

NAVAL POSTGRADUATE SCHOOL

Monterey, California



DTIC QUALITY INSPECTED 3

THESIS

**BENCH TEST MODEL OF THE HUMAN SKULL
FOR TESTING THE VARIABLE FREQUENCY
PULSE PHASE-LOCKED LOOP INSTRUMENT**

by

Amy Diana Burin

December, 1996

Thesis Advisor:

Sandra L. Scrivener

Approved for public release; distribution is unlimited.

19970616 125

REPORT DOCUMENTATION PAGE			Form Approved OMB No. 0704-0188	
Public reporting burden for this collection of information is estimated to average 1 hour per response, including the time for reviewing instruction, searching existing data sources, gathering and maintaining the data needed, and completing and reviewing the collection of information. Send comments regarding this burden estimate or any other aspect of this collection of information, including suggestions for reducing this burden, to Washington Headquarters Services, Directorate for Information Operations and Reports, 1215 Jefferson Davis Highway, Suite 1204, Arlington, VA 22202-4302, and to the Office of Management and Budget, Paperwork Reduction Project (0704-0188) Washington DC 20503.				
1. AGENCY USE ONLY (Leave blank)		2. REPORT DATE December 1996		3. REPORT TYPE AND DATES COVERED Master's Thesis
4. TITLE AND SUBTITLE BENCH TEST MODEL OF THE HUMAN SKULL FOR TESTING THE VARIABLE FREQUENCY PULSE PHASE-LOCKED LOOP INSTRUMENT			5. FUNDING NUMBERS	
6. AUTHOR(S) Burin, Amy Diana				
7. PERFORMING ORGANIZATION NAME(S) AND ADDRESS(ES) Naval Postgraduate School Monterey CA 93943-5000			8. PERFORMING ORGANIZATION REPORT NUMBER	
9. SPONSORING/MONITORING AGENCY NAME(S) AND ADDRESS(ES)			10. SPONSORING/MONITORING AGENCY REPORT NUMBER	
11. SUPPLEMENTARY NOTES The views expressed in this thesis are those of the author and do not reflect the official policy or position of the Department of Defense or the U.S. Government.				
12a. DISTRIBUTION/AVAILABILITY STATEMENT Approved for public release; distribution is unlimited.			12b. DISTRIBUTION CODE	
13. ABSTRACT (maximum 200 words) The Variable Frequency Pulse Phase-Locked Loop (VFPPLL) instrument is currently being used to non-invasively evaluate the human skull for increases in intracranial distances brought about by increases in intracranial pressure. It is designed to determine distance changes, in the sub-micron range, calculated from changes in frequency of an ultrasonic toneburst produced by a transducer, traversed through the skull and received back by the transducer. A bench test model of the human skull will calibrate the VFPPLL by comparing known distance changes to the VFPPLL derived distance changes, and thereby verify the accuracy of the instrument. Additionally, the bench test model will determine a broad range of operating limits on temperature, pressure and elongation over which the VFPPLL can operate accurately. Each of the three models made demonstrates a different effect on the frequency change based on the different parameters, i.e. temperature, pressure or elongation. The Open Channel Model compares closely approximated elongations with VFPPLL derived elongations, showing favorable results for calibration of the VFPPLL instrument. Specifications for creating a bench test model of the human skull for testing the VFPPLL instrument are established in this thesis.				
14. SUBJECT TERMS Human skull model, pulse phase-locked loop, intracranial pressure, intracranial distance			15. NUMBER OF PAGES 137	
			16. PRICE CODE	
17. SECURITY CLASSIFICATION OF REPORT Unclassified	18. SECURITY CLASSIFICATION OF THIS PAGE Unclassified	19. SECURITY CLASSIFICATION OF ABSTRACT Unclassified	20. LIMITATION OF ABSTRACT UL	

Approved for public release; distribution is unlimited.

**BENCH TEST MODEL OF THE HUMAN SKULL
FOR TESTING THE VARIABLE FREQUENCY
PULSE PHASE-LOCKED LOOP INSTRUMENT**

Amy Diana Burin
Lieutenant, United States Navy
B.S., University of Michigan, 1987

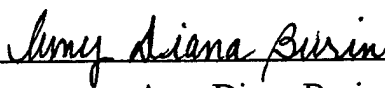
Submitted in partial fulfillment
of the requirements for the degree of

MASTER OF SCIENCE IN ASTRONAUTICAL ENGINEERING

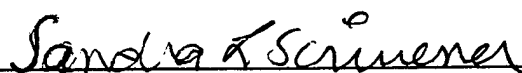
from the


**NAVAL POSTGRADUATE SCHOOL
December 1996**

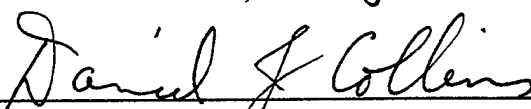
Author:


Amy Diana Burin

Approved by:


Sandra L. Scrivener, Thesis Advisor


Rudolf Panholzer, Second Reader


Daniel J. Collins, Chairman
Department of Aeronautics and Astronautics

ABSTRACT

The Variable Frequency Pulse Phase-Locked Loop (VFPPLL) instrument is currently being used to non-invasively evaluate the human skull for increases in intracranial distances brought about by increases in intracranial pressure. It is designed to determine distance changes, in the sub-micron range, calculated from changes in frequency of an ultrasonic toneburst produced by a transducer, traversed through the skull and received back by the transducer. A bench test model of the human skull will calibrate the VFPPLL by comparing known distance changes to the VFPPLL derived distance changes, and thereby verify the accuracy of the instrument. Additionally, the bench test model will determine a broad range of operating limits on temperature, pressure and elongation over which the VFPPLL can operate accurately. Each of the three models made demonstrates a different effect on the frequency change based on the different parameters, i.e. temperature, pressure or elongation. The Open Channel Model compares closely approximated elongations with VFPPLL derived elongations, showing favorable results for calibration of the VFPPLL instrument. Specifications for creating a bench test model of the human skull for testing the VFPPLL instrument are established in this thesis.

TABLE OF CONTENTS

I. INTRODUCTION	1
A. BACKGROUND AND SIGNIFICANCE	1
B. INTRACRANIAL PRESSURE (ICP) MEASUREMENT TECHNIQUES	2
II. THE PULSE PHASE-LOCKED LOOP INSTRUMENT	5
A. BACKGROUND	5
B. OPERATION	8
C. FREQUENCY EQUATIONS	11
III. PURPOSE OF TESTS	13
A. MOTIVATION	13
B. MODELS	13
1. Aluminum Model	13
a. Description	14
b. Set-up	17
c. Procedure	19
2. PVC Model	20
a. Description	20
b. Set-up	21
c. Procedure	23
3. Open Channel Model	23
a. Description	24
b. Set-up	26
c. Procedure	26
IV. RESULTS AND DISCUSSION	27
A. OPERATING LIMITS ON TEMPERATURE AND PRESSURE OF THE VFPPLL (ALUMINUM MODEL)	27
1. Frequency vs. Pressure	27
a. Results	27
b. Discussion	31
2. Elongation vs. Pressure	32
a. Results	32
b. Discussion	36

3.	Frequency vs. Elongation	36
a.	Results	36
b.	Discussion	40
B.	CALIBRATION	41
1.	PVC Model	41
a.	Results	41
b.	Discussion	43
2.	Open Channel Model	43
a.	Results	43
b.	Discussion	46
V.	CORRELATION TO THE HUMAN SKULL	47
A.	CADAVER STUDIES	47
1.	Background	47
2.	Discussion	47
VI.	FURTHER DISCUSSION AND CONCLUSIONS	53
A.	THEORY	53
B.	FUTURE STUDIES	62
APPENDIX A.	ALUMINUM MODEL	65
A.	NUMERICAL DATA	65
B.	GRAPHS	65
APPENDIX B.	PVC MODEL	83
A.	NUMERICAL DATA	83
B.	GRAPHS	83
APPENDIX C.	OPEN CHANNEL MODEL	93
A.	NUMERICAL DATA	93
B.	GRAPHS	93
APPENDIX D.	CADAVERS	111
A.	NUMERICAL DATA	111
B.	GRAPHS	111

LIST OF REFERENCES.....	115
INITIAL DISTRIBUTION LIST.....	117

LIST OF FIGURES

2.1	Block Diagram of the VFPPLL Instrument.	6
2.2	Block Diagram of the CFPPLL Instrument.	7
2.3	The VFPPLL Instrument.	9
2.4	The VFPPLL Instrument with PVC Model.	9
2.5	Artist Conception of the Human Skull.	10
3.1	The Aluminum Model.	13
3.2	Partial Testing Set-up with PVC Model.	19
3.3	The PVC Model.	20
3.4	Side View of PVC Model Set-up.	22
3.5	The Open Channel Model.	23
4.1	Individual HOT, ROOM TEMP and COLD Trials; Frequency vs. Pressure.	28
4.2	Average HOT, ROOM TEMP and COLD Trials; Frequency vs. Pressure.	30
4.3	Individual HOT, ROOM TEMP and COLD Trials; Elongation vs. Pressure.	33
4.4	Average HOT, ROOM TEMP and COLD Trials; Elongation vs. Pressure.	35
4.5	Individual HOT, ROOM TEMP and COLD Trials; Frequency vs. Elongation.	37
4.6	Average HOT, ROOM TEMP and COLD Trials; Frequency vs. Elongation.	39
4.7	PVC Model Run 1; Frequency vs. Elongation.	42
4.8	PVC Model Run 2; Frequency vs. Elongation.	42
4.9	Open Channel Model Run 2; Frequency vs. Elongation.	45
4.10	Open Channel Model Run 4; Frequency vs. Elongation.	45
5.1	Numerically Reduced Data on Cadaver A and Cadaver B.	49
5.2	Numerically Reduced Data on Cadaver C.	49
5.3	Cadaver A; ICD vs. ICP.	50
5.4	Cadaver B; ICD vs. ICP.	50
5.5	Cadaver C; ICD vs. ICP.	51
5.6	Pre-processed Cadaver B Data; Frequency vs. Time and ICP vs. Time [Ref. 2].	51
6.1	Example of Elongation.	54

6.2	C_1 vs. Temperature.	56
6.3	Slope of Elongation vs. Pressure, vs. Temperature.	57
A.1	Numerical Data for HOT Trials.	67
A.2	Numerical Data for ROOM TEMP Trials.	68
A.3	Numerical Data for COLD Trials.	69
A.4	Averaging Analysis for Frequency vs. Pressure Data.	70
A.5	Averaging Analysis for Elongation vs. Pressure Data.	71
A.6	Averaging Analysis for Frequency vs. Pressure Data.	72
A.7	HOT (1) Frequency and Axial Elongation vs. Pressure.	73
A.8	HOT (1) Frequency vs. Elongation.	73
A.9	HOT (2) Frequency and Axial Elongation vs. Pressure.	74
A.10	HOT (2) Frequency vs. Elongation.	74
A.11	HOT (3) Frequency and Axial Elongation vs. Pressure.	75
A.12	HOT (3) Frequency vs. Elongation.	75
A.13	ROOM TEMP (1) Frequency and Axial Elongation vs. Pressure.	76
A.14	ROOM TEMP (1) Frequency vs. Elongation.	76
A.15	ROOM TEMP (2) Frequency and Axial Elongation vs. Pressure.	77
A.16	ROOM TEMP (2) Frequency vs. Elongation.	77
A.17	ROOM TEMP (3) Frequency and Axial Elongation vs. Pressure.	78
A.18	ROOM TEMP (3) Frequency vs. Elongation.	78
A.19	COLD (1) Frequency and Axial Elongation vs. Pressure.	79
A.20	COLD (1) Frequency vs. Elongation.	79
A.21	COLD (2) Frequency and Axial Elongation vs. Pressure.	80
A.22	COLD (2) Frequency vs. Elongation.	80
A.23	COLD (3) Frequency and Axial Elongation vs. Pressure.	81
A.24	HOT (3) Frequency vs. Elongation.	81
B.1	PVC Model Numerical Data; Runs 1, 2 and 3.	84
B.2	PVC Model Numerical Data; Runs 4, 5 and 6.	85
B.3	PVC Model Numerical Data; Runs 7, 8 and 9.	86

B.4	PVC Model Run 1; Frequency vs. Elongation.	87
B.5	PVC Model Run 2; Frequency vs. Elongation.	87
B.6	PVC Model Run 3; Frequency vs. Elongation.	88
B.7	PVC Model Run 4; Frequency vs. Elongation.	88
B.8	PVC Model Run 5; Frequency vs. Elongation.	89
B.9	PVC Model Run 6; Frequency vs. Elongation.	89
B.10	PVC Model Run 7; Frequency vs. Elongation.	90
B.11	PVC Model Run 8; Frequency vs. Elongation.	90
B.12	PVC Model Run 9; Frequency vs. Elongation.	91
C.1	Open Channel Numerical Data; Runs 1 and 2.	94
C.2	Open Channel Numerical Data; Runs 3 and 4.	95
C.3	Open Channel Numerical Data; Runs 5 and 6.	96
C.4	Open Channel Numerical Data; Runs 7 and 8.	97
C.5	Open Channel Numerical Data; Runs 9 and 10.	98
C.6	Open Channel Numerical Data; Runs 11 and 12.	99
C.7	Open Channel Numerical Data; Runs 13 and 14.	100
C.8	Open Channel Numerical Data; Runs 15 and 16.	101
C.9	Open Channel Model Run 1; Frequency vs. Elongation.	102
C.10	Open Channel Model Run 2; Frequency vs. Elongation.	102
C.11	Open Channel Model Run 3; Frequency vs. Elongation.	103
C.12	Open Channel Model Run 4; Frequency vs. Elongation.	103
C.13	Open Channel Model Run 5; Frequency vs. Elongation.	104
C.14	Open Channel Model Run 6; Frequency vs. Elongation.	104
C.15	Open Channel Model Run 7; Frequency vs. Elongation.	105
C.16	Open Channel Model Run 8; Frequency vs. Elongation.	105
C.17	Open Channel Model Run 9; Frequency vs. Elongation.	106
C.18	Open Channel Model Run 10; Frequency vs. Elongation.	106
C.19	Open Channel Model Run 11; Frequency vs. Elongation.	107
C.20	Open Channel Model Run 12; Frequency vs. Elongation.	107

C.21	Open Channel Model Run 13; Frequency vs. Elongation.	108
C.22	Open Channel Model Run 14; Frequency vs. Elongation.	108
C.23	Open Channel Model Run 15; Frequency vs. Elongation.	109
C.24	Open Channel Model Run 16; Frequency vs. Elongation.	109
D.1	All Cadaver C Numerically Reduced Data.	112
D.2	All Cadaver C Data Points; ICD vs. ICP.	113
D.3	Data Points from Cadavers A, B and C; ICD vs. ICP.	113

LIST OF TABLES

3.1	Aluminum Model Parameters.	14
3.2	Temperature Data for Aluminum Model Testing.	18
3.3	Physical Dimensions of the PVC Model.	21
3.4	Physical Dimensions of the Open Channel Model.	25
4.1	Correlations and Slopes for HOT Temperature Trials.	29
4.2	Correlations and Slopes for ROOM TEMP Trials.	29
4.3	Correlations and Slopes for COLD Temperature Trials.	29
4.4	Correlations and Slopes for HOT Temperature Trials.	34
4.5	Correlations and Slopes for ROOM TEMP Trials.	34
4.6	Correlations and Slopes for COLD Temperature Trials.	34
4.7	Correlations and Slopes for HOT Temperature Trials.	38
4.8	Correlations and Slopes for ROOM TEMP Trials.	38
4.9	Correlations and Slopes for COLD Temperature Trials.	38
5.1	Equations Representing the Linear Relationship Between ICD and ICP and Corresponding Correlation Coefficients.	52
6.1	Values of C_2 and $\Delta f / \Delta x$ for the PVC Model.	60
A.1	Figure Number and Representative Graph, Aluminum Model.	66

ACKNOWLEDGEMENT

The author would like to thank Professor Scrivener for her guidance, patience and time spent in the preparation of this thesis. The author would also like to thank Boyd Ames, Norm Boivin and Tom Christian for their assistance with the bench test models.

I. INTRODUCTION

A. BACKGROUND AND SIGNIFICANCE

Space motion sickness and headaches can be significant problems astronauts will experience during spaceflight. Seventy-three percent of Shuttle astronauts exhibit symptoms of space motion sickness which may persist through the first three days of flight and have an adverse affect on crew performance and mission progress [Ref. 1]. These symptoms can include, but are not limited to, headache, nausea, vomiting, lethargy, disorientation, and malaise, which may significantly impair astronaut performance during that period. A definitive cause for these headaches and space motion sickness still remains unclear, but the symptoms may result, at least in part, from alterations in intracranial circulation and intracranial pressure (ICP) [Ref. 2]. On Earth, abnormally elevated ICP occurs in 50-75% of patients experiencing severe head trauma [Ref. 3]. In documented cases where ICP increases to values exceeding 20 mmHg, a 95% mortality rate has been observed. Secondary brain injury due to severe head trauma can therefore be greatly reduced by immediate detection and treatment of elevated ICP. Of military significance, historically nearly 20% of all head injuries sustained in combat have been non-skull-penetrating [Ref. 4]. With better protective equipment, i.e., Kevlar helmets, and the use of armored vehicles on the battlefield, the relative frequency of severe non-skull-penetrating head injuries will likely increase. Reduction, and eventual prevention, of secondary brain injuries in the field following head trauma can be accomplished most easily by the prompt detection and treatment of hematomas

and of waves on intracranial pressure elevation that accompany loss of cerebrovascular autoregulation, cerebral edema, seizures and infection [Ref. 5].

Intracranial pressure has the potential to be a critical parameter for understanding physiological responses during exposure to microgravity. A better understanding of time course changes in ICP during exposure to microgravity could aid our understanding of the pathophysiology of space adaptation syndrome and improve treatment and performance of astronauts during early flight. Elevated intracranial pressure can lead to reduced brain perfusion, which in turn leads to reduced brain oxygenation and ultimately impairs crew performance. It can also lead to vestibular dysfunction, which leads to space adaptation syndrome (SAS), and further reduces crew performance. In the January 1994 Joint National Aeronautics and Space Administration (NASA)/National Institutes of Health (NIH) Workshop on Research in the Microgravity Environment, intracranial pressure was labeled as one of the most important parameters to investigate for problems astronauts can experience during spaceflight and for several diseases or cases of traumatic head injuries of patients on Earth. Intracranial pressure though has been an extremely difficult parameter to measure because of the invasive nature of the techniques currently available [Ref. 6], techniques which are impractical for use in space or in the combat environment.

B. INTRACRANIAL PRESSURE (ICP) MEASUREMENT TECHNIQUES

Several invasive methods are available for clinical use in life threatening situations [Refs. 7 and 8]. The intraventricular pressure (IVP) method involves the insertion of a catheter into the lateral ventricle and the fluid-coupling of this catheter to a strain gage. This procedure is still used as a reference method of monitoring intracranial pressure [Ref. 9].

Extraventricular ICP systems employ subdural fluid filled pressure monitoring devices [Ref. 7] and semi-conductor pressure transducers [Refs. 10 and 11]. Commercially available extradural pressure (EDP) monitoring devices have been used in clinical settings, but show unacceptable discrepancies between intraventricular pressure (IVP) and EDP recordings [Refs. 9 and 12]. Other types of indirect long term ICP measurement techniques can be utilized, but all require substantial surgical intervention which involves considerable high risk to the patient due to the risk of infection and limited monitoring periods.

The inherent limitations of the above invasive methods of measuring and monitoring intracranial pressure indicate the need for an ICP measurement technique that is noninvasive and accurate. The noninvasive monitoring technique employed should have direct correlation with ICP and be highly sensitive to changes in ICP, as the changes are small in magnitude and difficult to detect. Of great importance, in addition to the former, the technique should be safe, reliable and easily performed [Ref. 13].

Although the skull is often assumed to be a rigid container with constant volume, sensitive measurements indicate that the skull expands with increasing intracranial pressure [Refs. 14 and 15]. Early noninvasive diagnosis of increasing ICP may help manage and prevent secondary brain injury caused by head trauma, brain tumors, brain edema, or infection. Investigation into the use of ultrasound to noninvasively measure the slight changes in intracranial volume (ICV), assuming ICV is directly proportional to intracranial diameter (or distance) (ICD), that occur coincidentally with changes in ICP is ongoing. A relatively new instrument based on a pulsed phase-lock loop (PPLL) technology concept has been developed to measure the ultrasonic phase velocity accurately in condensed matter [Ref. 16].

The instrument transmits a 500 kHz ultrasonic toneburst through the cranium via a transducer placed on the side of the skull. The ultrasonic wave passes through the cranial cavity, reflects off the inner surface of the skull on the opposite side, and is received back by the same transducer. The device then uses a phase comparison technique to quantify distance across the skull [Ref. 16].

The purpose of the experimentation done for this thesis is to develop and test a bench test model for the PPLL instruments. The main requirements of the bench test model are to calibrate the PPLL and establish broad operating limits on temperature, pressure and elongation over which the PPLL can operate accurately.

II. THE PULSE PHASE-LOCKED LOOP INSTRUMENT

A. BACKGROUND

Dr. W. Tom Yost and Dr. John H. Cantrell, of the NASA-Langley Research Center have patented the constant frequency pulse phase-locked loop (CFPPLL) instrument. The variable frequency pulse phase-locked loop (VFPPLL) instrument elements are identical to the CFPPLL, with the exception of the constant frequency source and the phase shift circuitry. The VFPPLL is a device whose operating frequency is changed during the course of a measurement procedure. It was developed through measurements of externally simulated small changes in velocity and path lengths in different types of solid media. Both the CFPPLL and the VFPPLL operate by using the output of a phase detector that compares the phase of a signal from a sample, in this case a human subject, to a reference signal. A selected portion of the signal received back from the subject is fed through an integrator circuit to a control loop that alters the signals to the phase detector until its output is nulled. At the point when the phase detector's output is nulled, the system stabilizes and the instrument output signal is recorded [Ref. 16]. Figure 2.1 is a block diagram of the CFPPLL instrument for comparison with Figure 2.2, the VFPPLL instrument [Ref. 16].

All model testing for this thesis was done using the VFPPLL, but they could be used with the CFPPLL, by measuring different parameters; i.e., the VFPPLL measures changes in frequency while the signal phase is held constant (phase comparison), and the CFPPLL measure changes in signal phase while the frequency is held constant (frequency comparison). The CFPPLL was not available for testing.

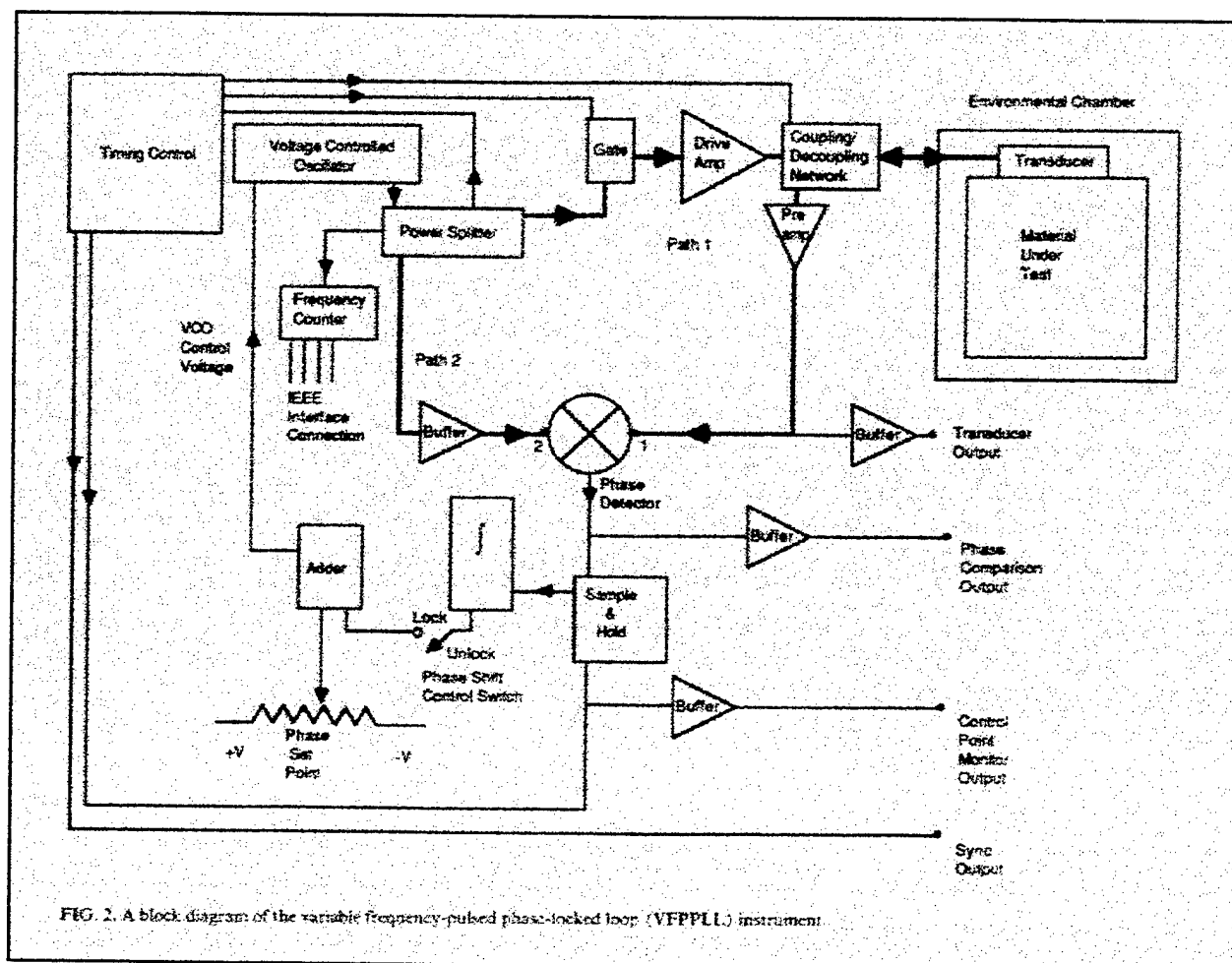


Figure 2.1 Block Diagram of the VFPLL Instrument [Ref. 16].

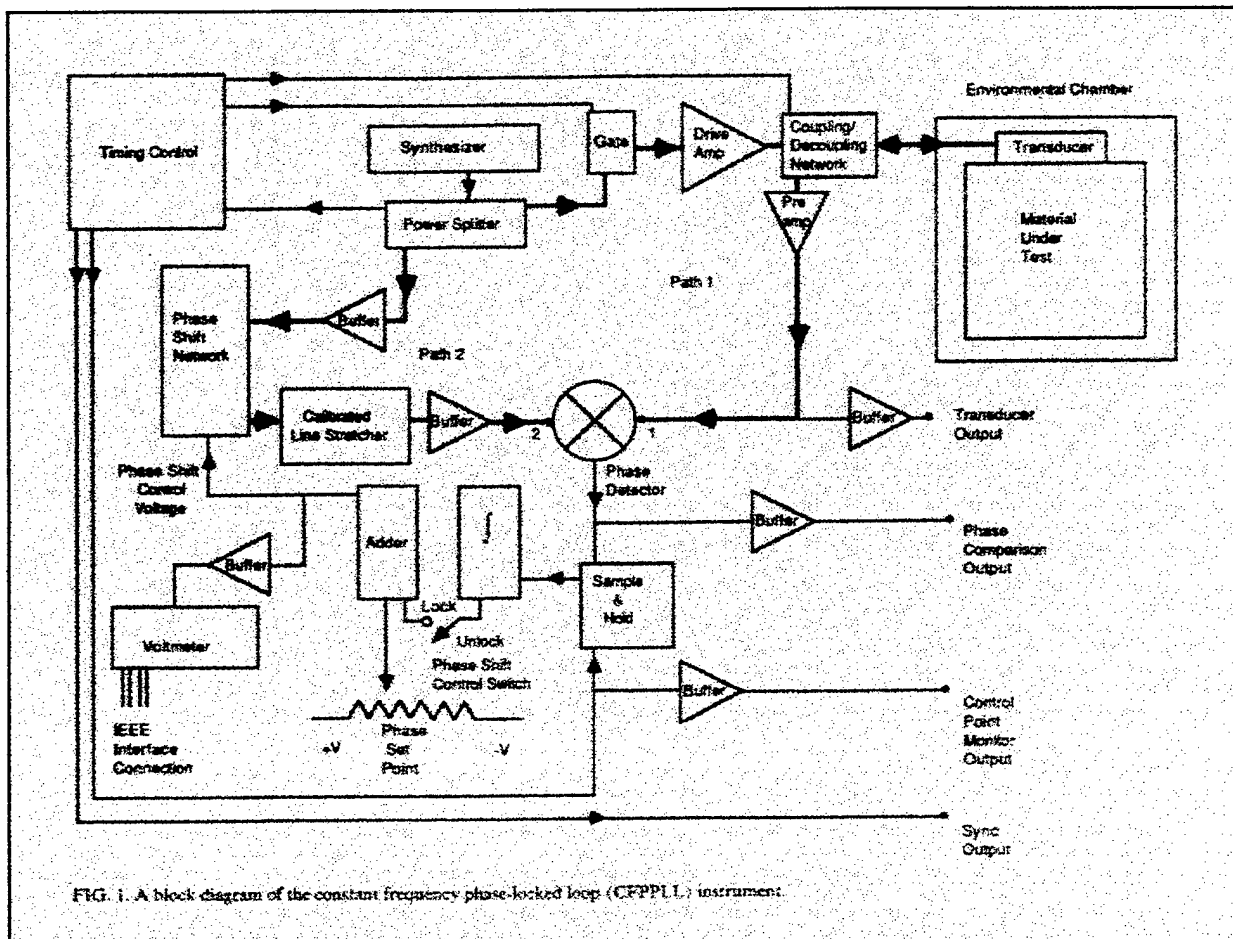


Figure 2.2 Block Diagram of the CFPPLL Instrument [Ref. 16].

B. OPERATION

Basic operation of the VFPPLL can be understood by first discussing the basic principles of the CFPPLL instrument. It begins with a constant frequency oscillator and two signal paths. Along the measurement path, the acoustic signal is generated and amplified after traveling through the acoustic medium and after the signal has been electroconverted by the transducer. The second path, including a voltage-controlled phase shifter, is the reference path used for the phase comparison with the measurement path. The phase detector then detects the relative phase difference between the reference path and the measurement path with an output voltage that is directly proportional to the cosine of that phase difference. The control voltage to the voltage-controlled phase shifter is automatically changed until the output is zero volts, a condition of quadrature between the reference path signal and the measurement path signal. A calibration procedure utilizing a line stretcher in the reference path permits the conversion of the change in control voltage to a change in phase shift between the two paths. This change in phase shift is the parameter from which changes in intracranial distance are determined by calculation. In the VFPPLL instrument, the frequency of the voltage control oscillator is changed by the loop control circuit until quadrature between the reference path signal and the measurement path signal is obtained, and the frequency observation is the parameter from which intracranial distance changes are calculated [Ref. 16]. Figure 2.3 shows the actual VFPPLL instrument used in the Space Physiology Laboratory at NASA Ames Research Center. Figure 2.4 is the VFPPLL with a view of the Polyvinyl Chloride (PVC) model connected for testing and is a full set-up, excluding the strain gage box and switching unit (discussion to follow in Chapter III).

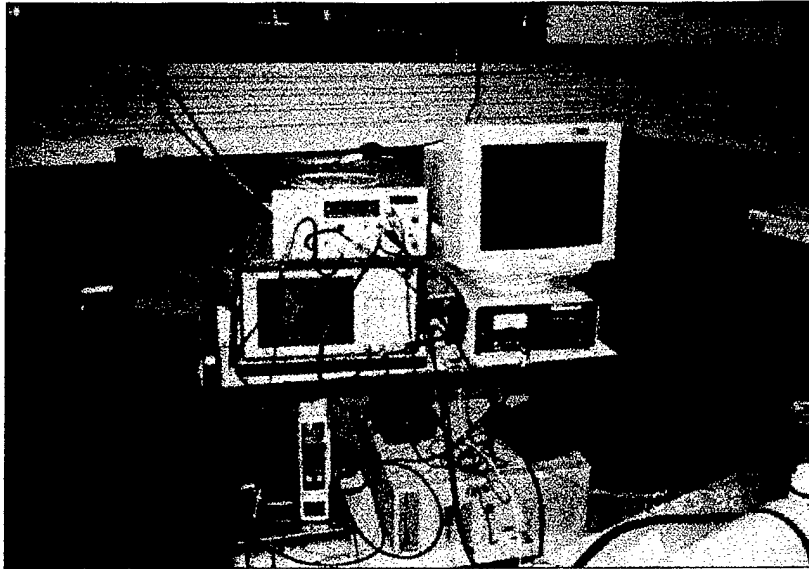


Figure 2.3 The VFPPLL Instrument.

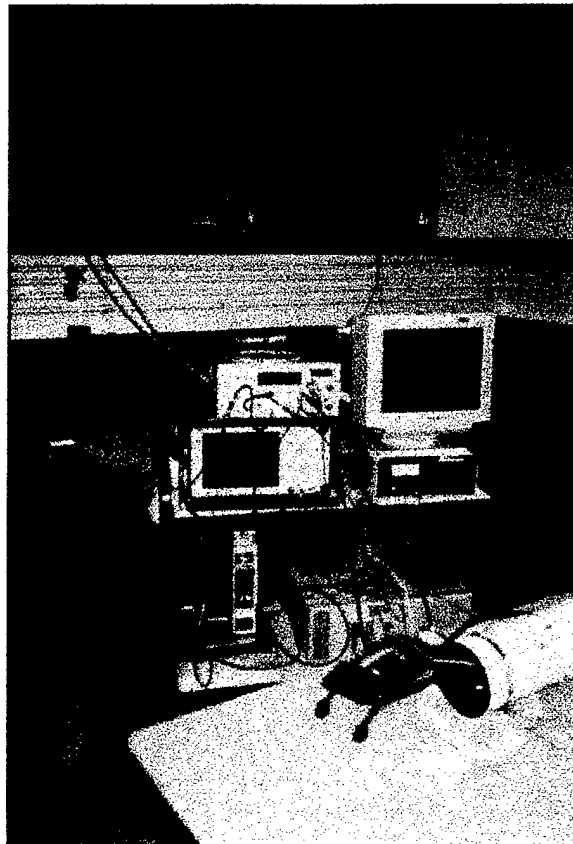


Figure 2.4 The VFPPLL Instrument with PVC Model.

Figure 2.5 is an artists' conception of a human skull with transducer attached on the right side of the skull, to the left in the figure [Ref. 2]. It depicts the path the ultrasound toneburst takes when traversing the skull and shows the equation relating frequency to elongation.

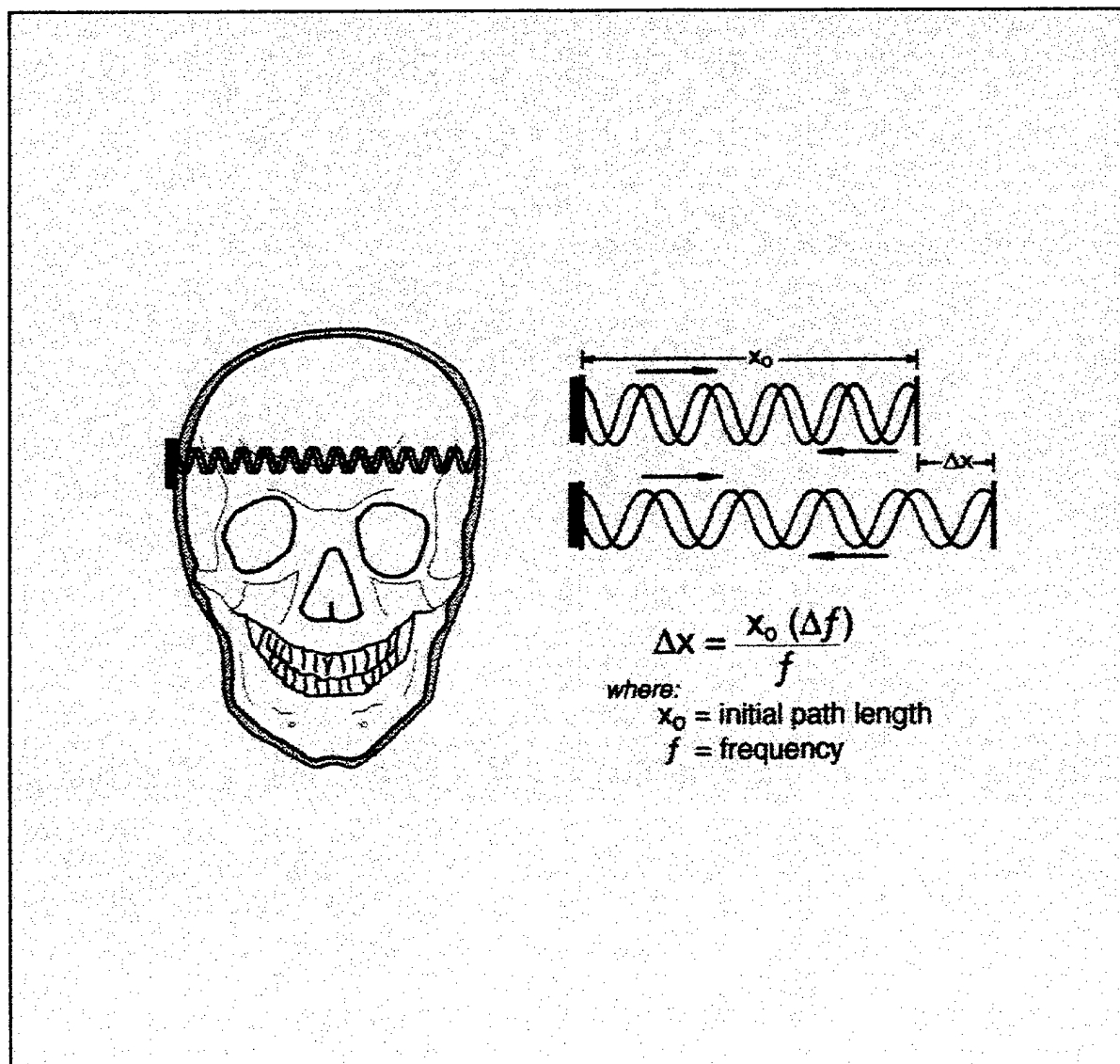


Figure 2.5 Artist Conception of the Human Skull [Ref. 2].

C. FREQUENCY EQUATIONS

The basic governing equation used to calculate elongation in the human skull, i.e., intracranial distance changes from frequency readings of the VFPPLL is given by

$$\Delta x = -x_0 \cdot \left(\frac{\Delta f}{f_0} \right) \quad (2.1)$$

[Ref. 2]

or rearranged,

$$\Delta f = - \left(\frac{\Delta x}{x_0} \right) \cdot f_0 \quad (2.2)$$

where

Δf = the change in frequency

f_0 = the initial frequency of the comparing frequency observations

x_0 = the initial path length or intracranial distance

Δx = the change in path length, i.e., the change in intracranial distance.

The change in intracranial distance, however, is affected by the other parameters, specifically temperature and pressure. The proposed expanded frequency equation shows that the change in frequency observed by the VFPPLL when measuring intracranial distances changes is given as

$$\Delta f (\Delta x, T, p) = c_1(T) \cdot \Delta p + c_2(T) \cdot \Delta x \quad (2.3)$$

where

T = temperature

p = pressure

Δx = initial intracranial distance

c_1 = constant for pressure term

c_2 = constant for elongation term

The effects of temperature, pressure and elongation on the operating accuracy of the VFPPLL are explored in this thesis, as well as the proposed expanded frequency equation. Chapter IV will detail the results of the three different models tested and indicate when the frequency observations of the VFPPLL are affected more by the pressure term of the frequency equation than by the elongation term, and when the elongation term of the frequency equations outweighs the effect of the pressure term.

III. PURPOSE OF TESTS

A. MOTIVATION

The bench test model needs to simulate and accurately measure the expansion in an actual human skull. The VFPPLL has certain operating limits on parameters such as elongation, temperature and pressure, and the bench test models will determine rough limits on these parameters. The VFPPLL must also be calibrated, and the bench test model needs to calibrate the measurement capability of the device. The tests discussed in this chapter are initial tests used to determine broad ranges for the operating parameters, and further studies with more refined equipment is needed to establish tighter upper and lower limits.

B. MODELS

a. Aluminum Model

Figure 3.1 is the Aluminum Model.

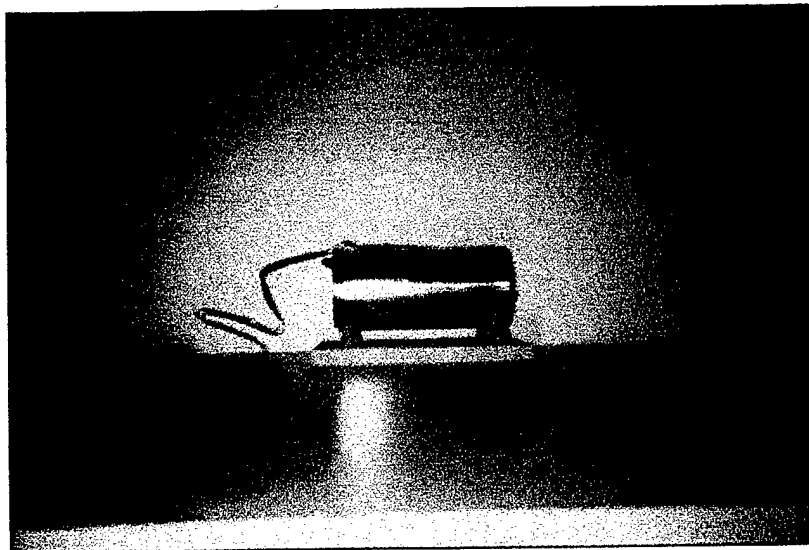


Figure 3.1 The Aluminum Model.

a. Description

When testing this model, it became apparent that both temperature and pressure had significant effects on the operating limits of the VFPPLL. This afforded the opportunity to explore the ranges of these parameters for correct operation of the VFPPLL.

This model, as seen in Figure 3.1, is made of 6061-T6 Aluminum with steel endcaps. The physical dimensions were taken with a micrometer, and are accurate to within $\pm 0.5 \mu\text{m}$. The dimensions and physical parameters as listed in Table 3.1.

Material	E (GPa)	G (MPa)	ν	ρ (kg/m ³)	σ_y (MPa)	outer radius (mm)	inner radius (mm)	thickness (mm)	length (mm)
Aluminum	70.00	25.51	0.3719	2710	95.00	49.986	48.486	1.5	149.586
Steel	200.00	79.29	0.2611	7860	250.00	49.986	solid	solid	30.044

Table 3.1 Aluminum Model Parameters.

where E = the modulus of elasticity, G = the shear modulus, ν = Poisson's ratio, ρ = density and σ_y = yield strength. [Ref. 17]

The steel endcaps are threaded and screw into both ends of the thin aluminum cylinder, and a water and pressure tight seal is provided by an o-ring. The outer ends of the steel endcaps have grooves for placement of a spanning wrench, and during testing the aluminum cylinder is filled with water by removing the steel endcaps with this spanning wrench. The model is elongated, both radially and axially, by increasing the pressure inside

the model through a Schraeder valve using a standard bicycle pump. The elongation is measured using two strain gages, one attached in the axial direction and the other attached in the radial direction. They are strategically glued to the top of the model, with the wires taped down for protection from outside influence. Finally, a half-circle shaped piece of acrylic, with a diameter of approximately 1.75", is glued to an outer steel endcap (opposite end from the Schraeder valve) to hold the transducer in place.

The aluminum model (as well as the Polyvinyl Chloride (PVC) model, discussion to follow) is supported using a cradle-like wooden structure, as seen in Figure 3.1. It is constructed out of pine, and leveled to provide a relatively flat surface area on which the model was supported for testing. The purpose of the cradle is to reduce surface area contact of the model to minimize friction, allowing for optimum elongation.

The aluminum model is designed as a thin-walled cylindrical pressure vessel. Equations for stress and strain in the axial and hoop directions are given as

$$\sigma_h = \frac{pr_i}{t} \quad (3.1)$$

[Ref. 18]

$$\sigma_a = \frac{pr_i}{2t} \quad (3.2)$$

[Ref. 18]

where σ_h is the hoop stress and σ_a is the axial stress, and

$$\epsilon_h = \frac{1}{E} \left(\sigma_h - \nu \sigma_a \right) = \frac{1}{E} \left(\frac{pr_i}{t} - \nu \frac{pr_i}{2t} \right) = \frac{pr_i}{Et} \left(1 - \frac{\nu}{2} \right) \quad (3.3)$$

[Ref. 18]

$$\epsilon_a = \frac{1}{E} \left(\sigma_a - \nu \sigma_h \right) = \frac{1}{E} \left(\frac{pr_i}{2t} - \nu \frac{pr_i}{t} \right) = \frac{pr_i}{Et} \left(\frac{1}{2} - \nu \right) \quad (3.4)$$

[Ref. 18]

where ϵ_h is the hoop strain and ϵ_a is the axial strain, and

E = modulus of elasticity

p = pressure

r_i = radius, inner

t = thickness

The elongation of the model is directly proportional to the axial strain, assuming first order strain as an approximation. The relationship of axial strain to elongation in the axial direction is given as

$$\epsilon_a = \frac{\Delta x}{x_0}$$

where x_0 is the initial length. (3.5)

Rearranging Equation (3.5) yields elongation in the axial direction as

$$\Delta x = \epsilon_a \cdot x_0 \quad (3.6)$$

The theoretical expansion of this model in the axial direction is based on a combination of Equations (3.4) and (3.6) and is given as

$$\Delta x = \epsilon_a \cdot x_0 = \left[\frac{Pr_i}{Et} \left(\frac{1}{2} - \nu \right) \right] \cdot x_0 \quad (3.7)$$

The elongation of the model in the axial direction is primarily due to the expansion of the aluminum in the same direction, although a small amount of expansion can be attributed to the steel endcaps. Using Equation (3.7), the elongation of the steel endcaps accounts for less than 3 percent of the total elongation and is therefore considered negligible.

b. Set-up

Testing of the aluminum model concentrated on finding the combined effects of temperature and pressure on the function of the VFPPLL. Three temperature ranges were explored for their individual effects on the operation of the device. Three trials were conducted in the "hot" temperature range, three in the "room" temperature range and three in the "cold" temperature range. Table 3.2 illustrates the temperatures recorded in each trial and the average temperature used in the overall analysis.

	trial 1	trial 2	trial 3	<i>average</i>
	(°F)	(°F)	(°F)	(°F)
HOT	122	not available	112	117
ROOM	79	not available	80	79.5
COLD	48	not available	60	54

Table 3.2 Temperature Data for Aluminum Model Testing.

One endcap of the model is removed and the cylinder is filled with water, enough so the ultrasound wave will travel through water, but not too much so that air cannot be pumped in to pressurize the model. The temperature of the water is initially observed and recorded, and the endcap is replaced. The model is placed in the wooden cradle and the strain gage wires are checked for proper operation. The pump is then connected to the aluminum model's Schraeder valve for pressurization during testing. The transducer is placed in the acrylic cradle, and the testing is ready to proceed. Figure 3.2 illustrates a partial set-up, which includes the strain gage box and switching unit, connections to the model, and bicycle pump. The white wire to the right of the PVC model in Figure 3.2 is the transducer wire which connects to the circuitry of the VFPPLL. Note the model illustrated in this figure is the PVC model, not the aluminum model.

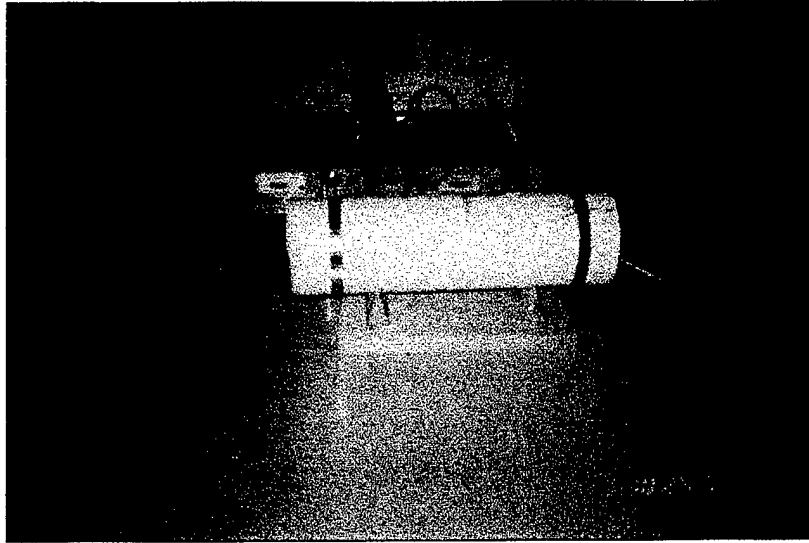


Figure 3.2 Partial Testing Set-up with PVC Model.

c. Procedure

Three trials were conducted for each of the three temperature ranges. Data collected includes the date, the time of the trial (to ensure the temperature remained relatively constant over the data collection period), the temperature (for the first and third trial; for the second trial no temperature was recorded due to the difficulty of removing the steel endcaps quickly), the pressure introduced to into the aluminum model, the strain gage readings from both the axial and radial strain gages (in microstrain), and the frequency of the VFPPLL. Pressure was steadily increased inside the model from 0 - 140 psi, while each temperature range was kept relatively constant, i.e., over the short duration of the test (approximately ten minutes), the temperature was assumed to be constant and the value used for analysis was an average of the first and third temperature readings as seen in Table 3.2. Recorded data was analyzed using Microsoft EXCEL and will be shown in Chapter IV.

2. PVC Model

Figure 3.3 is the PVC Model.

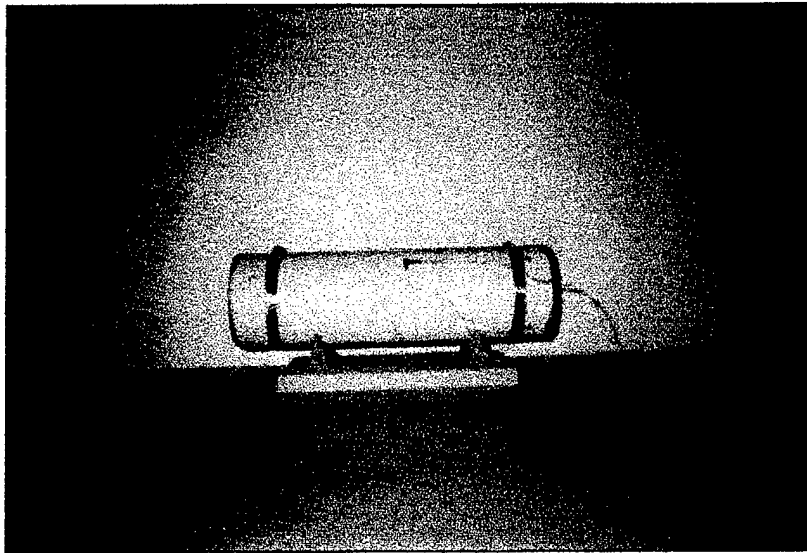


Figure 3.3 The PVC Model.

c. Description

The PVC model is designed to calibrate the VFPPLL. It is made of the composite material Polyvinyl Chloride. The endcaps are made of a strong plastic used in standard plumbing projects. The endcaps are glued to the PVC piping using a PVC adhesive compound that melts the plastic and the PVC materials together to form a water and pressure tight seal. The attachment of the endcaps to the PVC piping is further reinforced by four bolts per end for safety. Due to the yield strength of the material and the strength of the endcap bonds, the PVC pipe model will not withstand near the pressure increase within its walls as the aluminum model. For this reason, and the fact that the attachment of the endcaps is much more rigid in the aluminum model than in the PVC model (due to the threaded endcaps), the PVC model requires that additional safety measures be taken. Since the

endcaps are fixed, the introduction of water into the model had to be accomplished by different means. A pipe fitting was used with a threaded screw for water tight integrity, and a funnel was used to pour water into the model. Pressure was again pumped into the model via a Schraeder valve using a standard bicycle pump. Two strain gages were fixed to the top of the PVC model, as on the aluminum model, and the wires were taped for equipment safety. A transducer holder was not needed for this model, as the shape of the endcap allowed it to act as a natural holder. Table 3.3 gives approximate values for the dimensions of the PVC model.

	length (mm)	radius (mm)
cylinder	350	50
endcap	50	50

Table 3.3 Physical Dimensions of the PVC Model.

b. Set-up

Testing of the PVC model concentrated on the relationship between frequency and elongation of the model, and interaction with the VFPLL. In the aluminum model, the observed relationship between frequency and elongation was: as elongation increased, frequency increased due to greater effects by the pressure rather than by the elongation. In this model, a much more compliant material was used, so that the elongation would have a greater effect than the pressure on frequency.

The PVC model cylinder was filled with water using a funnel, to the same relative level as in the aluminum model; enough water so the ultrasound wave would pass through the water to simulate human brain tissue, but not too much that air could not be pumped into the model to pressurize it. The trials were run with water at room temperature, as there was no concern here the effect of temperature, just the effect of pressure. Since there were no temperature concerns, the strain gages were connected last with no time constraints on equipment set-up. The model was again placed in the wooden cradle for support and resistance to frictional effects during the elongation testing of the model. Finally, the pump connection was made to the Schraeder valve on the PVC model, the transducer is placed in the endcap and testing is ready to begin. Figure 3.4 is a side view of the PVC model partial set-up with the model connected to the strain gage box and switching unit equipment. The transducer is cradled in the endcap of the model, and the wire (to the left in the figure) stretches outward to connect to the VFPPLL instrument circuitry.

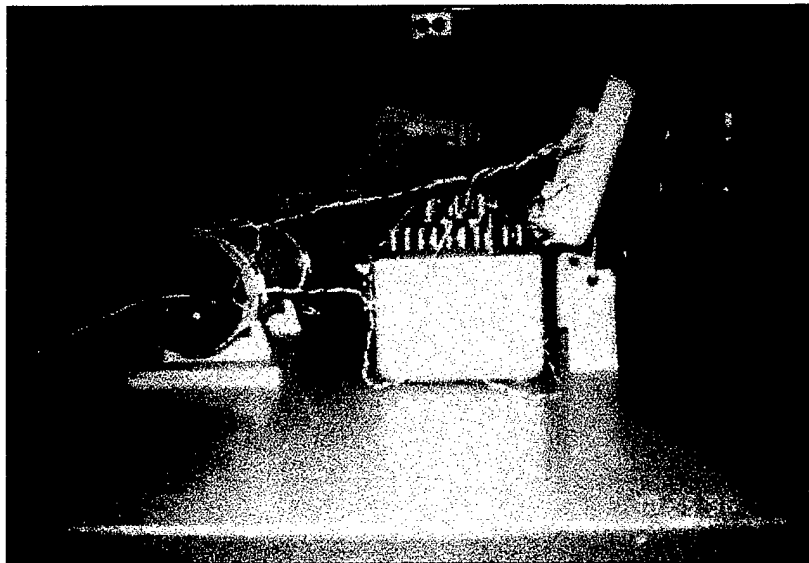


Figure 3.4 Side View of PVC Model Set-up.

c. Procedure

Data collection in testing the PVC model is not time or temperature critical, so more trials can be conducted without worrying about temperature effects. Since the accuracy of measurement of the VFPPLL is limited to small elongations, possibly only one wavelength, and the pressure threshold is considerably less than that of the aluminum model, these trials require fewer pressure steps than in the aluminum model. In the PVC model, the pressure is increased much more gradually, to a maximum pressure of less than 20 psi, whereas in the aluminum model the pressure increases in steps of 10 psi up to 140 psi. Data collected includes frequency readings by the VFPPLL and radial (hoop) strain. Pressure readings were not collected as the graduations were too small to be read by the pressure gage. Both strain readings could not be read at the same time with the equipment available. A strain box and switching unit were available, but considerable fluctuations in the strain values resulted when attempting to switch from reading one strain gage to reading the other due to continual pressure loss from the PVC model. Detailed analysis and results are presented with Microsoft EXCEL files in Chapter IV.

3. Open Channel Model

Figure 3.5 is the Open Channel Model.

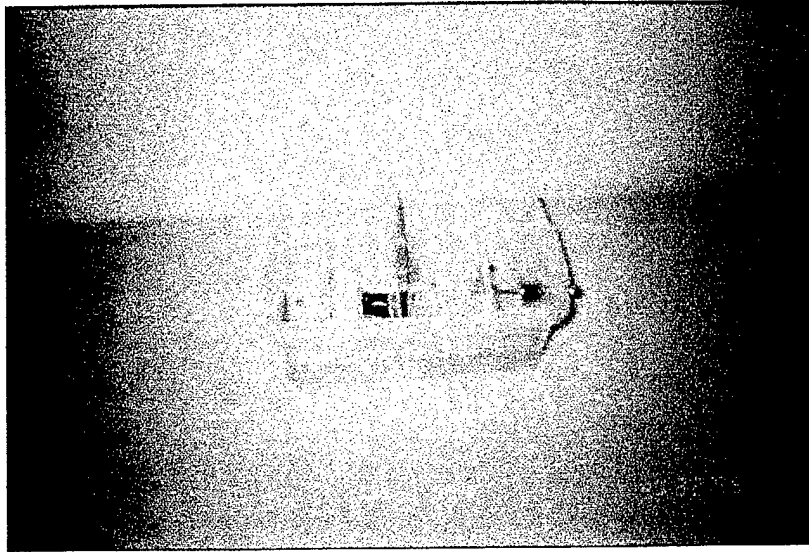


Figure 3.5 The Open Channel Model.

a. Description

The open channel model is the final "bench test" calibration model for the VFPPLL instrument (for purposes of this thesis). It primarily demonstrates the relationship between frequency and elongation, but does not have the accuracy required to be a stand alone model for calibration purposes. This model uses a rough measurement technique, utilizing a 4.25" long screw with 1/32" threads, to effect elongation. It lacks precision due to the fact that, when the screw is turned to effect elongation, human error can account for a major difference between effected (theroetical) and measured elongation.

The open channel model, as seen in Figure 3.5, is simplistic in design. Primary operation of this model is based on two reflective surfaces, one at each end, off which the ultrasound wave from the VFPPLL instrument is reflected and the distance between them indirectly measured through a change in frequency (see Chapter II on the VFPPLL instrument for details on how this is accomplished). The two surfaces are of acrylic material which act

as good reflectors, i.e., they show a clear reflection of the ultrasound wave from the VFPPLL off their surfaces, which is necessary in determining the initial measured distance (x_0). On one end the reflective acrylic surface is fixed to stand at a 90° angle to the base and is riveted in place with a piece of aluminum to hold the plate firmly in place. The other reflective surface is not fixed, but is allowed to move to effect distance changes. It is riveted to "L" shaped aluminum flanges to allow it to be as level as possible with the base of the model for smooth movement along the flat surface. The base of the open channel model is aluminum and painted with non-reflective black paint on the bottom. Table 3.4 gives approximate values for the physical dimensions of this model.

	color	length (mm)	height [width] (mm)
reflective surface - fixed	clear	85	110
reflective surface - moveable	black	85	125
base	n/a	230	[90]
screw hold	n/a	75	40
screw	n/a	100	n/a

Table 3.4 Physical Dimensions of the Open Channel Model.

The elongation of this model is effected by turning the screw and pushing the moveable reflective surface along the base of the model. Each complete turn of the screw moves it approximately $1/32"$. The screw is held level by a screw hold made of aluminum and

riveted securely to the aluminum base. On the base of the model, in viewing area of the reflective surface movement, are graduated etched markings reflecting measured known distances of $1/10''$ and $1/20''$ for theoretical comparison to measured elongations derived from changes in frequency. Finally, the model is in a square plastic container slightly larger than the base of the model and 105 mm in height to hold water during testing.

b. Set-up

Testing with the open channel model does not depend on pressure or temperature. The total elongation effected during each trial is limited, however, by the maximum elongation accurately determined by the VFPPLL. The model is placed in the plastic container and the container is filled with water. The transducer is attached to the moveable reflective plate using ultrasound transmission gel only, and the model is ready for testing.

c. Procedure

The procedure for testing the open channel model is relatively easy, but care must be taken since the majority of error in testing this model will be due to human interaction. Data collected during these trials will consist of frequency values from the VFPPLL and approximate values of elongation effected by an operator. One operator will induce an elongation by turning the screw in the screw hold, and the other operator will record the amount of approximate elongation and while simultaneously taking a frequency reading. The results of these trials are presented in Chapter IV.

IV. RESULTS AND DISCUSSION

In general, the data collected in testing and presented in this chapter will be in the form of graphs and charts. For all graphical representations, RED circles represent data for the HOT trials, YELLOW triangles represent data for ROOM TEMPERATURE trials, and BLUE squares represent data for COLD trials. The raw data, most often in the form of Microsoft EXCEL files, are in appendices and labeled as to their content.

A. OPERATING LIMITS ON TEMPERATURE AND PRESSURE OF THE VFPPLL (ALUMINUM MODEL)

1. Frequency vs. Pressure

a. Results

The effect of temperature on the frequency of the VFPPLL instrument, and therefore the measured elongation, was analyzed for temperatures in the broad ranges HOT, COLD and ROOM TEMPERATURE. A comprehensive graph relating frequency to pressure, of the nine individual trials performed, three each in the three temperature ranges, is shown as Figure 4.1. Tables 4.1, 4.2 and 4.3 represent the values for the correlation coefficients of the data for the relationship between frequency and pressure and the slope of the line representing the relationship of frequency to pressure for each temperature range, for the HOT, ROOM TEMP and COLD trials respectively. Each table lists the average value of the three individual trials, which is used in the final analysis. Figure 4.2 represents the processed data; the average values for each temperature range of frequency vs. pressure for the HOT, COLD and ROOM TEMPERATURE trials.

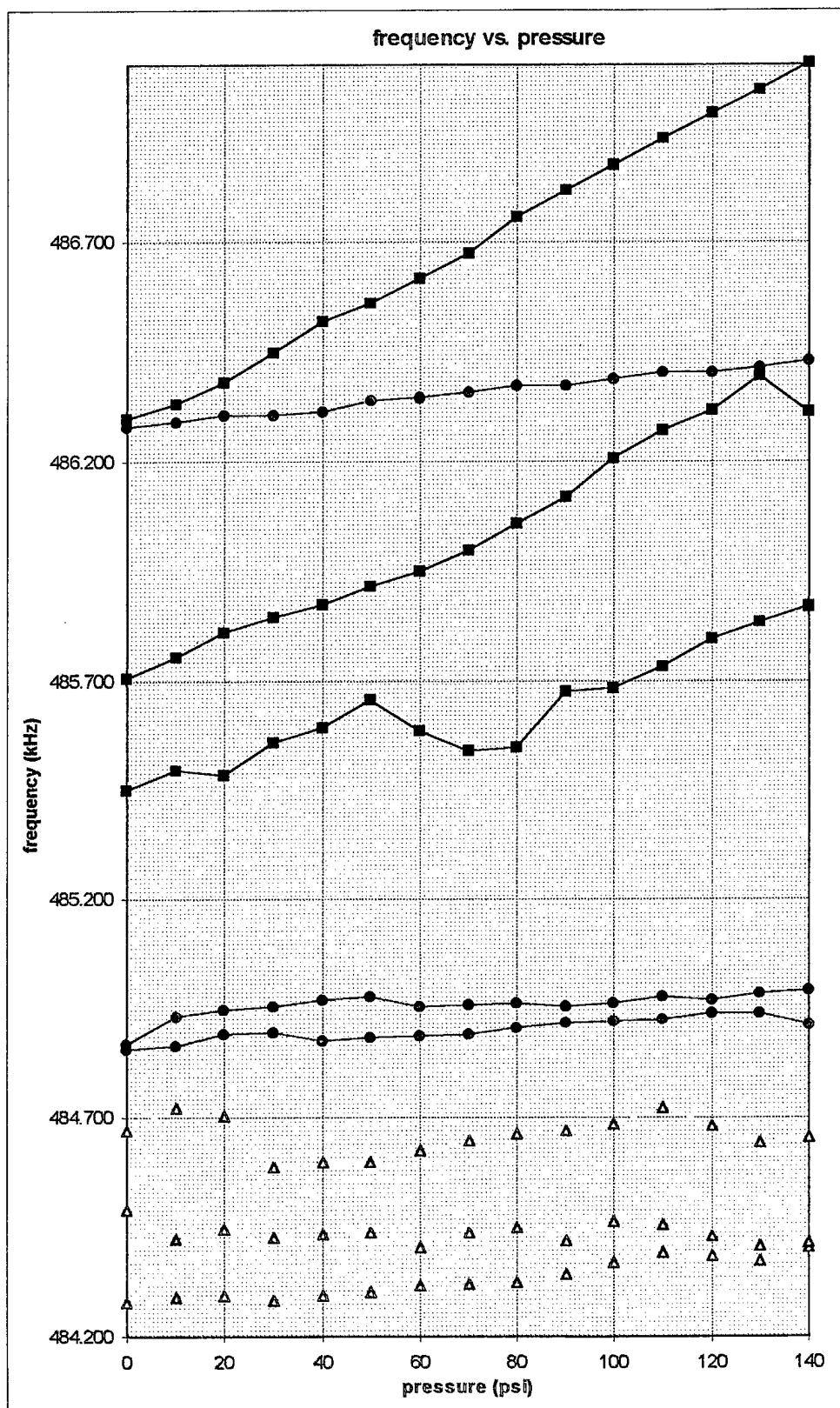


Figure 4.1 Individual HOT, ROOM TEMP and COLD Trials, Frequency vs. Pressure.

<i>Frequency vs. Pressure</i>	Correlation Coefficient	Slope
HOT (1)	0.99372	0.00108
HOT (2)	0.90629	0.00052
HOT (3)	0.73628	0.00047
<i>average * used</i>	<i>0.89369</i>	<i>0.00050</i>

Table 4.1 Correlation Coefficients and Slopes for HOT Temperature Trials.

<i>Frequency vs. Pressure</i>	Correlation Coefficient	Slope
ROOM TEMP (1)	-0.43110	-0.00027
ROOM TEMP (2)	0.96064	0.00101
ROOM TEMP (3)	0.10603	0.00010
<i>average * used</i>	<i>0.96594</i>	<i>0.00106</i>

Table 4.2 Correlation Coefficients and Slopes for ROOM TEMP Trials.

<i>Frequency vs. Pressure</i>	Correlation Coefficient	Slope
COLD (1)	0.91881	0.00268
COLD (2)	0.98808	0.00493
COLD (3)	0.99914	0.00594
<i>average * used</i>	<i>0.96356</i>	<i>0.00451</i>

Table 4.3 Correlation Coefficients and Slopes for COLD Temperature Trials.

* see discussion for actual averaging analysis

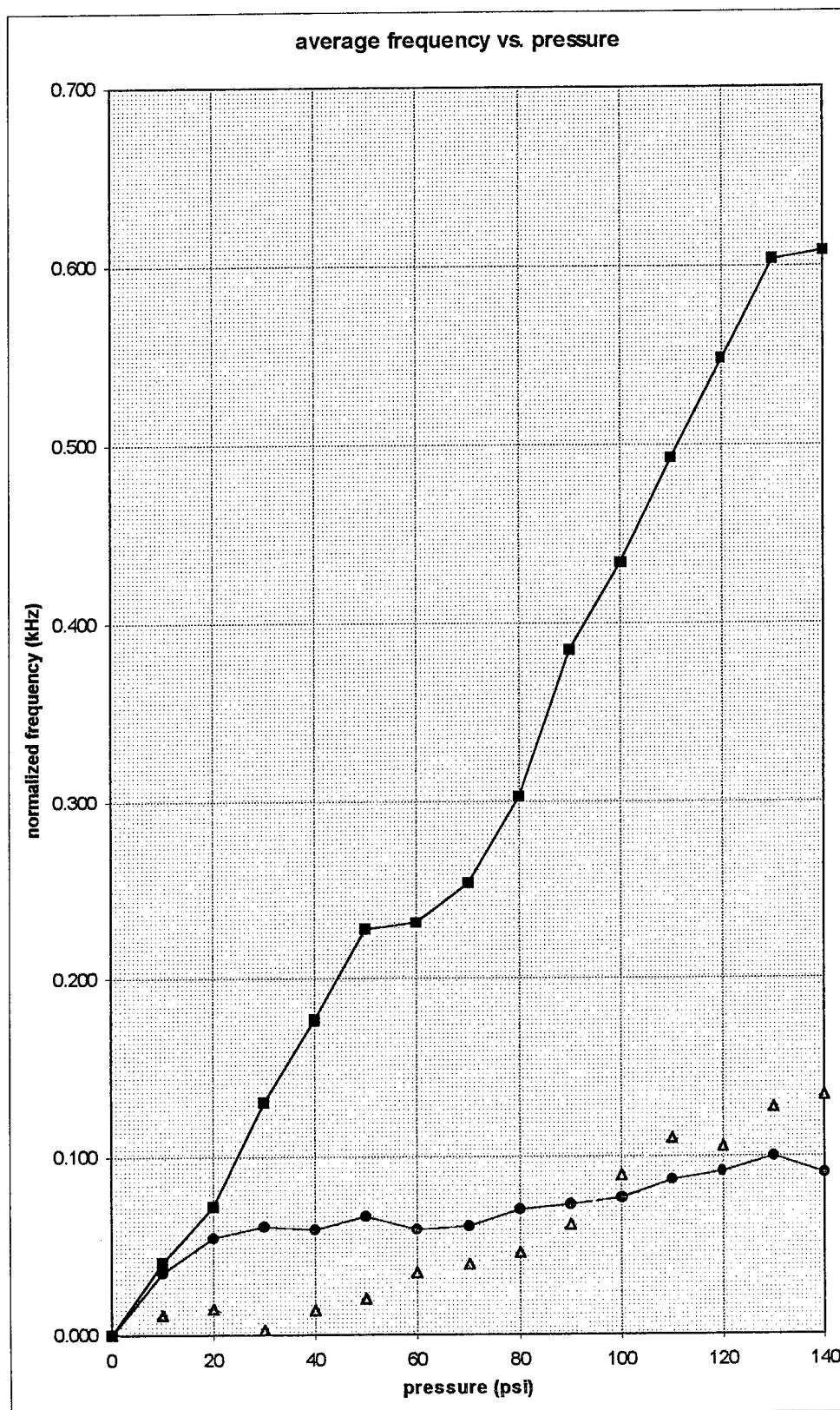


Figure 4.2 Average HOT, ROOM TEMP and COLD Trials; Frequency vs. Pressure.

b. Discussion

The average slope of the line relating frequency to pressure for the HOT, ROOM TEMP and COLD trials were compared for analysis of temperature effects on the operation of the VFPPLL. For all of the temperature trials, the range of pressure over which the VFPPLL was tested was kept constant (0-140 psi). From Tables 4.1, 4.2 and 4.3 the average slope of the line for each temperature range indicates there is a larger slope, and therefore a greater effect on the frequency of the VFPPLL, over the same pressure range, as temperature decreases. The cold temperature range has the greatest effect on the frequency, the room temperature range has the next greatest effect, and the hot temperature range has the least effect on the frequency of the VFPPLL instrument as the pressure is increased.

Not all the data was included in the averaging analysis. In the hot trials, the first trial was not used due to incorrect usage of the VFPPLL instrument; the wave peak locked onto was not the correct wave peak and that trial was discarded. In that trial, the peak that was used to lock the instrument initially did not correspond to the reflection off the back surface (steel endcap). The data is included to show trend, but is not of sufficient quality to warrant inclusion in the more detailed analysis. In the room temperature trials, the first trial was not considered, and only the values of frequency for pressures between 30 and 110 psi were considered from the third trial. The first trial produced data that was extremely erratic, most likely due to the sensitivity of the equipment or an equipment malfunction. The third trial had inconsistencies at the beginning and at the end of the run, but the center values were consistent with the ongoing trend and were utilized. In the cold trials, all data had consistent trends and was used.

The numerical data collected in each of the HOT, ROOM TEMP and COLD trials and the individual trial graphs of frequency vs. pressure are presented in Appendix A.

2. Elongation vs. Pressure

a. Results

Along with the analysis of the relationship between frequency and pressure, the relationship between elongation and pressure was also examined, representing an intermediate step to the ultimate analysis of the relationship between frequency and elongation. Figure 4.3 represents the initial graphical data of the nine individual temperature trials relating elongation and pressure. Tables 4.4, 4.5 and 4.6 show the individual trial values for the correlation coefficient between elongation and pressure, and the slope of the line representing that relationship, for the HOT, ROOM TEMP and COLD trials respectively. The average value is listed in each table last, and is the value used in the final analysis. Once processed, the average values for elongation vs. pressure are shown for each temperature range as Figure 4.4.

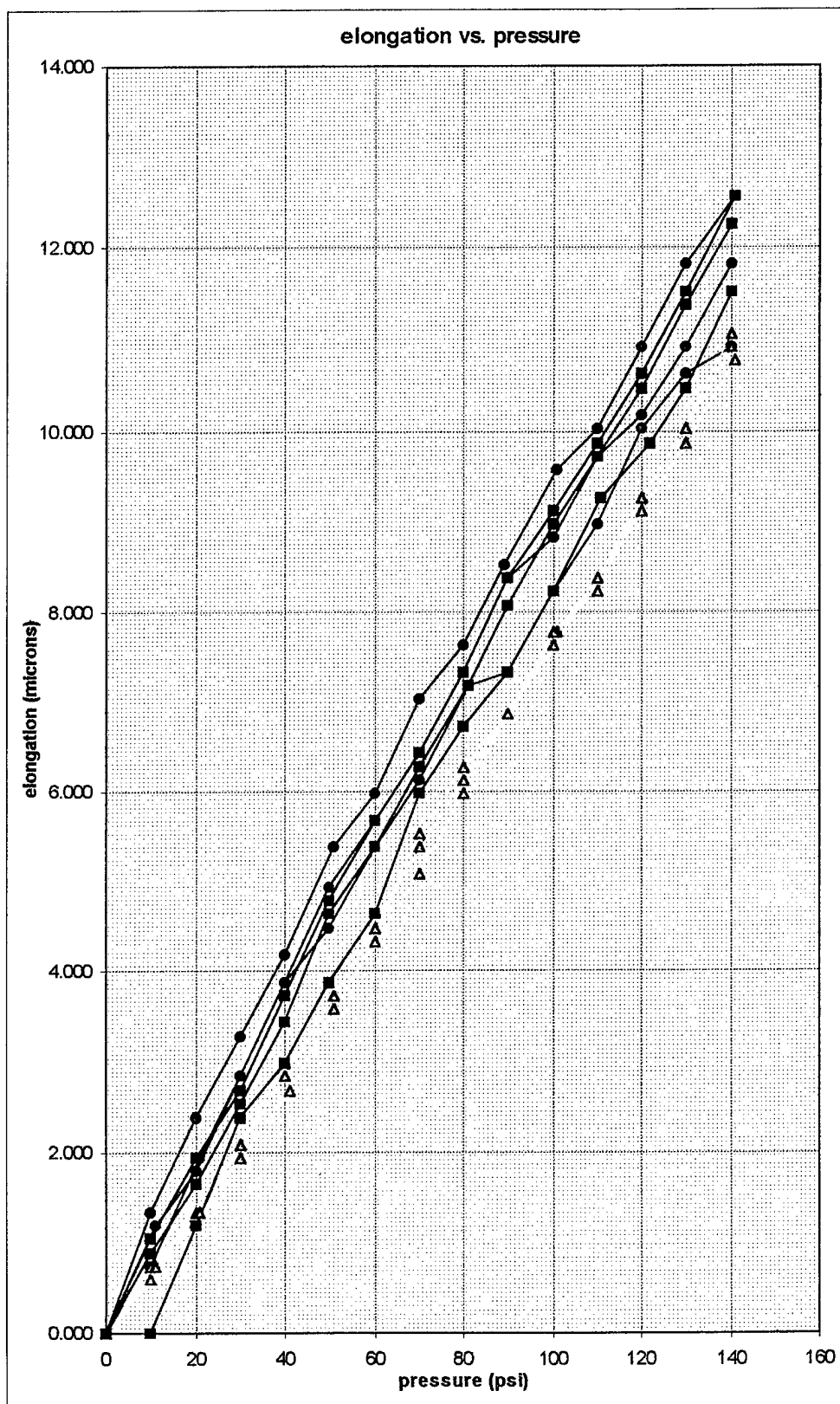


Figure 4.3 Individual HOT, ROOM TEMP and COLD Trials; Elongation vs. Pressure.

<i>Elongation vs. Pressure</i>	Correlation Coefficient	Slope
HOT (1)	0.99790	0.08730
HOT (2)	0.99668	0.07897
HOT (3)	0.99733	0.08351
<i>average * used</i>	<i>0.99779</i>	<i>0.08124</i>

Table 4.4 Correlation Coefficients and Slopes for HOT Temperature Trials.

<i>Elongation vs. Pressure</i>	Correlation Coefficient	Slope
ROOM TEMP (1)	0.99924	0.07795
ROOM TEMP (2)	0.99942	0.07801
ROOM TEMP (3)	0.99962	0.07897
<i>average * used</i>	<i>0.99964</i>	<i>0.07814</i>

Table 4.5 Correlation Coefficients and Slopes for ROOM TEMP Trials.

<i>Elongation vs. Pressure</i>	Correlation Coefficient	Slope
COLD (1)	0.99807	0.08538
COLD (2)	0.99942	0.08853
COLD (3)	0.99957	0.08816
<i>average * used</i>	<i>0.99956</i>	<i>0.08736</i>

Table 4.6 Correlation Coefficients and Slopes for COLD Temperature Trials.

* see discussion for actual averaging analysis

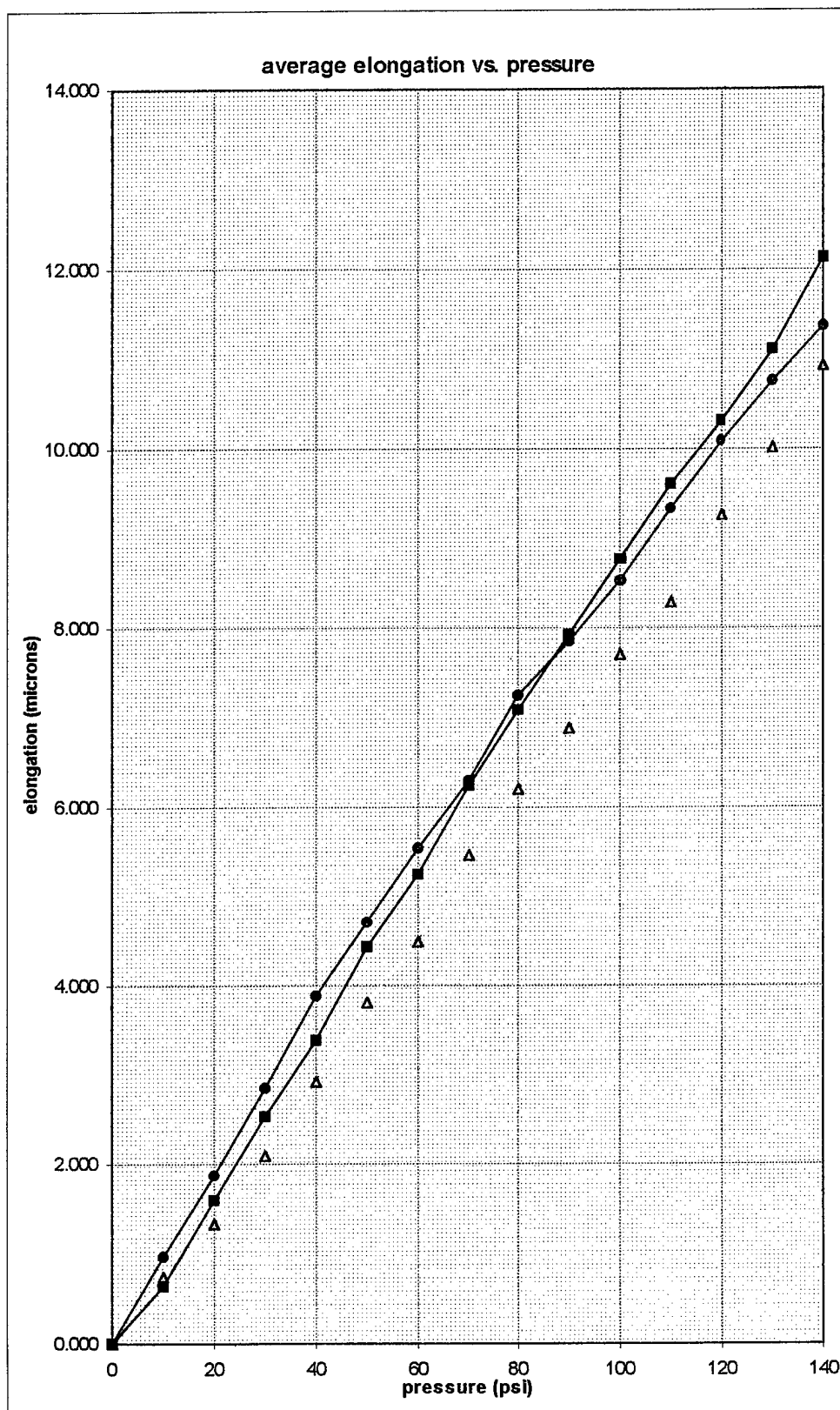


Figure 4.4 Average HOT, ROOM TEMP and COLD Trials; Elongation vs. Pressure.

b. Discussion

The average slope of the line relating elongation to pressure for the HOT, ROOM TEMP and COLD trials provides no conclusive evidence that temperature affects elongation when the range of pressure is kept constant. The results of analyzing elongation in relation to pressure are independent of the operation of the VFPPLL, but were considered as an intermediate step to analyzing the relationship of frequency to elongation.

The same portions of trials were used in this analysis as in the frequency vs. pressure analysis in part one of this chapter, i.e., the first of the hot trials was not used, the first of the room temperature trials was not used, only the values of elongation for pressures between 30 and 110 psi were used from the third room temperature trial and all data from the cold trials was used.

The numerical data collected in each of the HOT, ROOM TEMP and COLD trials and the individual trial graphs of elongation vs. pressure are included in Appendix A.

3. Frequency vs. Elongation

a. Results

The effect of temperature on the frequency of the VFPPLL when measuring elongation, and ultimately the relationship between frequency and elongation for three broad temperature ranges was analyzed. Individual values of the correlation coefficients and slopes of the lines relating frequency to elongation are shown in Tables 4.7, 4.8 and 4.9. Average values for each temperature range that are used in the final analysis are listed last in the tables. A collective graph of the nine individual trials, three trials each in the temperature ranges of HOT, ROOM TEMP and COLD, is presented as Figure 4.5.

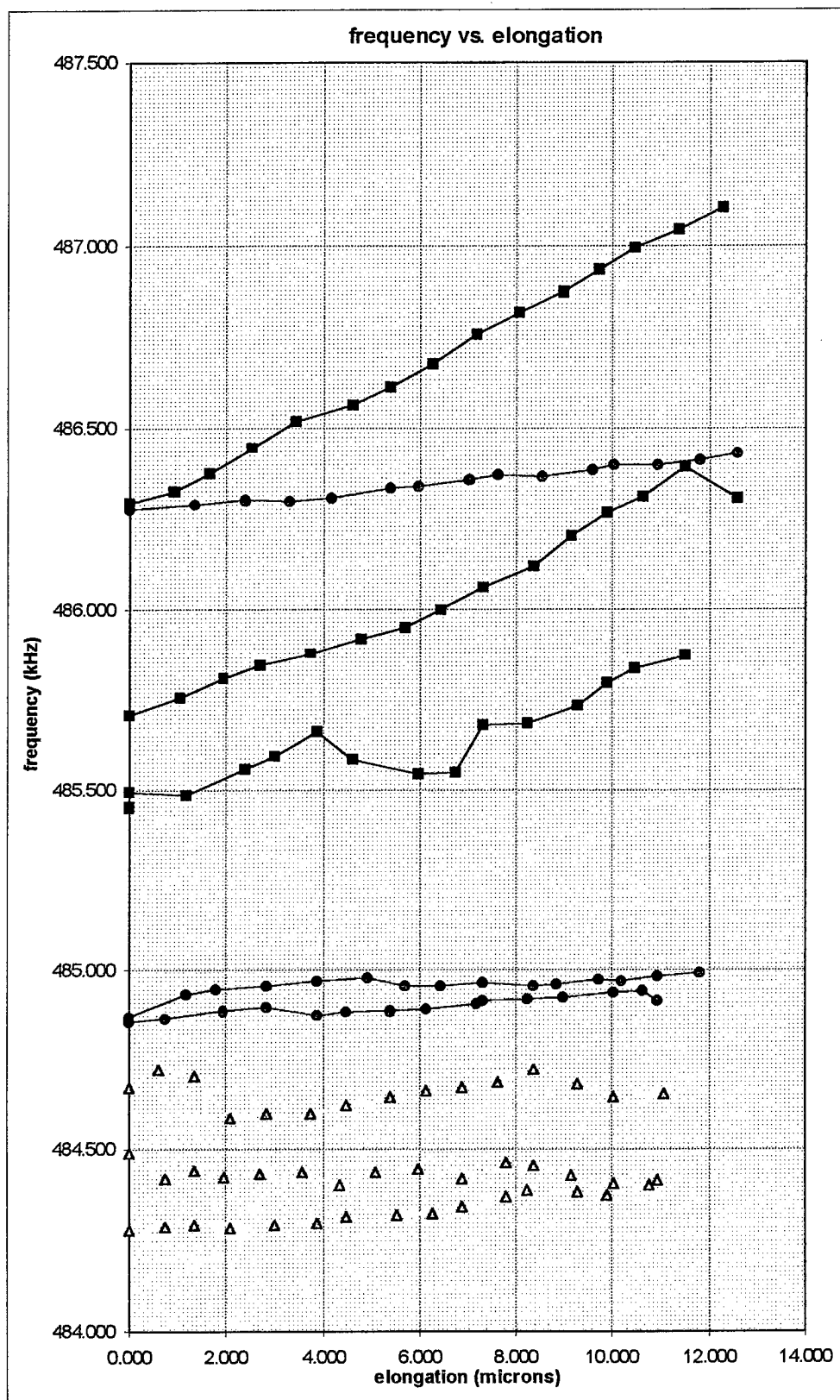


Figure 4.5 Individual HOT, ROOM TEMP and COLD Trials; Frequency vs. Elongation.

Figure 4.6 shows the processed data, the average values of the frequency and elongation for each of the three temperature categories, HOT, ROOM TEMP, and COLD.

<i>Frequency vs. Elongation</i>	Correlation Coefficient	Slope
HOT (1)	0.99271	0.01229
HOT (2)	0.91011	0.00655
HOT (3)	0.75364	0.00578
<i>average * used</i>	<i>0.90474</i>	<i>0.00616</i>

Table 4.7 Correlation Coefficients and Slopes for HOT Temperature Trials.

<i>Frequency vs. Elongation</i>	Correlation Coefficient	Slope
ROOM TEMP (1)	-0.41625	-0.00328
ROOM TEMP (2)	0.95818	0.01297
ROOM TEMP (3)	0.10902	0.00131
<i>average * used</i>	<i>0.95818</i>	<i>0.01297</i>

Table 4.8 Correlation Coefficients and Slopes for ROOM TEMP Trials.

<i>Frequency vs. Elongation</i>	Correlation Coefficient	Slope
COLD (1)	0.90512	0.03081
COLD (2)	0.98445	0.05541
COLD (3)	0.99875	0.06827
<i>average * used</i>	<i>0.99106</i>	<i>0.05150</i>

Table 4.9 Correlation Coefficients and Slopes for COLD Temperature Trials.

* see discussion for actual averaging analysis

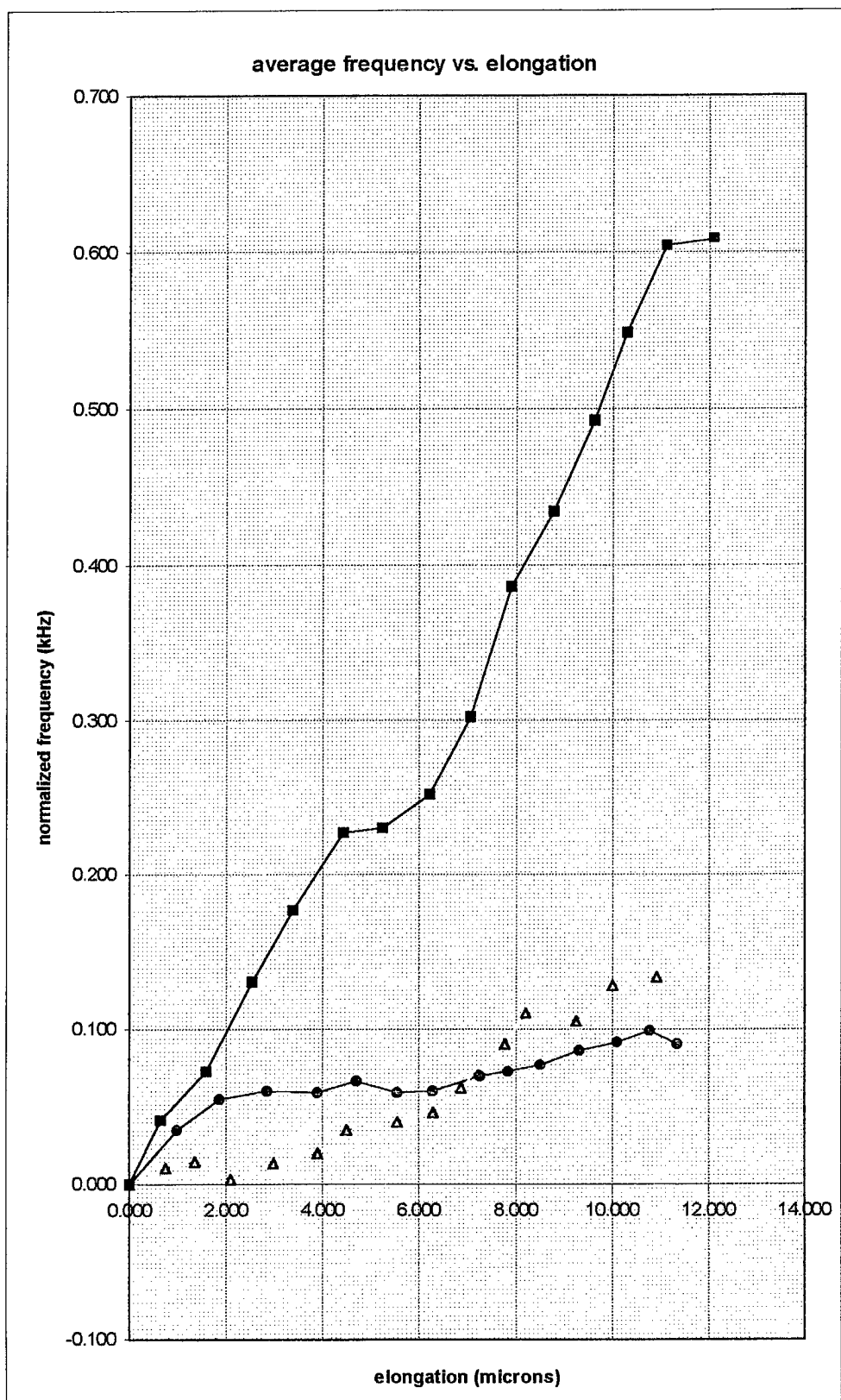


Figure 4.6 Average HOT, ROOM TEMP and COLD Trials; Frequency vs. Elongation.

b. Discussion

The average slope of the line for all three temperature ranges HOT, ROOM TEMP and COLD, relating frequency to elongation, were compared to determine whether or not temperature and pressure affected the operation of the VFPPLL by affecting the frequency values. For all the temperature ranges and trials, the range of pressure over which the VFPPLL instrument was tested was 0 - 140 psi. From Tables 4.6, 4.7 and 4.8 it is shown that the effect temperature has on the relationship of frequency to elongation is the same as the effect temperature has on the relationship of frequency to pressure. The average slope of the line relating frequency to elongation increases with decreasing temperature when the pressure range over which the testing occurs is held constant. In other words, cold temperatures have the greatest effect on frequency, room temperatures have the next greatest effect, and hot temperatures have the least effect on the frequency of the VFPPLL over a range of pressure increase.

The averaging analysis did not include all the data. In the hot trial data, the first trial data was excluded again, as the wave peak locked onto was not the correct wave peak. Of the room temperature trials, the first trial data was again excluded due to equipment sensitivity problems and this time the center portion of elongation data related to pressures between 30 and 110 psi, was not used. Averaging was not possible combining the second trial and the 30 to 110 psi pressure range of elongation data for the third trial due to using normalized frequencies. All cold trial data was successfully used in the averaging analysis.

The numerical data collected in each of the HOT, ROOM TEMP and COLD trials and the individual trial graphs of frequency vs. elongation are included in Appendix A.

B. CALIBRATION

1. PVC Model

a. Results

The concept behind the PVC model was to create a model made of a material that will behave more like the human skull when expanded. Therefore this model is more suited to the purpose of calibration of the VFPPLL instrument. The pressure increase within a human skull to effect elongation is extremely small compared to the pressure needed to effect elongation in the aluminum model. The PVC model needs much less pressure to effect elongation and ultimately the elongation term in the frequency equation becomes more significant than the pressure term. The PVC model has similar frequency to pressure and frequency to elongation relationships as the human skull, and for that reason is a better bench test model than the aluminum model. The proposed frequency equation is restated here for clarity and convenience of the reader as Equation (2.3)

$$\Delta f (\Delta x, T, p) = c_1(T) \cdot \Delta p + c_2(T) \cdot \Delta x$$

Figures 4.7 and 4.8 demonstrate the relationship between frequency and elongation and are two representative elongation trials of the PVC model with small amounts of pressure, i.e., less than 25 psi. As the figures show, frequency is directly proportional to elongation; when elongation increases, frequency decreases, and positively correlates to the same relationship within the human skull. Appendix B contains the graphs of all nine trials of the PVC model testing, as well as the data collected.

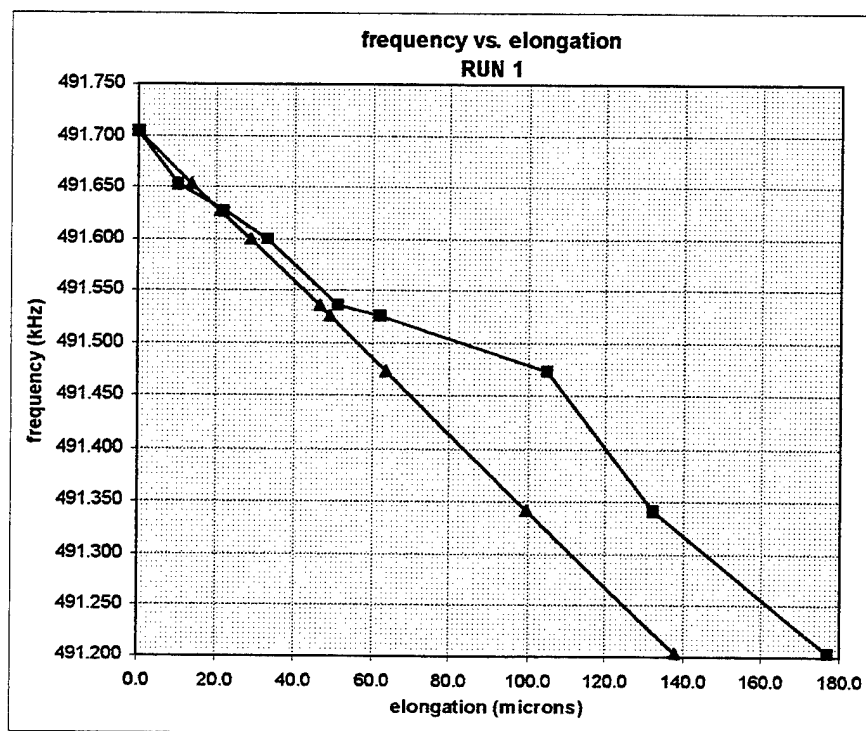


Figure 4.7 PVC Model Run 1; Frequency vs. Elongation.

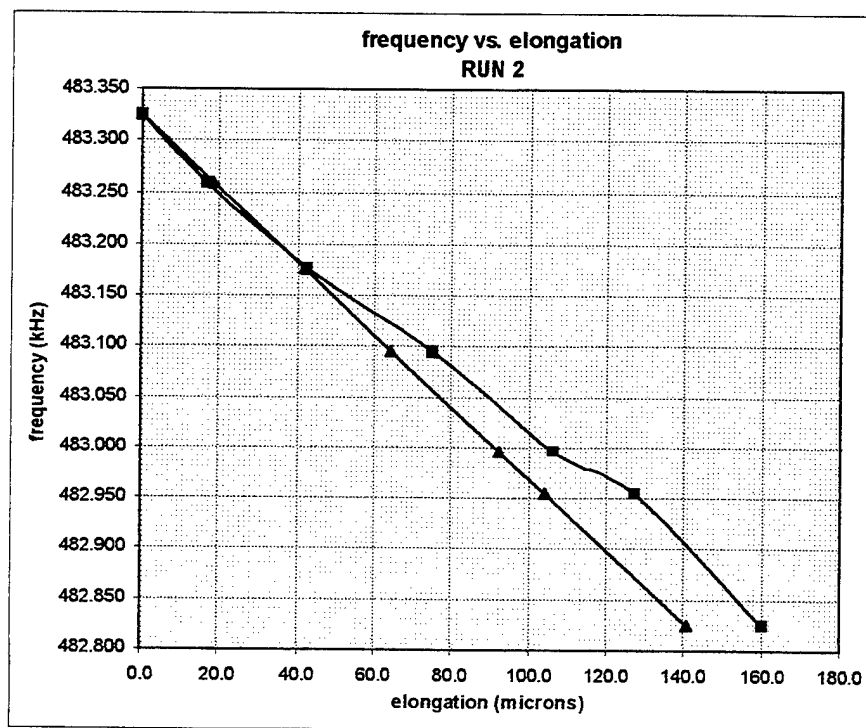


Figure 4.8 PVC Model Run 2; Frequency vs. Elongation.

b. Discussion

The purpose behind development and testing of the PVC model is to establish the same relationship, or trend, between frequency and pressure as that seen in the human skull. In the human skull, the frequency measurements are used to calculate elongation using the frequency equation, and this elongation is compared to the elongation calculated from the strain gage readings from the PVC model. With this accomplished, the elongation to pressure trend in the PVC model can be compared to the same trend in the human skull and a multiplicative factor assigned to mathematically relate the two. In the preliminary testing done for this thesis, no definitive pressure measurements could be made from the PVC model, and therefore no comparison between frequency and pressure, and consequently elongation and pressure, could be made.

2. Open Channel Model

a. Results

The purpose of the open channel model is to compare physical measurements with measurements derived from the frequency observations of the VFPPLL. Both the PVC model and the Open Channel model are for the purpose of calibration of the VFPPLL, but the Open Channel model allows for physical elongation to be compared to elongation calculated from frequency observations vice elongation effected by an increase in pressure as in the PVC model. The results of the Open Channel model are favorable, i.e., they compare well to approximate elongations effected by the operator, but there is a large degree of human "eye-balling" of physical distance which can account for large amounts of error. Figures 4.9 and 4.10 are graphical representations of the results of the comparison of physical elongation

to the elongation calculated from the frequency observations of the VFPPLL. A total of 16 trials were completed with the Open Channel model, and all the trial graphs are listed in Appendix C. Along with the graphs in Appendix C is the numerical data collected from each of the 16 trials.

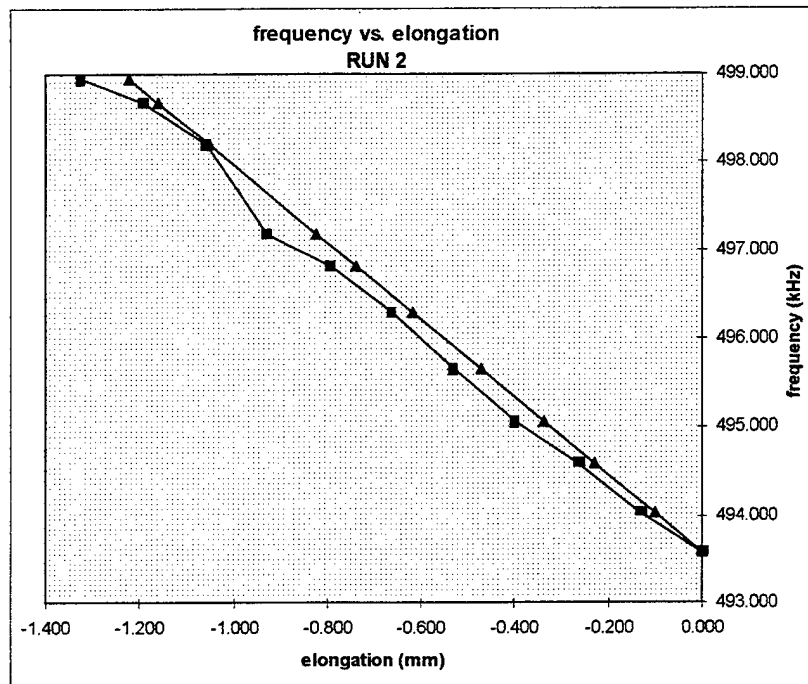


Figure 4.9 Open Channel Model Run 2; Frequency vs. Elongation.

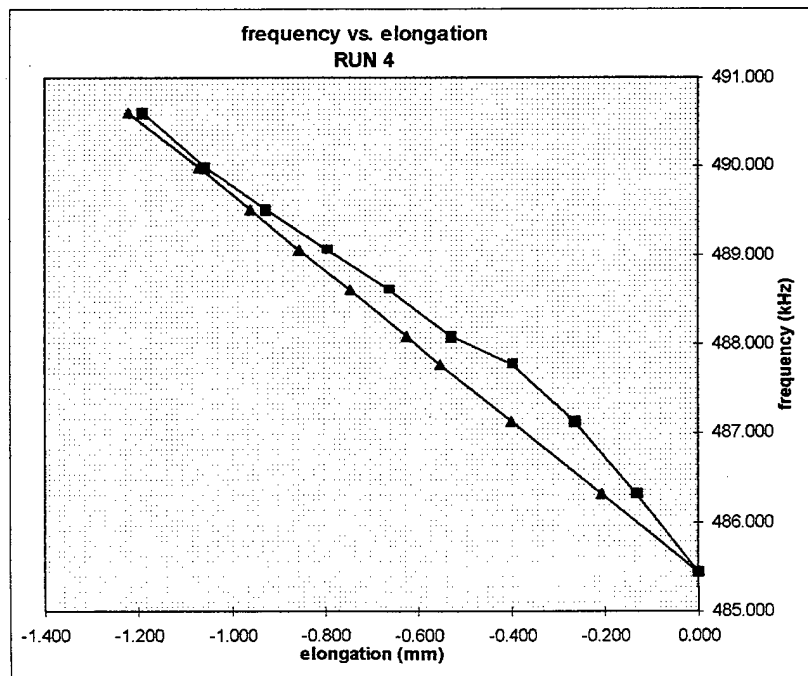


Figure 4.10 Open Channel Model Run 4; Frequency vs. Elongation.

b. Discussion

The testing of the Open Channel model, as in the testing of the PVC model, could be improved. The pressure data in the PVC model testing was not available to get a relationship between frequency and pressure, so only frequency and elongation data could be used to establish a trend between the two values. As in the PVC model, use of the Open Channel model is limited in that the values of physical elongation are approximate. When the physical values are compared to the elongation calculated from the frequency observations of the VFPPLL, only a trend can be established. No precise determination of the comparison between physical and calculated elongation from frequency measurements of the VFPPLL instrument can be made with this model.

V. CORRELATION TO THE HUMAN SKULL

A. CADAVER STUDIES

1. Background

Invasive methods of measuring and monitoring intracranial pressure are dangerous to a live human subject. Cadavers are therefore utilized as a replacement subject for study of intracranial pressure and intracranial distance measurements. The VFPPLL collects frequency data, elongation is calculated from the frequency data, and from these intracranial distance measurements, intracranial pressure can be inferred based on the results of these cadaver studies. Of note, these cadaver studies are not yet complete, so a definitive relationship between intracranial pressure and effected intracranial elongation is not yet available. This study has been ongoing for the last several years and will be continuing for several years to come.

2. Discussion

Since this thesis was done in conjunction with the NASA Ames Research Center, Space Physiology Laboratory, and two cadaver studies had already been completed prior to this thesis, cadaver data was readily available. One additional cadaver was available and studied during the timespan of this thesis and is included as part of the data collection for this thesis. Results from all three cadavers will be represented, but only Cadaver C was studied by the author.

A relationship between intracranial pressure and intracranial distance (elongation) is desired so that when frequency measurements are taken on a live human subject and

elongation is calculated from these frequency measurements, intracranial pressure can be accurately inferred. Figure 5.1 is the reduced and processed data collected on Cadaver A and Cadaver B, provided for instructional purposes only by the Space Physiology Laboratory at NASA Ames Research Center [Ref. 2]. Figure 5.2 is the reduced and processed data collected on Cadaver C [Ref. 2]. Actual data collected included frequency observations and intracranial pressure measurements effected by infusing saline solution into a burr hole in the lateral ventricle of a human cadaver, at a rate of 50 samples/second. Data reduction was done on the raw accumulated data to get a reasonable number of data points for graphing purposes. Following the numerical data are Figures 5.3, 5.4 and 5.5, the graphical representations of the processed data in Figures 5.1 and 5.2, and demonstrate the linear relationship between intracranial distance and intracranial pressure for Cadaver A, Cadaver B, and Cadaver C, respectively. The raw data graph, before data reduction, of frequency and intracranial pressure plotted over time for Cadaver B is also shown as Figure 5.6 [Ref. 2].

Cadaver A		Cadaver B	
ICP (mmHg)	ICD (mm)	ICP (mmHg)	ICD (mm)
10	0	1	0
22	0.017	30	
28	0.06	0	
40	0.109	12	0.0561
30	0.07	22	0.0719
21	0.04	31	0.07876
12	0.01	42	0.0946

Figure 5.1 Numerically Reduced Data on Cadaver A and Cadaver B.

Cadaver C			
run 1		run 2	
ICD (mm)	ICP (mmHg)	ICD (mm)	ICP (mmHg)
4.9	0	5.15	0
15.01	0.058	17.25	0.038
25.27	0.213	26.21	0.174
34.65	0.324	36.59	0.369
44.26	0.405	45.76	0.424
35.04	0.396	34.34	0.38
23.66	0.296	23.46	0.274
12.95	0.162	12.63	0.088
4.95	0.029	3.04	-0.167

Figure 5.2 Numerically Reduced Data on Cadaver C.

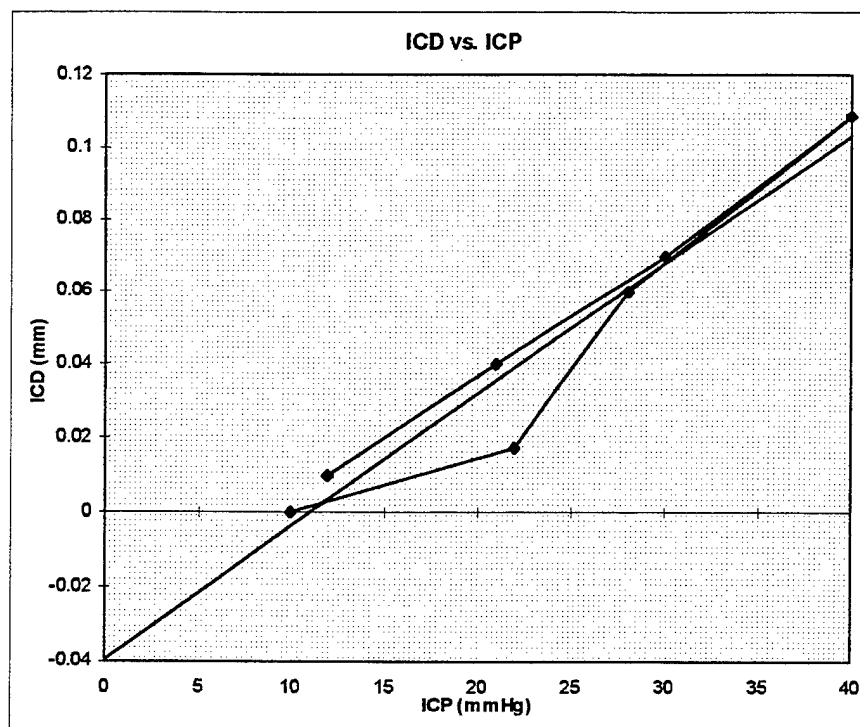


Figure 5.3 Cadaver A; ICD vs. ICP.

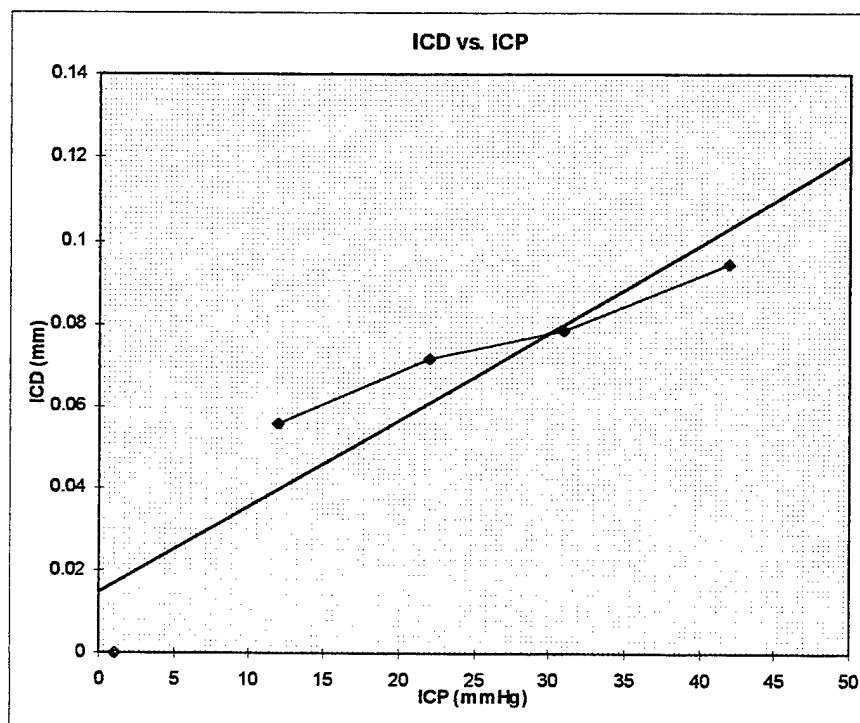


Figure 5.4 Cadaver B; ICD vs. ICP.

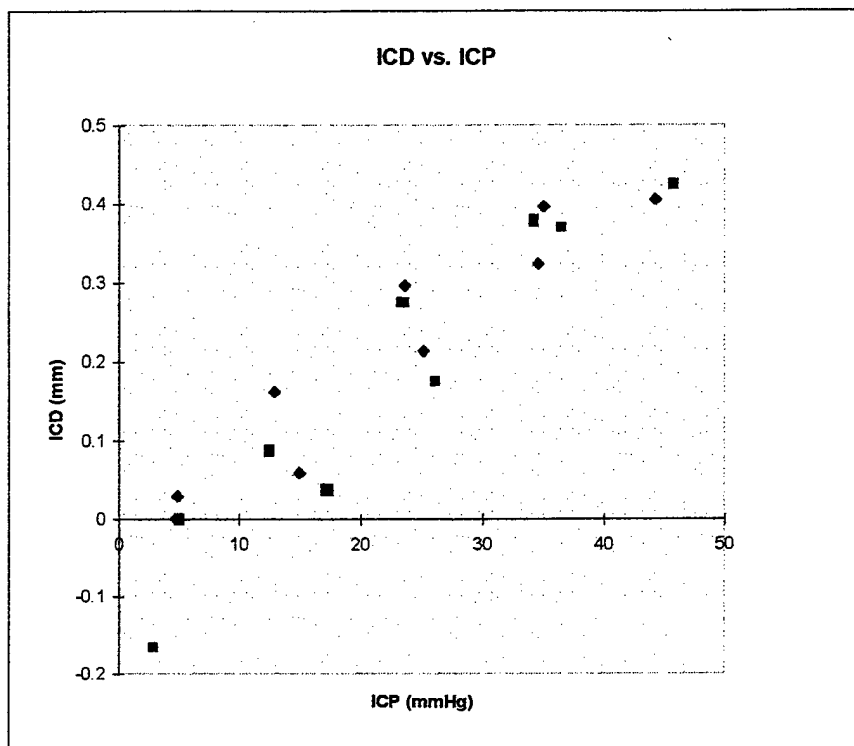


Figure 5.5 Cadaver C; ICD vs. ICP.

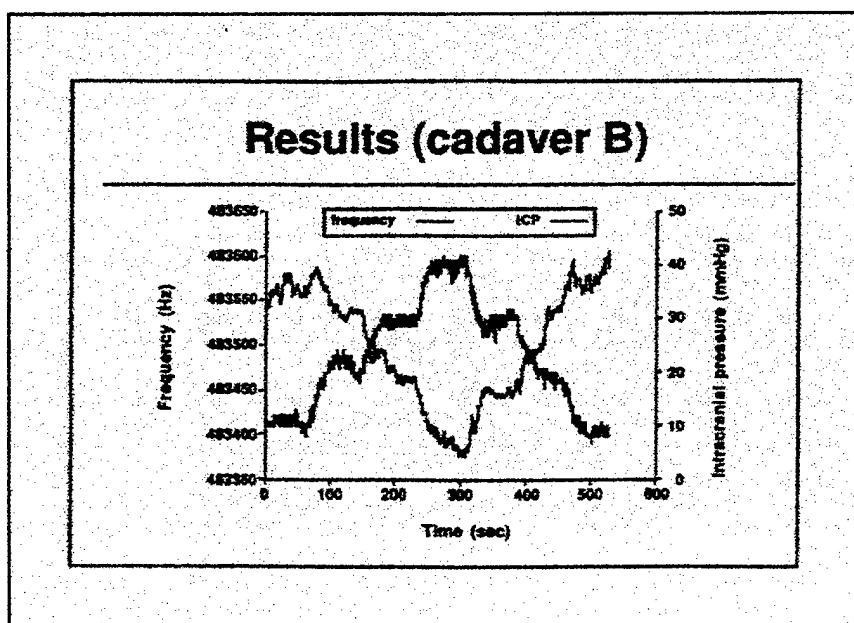


Figure 5.6 Pre-processed Cadaver B Data; Frequency vs. Time and ICP vs. Time [Ref. 2].

The linear relationship between intracranial distance and intracranial pressure for the three cadavers is shown by the slope of the line relating the two parameters. Table 5.1 gives the equation of the line (including slope and y-intercept) and the correlation coefficient between them.

	equation of the line	correlation coefficient
<i>Cadaver A</i>	$y = 0.004 x - 0.039$	0.966
<i>Cadaver B</i>	$y = 0.002 x + 0.015$	0.928
<i>Cadaver C</i>	$y = 0.012 x - 0.076$	0.938

Table 5.1 Equations Representing the Linear Relationship Between ICD and ICP and Corresponding Correlation Coefficients.

For the equations in Table 5.1,

y = intracranial distance calculations (ICD)

x = intracranial pressure measurements (ICP).

These three cadavers represent only initial studies and more data is required to make a deterministic evaluation of the relationship between ICD and ICP. Once a definitive baseline is developed of the relationship between ICD and ICP, future comparisons to frequency, and ultimately elongation and therefore pressure of the VFPPLL instrument can be evaluated.

VI. FURTHER DISCUSSION AND CONCLUSIONS

A. THEORY

Relating back to the purpose of this thesis, to develop a bench test model that will calibrate the PPLL and establish broad operating limits on the parameters temperature, pressure, and elongation over which the PPLL can accurately operate, the data collected is condensed and all conclusions are discussed within this chapter. The proposed frequency equation, Equation (2.3), is restated here for convenience of the reader.

$$\Delta f (\Delta x, T, p) = c_1(T) \cdot \Delta p + c_2(T) \cdot \Delta x$$

Figure 6.1 is a simple drawing of an example of "elongation", or Δx . The container, whether an open channel type or a thin-walled pressure vessel type as in the PVC model, contains water and is the medium through which the ultrasound toneburst travels. It is of original length x_0 , and final length x_0 plus some finite value of Δx ; i.e.,

$$x_f = x_0 + \Delta x \quad (6.1)$$

where

x_f = final length

x_0 = initial length

Δx = effective change in length, which is comparatively calculated from observed frequencies on the VFPPLL instrument digital readout.

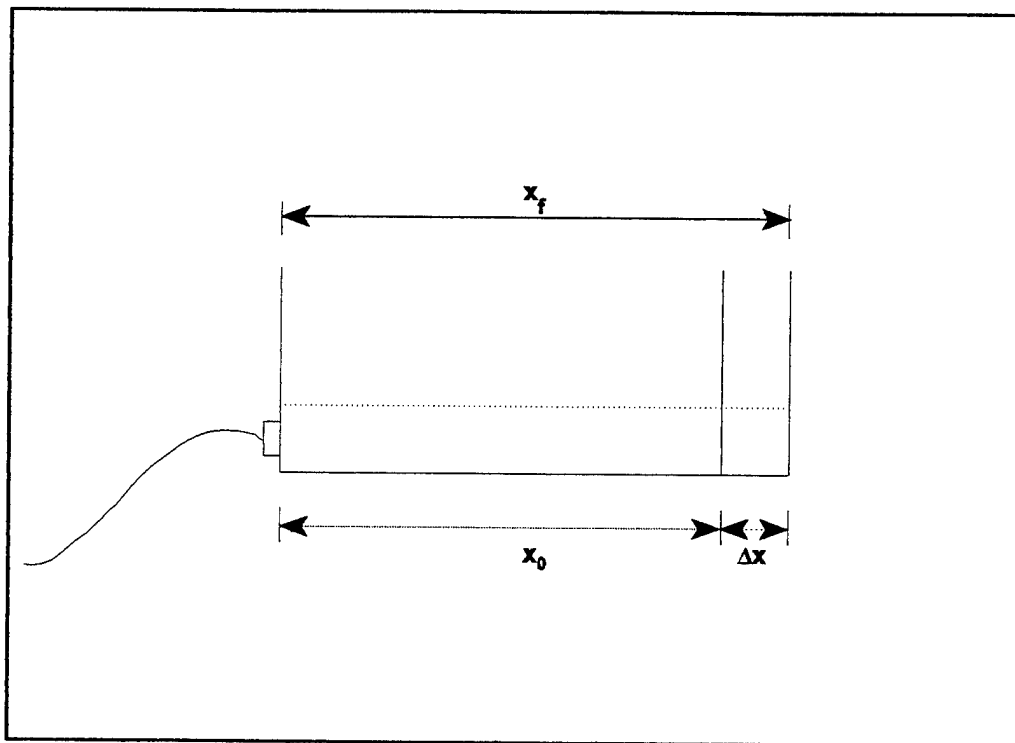


Figure 6.1 Example of Elongation.

The PPLL instruments calculate this elongation using the parameters observed as output from either the constant frequency or the variable frequency version of this instrument.

For a constant speed of sound in water, as Δx increases, Δf should decrease; i.e., it takes longer for the sound wave to traverse a greater distance and since frequency is the inverse of time, frequency should decrease. However, in the case of the aluminum model, the opposite is occurring: as Δx increased, frequency increased as well. This is explained with basic physics. The pressure on the water in the aluminum pressure vessel is being continually increased, which increases the density of the water. The speed of sound increases when the density of the medium increases [Refs. 19 and 20], and even though Δx is increasing, the traversal takes less time, so frequency increases. This pressure effect changes when temperature differences are also involved, which complicates things. The density of the

medium is affected by temperature as well as pressure. As the temperature increases the density decreases, therefore the speed of sound decreases and the effects of temperature and pressure on density and the speed of sound in water have opposing effects on each other.

Of the two terms in the proposed expanded frequency equation, both terms are a function of temperature, i.e., pressure is affected by temperature in the first term and elongation is affected by temperature in the second term. The results of the testing of the three bench test models provide the following conclusions.

In the aluminum model, temperature affects frequency observations of the VFPPLL instrument. Under conditions of increasing pressure, the first term involving pressure dominates the frequency change and the second term involving elongation, is considered negligible in comparison. Results of the HOT, ROOM TEMP and COLD trials show that as elongation increases, frequency increases; the inverse relationship of what occurs in the human skull, which indicates dominance of the pressure term over the elongation term. When the elongation term is considered negligible, the proposed frequency equation is reduced to

$$\Delta f (\Delta x, T, p) = c_1(T) \cdot \Delta p \quad (6.2)$$

where the constant c_1 is simply the slope of the line relating frequency and pressure, and is given as

$$c_1 = \frac{\Delta f}{\Delta p} \quad (6.3)$$

The values of c_1 clearly indicate that temperature affects the frequency observations of the VFPPLL. COLD temperatures have the greatest effect, ROOM temperatures have the next greatest effect and HOT temperatures have the least effect on frequency observations of the VFPPLL. Figure 6.2 reflects the relative effect of the broad temperature ranges on frequency readings observed; average values of the slopes of the frequency vs. pressure lines from Tables 4.1, 4.2 and 4.3 (c_1 values) which are graphed against temperature.

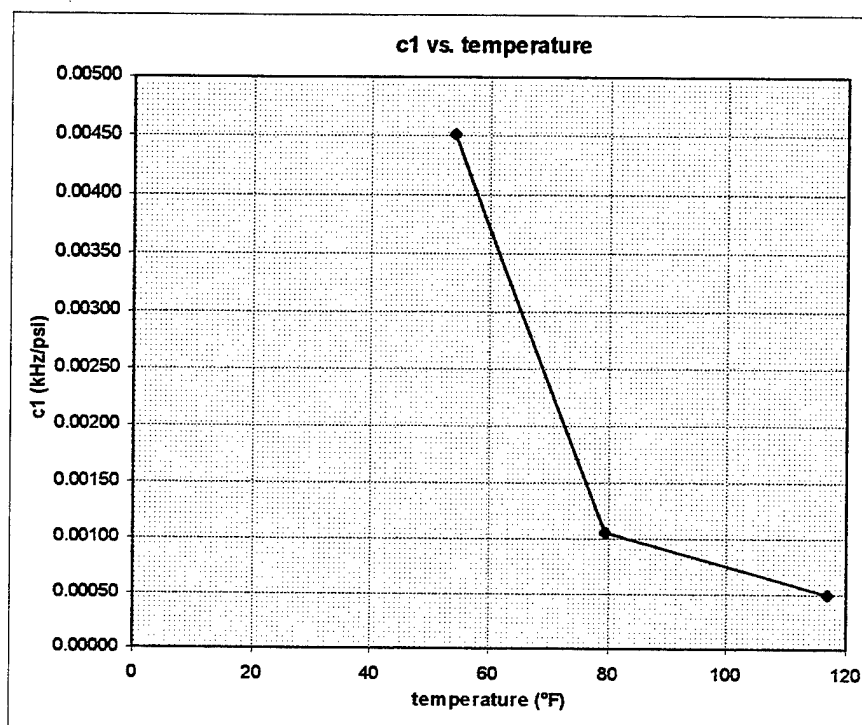


Figure 6.2 C_1 vs. Temperature.

The temperature trials also indicate, in the graphs of elongation vs. pressure, that the elongation term in the proposed frequency equation is not a function of temperature over the range of temperatures investigated. The slopes of the lines relating pressure and elongation are relatively equal in magnitude, indicating no dependence on temperature in the ranges investigated. Figure 6.3 reflects this conclusion, where average values of the slopes of the

of the lines relating elongation to pressure are from Tables 4.4, 4.5 and 4.6. This reduces the proposed frequency equation to

$$\Delta f (\Delta x, T, p) = c_1(T) \cdot \Delta p + c_2 \cdot \Delta x \quad (6.4)$$

which becomes the frequency equation relevant to the Aluminum model.

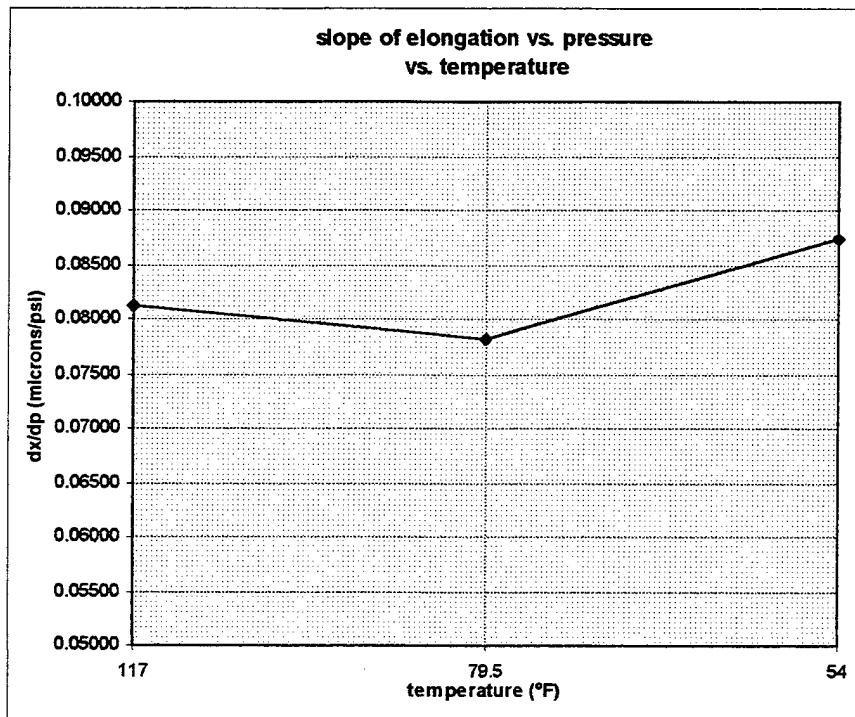


Figure 6.3 Slope of Elongation vs. Pressure, vs. Temperature.

Since the frequency of the VFPLL is affected by more parameters than just elongation, i.e., temperature and pressure, thought must be given to the environmental conditions where it will be in use. When the instrument is used in a military combat field setting or in conjunction with the U.S. Space Shuttle Program, environmental conditions such as temperature will most likely be within the limits the instrument is capable of tolerating.

Normal body temperature of about 100°F is most comparable with the HOT temperature trials, which least affected the frequency of the PPLL, so operation of the instrument in this temperature range minimizes temperature effects. It should be noted however, that fluctuating temperature will affect frequency observations, and the instrument should be used in the same operating regime as it is calibrated in, i.e., if operating in the normal body temperature range (~100°F), the bench test model should calibrate the instrument with water in the same temperature range (see Figure 6.2 for relative effects of the broad temperature ranges on the frequency of the VFPPLL). Pressure limits will not be exceeded when the pressures are comparable to those observed inside the skull of a living human subject, which are *much* less than 20 psi (1 psi = 51.71 mmHg), which the instrument is capable of tolerating.

In the PVC model, the effects of pressure and elongation on frequency are of the same relationships as those seen in a human subject; i.e., as pressure increases, frequency decreases, as pressure increases, elongation increases, and as elongation increases, frequency decreases. The elongation term of the proposed expanded frequency equation dominates over the pressure term, having a much greater effect on the frequency of the VFPPLL. This is demonstrated by the relationship of frequency to elongation; as elongation increases, frequency decreases as expected and with the same relationship when compared to the human skull. The proposed frequency equation, Equation (2.3), is restated here for reader convenience as

$$\Delta f (\Delta x, T, p) = c_1(T) \cdot \Delta p + c_2(T) \cdot \Delta x$$

where c_2 is given as (from Equation 2.2)

$$c_2 = - \frac{f_0}{x_0} \quad (6.5)$$

To attempt to consider the pressure term negligible in the frequency equation used for the PVC model, and further reduce the proposed frequency equation down to its original form (Equation 2.2), a comparison between $\Delta f / \Delta x$ and the constant c_2 was made. The value of $\Delta f / \Delta x$, compared to the c_2 constant calculated, indicate that although the elongation term is the dominating term of the two terms in the proposed frequency equation, the pressure term still has some effect on frequency and cannot be considered negligible. The frequency equation relevant to the PVC model is therefore given as Equation (2.3). Table 6.1 shows the relative magnitudes of the average $\Delta f / \Delta x$ for each trial compared to the calculated constant c_2 , and the percent difference between the two values. All PVC model trial data is listed in Appendix B, including values of $\Delta f / \Delta x$ for each consecutive data point in each individual trial, and the values of the c_2 constants for each trial.

	<i>ave $\Delta f / \Delta x$</i>	<i>c_2</i>	<i>% difference</i>
Run 1	-0.00141	-0.00181	22.10
Run 2	-0.00156	-0.00178	12.36
Run 3	-0.00156	-0.00179	12.85
Run 4	0.00023	-0.00179	112.85
Run 5	-0.00550	-0.00180	205.56
Run 6	-0.00141	-0.00180	21.67
Run 7	-0.00182	-0.00180	1.11
Run 8	-0.00147	-0.00175	16.00
Run 9	-0.00156	-0.00176	11.36
<i>average</i>	-0.00178	-0.00179	46.21

Table 6.1 Values of C_2 and $\Delta f / \Delta x$ for the PVC Model.

In conclusion, it is established there is a need for a compliant material model that will be capable of elongations in the sub-micron range, and measurements derived from the PPLL instruments must have an accurate, comparable external source for comparison, i.e., an extensometer or strain gage on the PVC Model. The pressure introduced into the bench test model must also be accurately recorded. A manometer, which accurately measures pressures with a range of approximately 0-100 mmHg (equivalently 0-1.93 psi) will work well with the small pressure changes needed to elongate compliant materials.

In the open channel model, the actual "bench test" model for purposes of this thesis, the proposed expanded frequency equation includes only the elongation term, as pressure is not a factor in the elongation of the model. The frequency equation relevant to the open channel model is therefore simply given as

$$\Delta f(p, T, \Delta x) = c_2(T) \cdot \Delta x \quad (6.6)$$

where c_2 is again given as Equation (6.5)

$$c_2 = - \frac{f_0}{x_0}$$

There is good correlation of the comparison between c_2 and the slope of the line relating frequency and elongation. The average value of c_2 is -4.37, the average value of the slope of the line relating frequency and elongation is -3.47, and the average percent difference between the two values is 20.89%. The numerical values for c_2 and the slope of the frequency vs. elongation line for each trial are included in the Open Channel model data found in Appendix C. Even though the PPLL instruments measure typical elongations in the sub-micron range, there is strong evidence that elongations in the millimeter range are reasonably measured.

Specifications have been established for creating a calibration bench test model of the human skull for testing either PPLL instrument. The bench test model must have accurately measurable elongation in the sub-micron range and be externally measurable with the use of strain gages or an extensometer. If elongation is to be effected by the introduction of pressure, that pressure should be in the 0-20 psi range (low pressure range) and be accurately recorded, i.e., by a manometer, for comparison with cadaver intracranial pressure (ICP) readings. The temperature range of the bench test model should be limited, i.e., if the

operation of the PPLL instrument will be in a range near 100°F, the bench test model should be calibrated in this limited temperature range.

The Variable Frequency Pulse Phase-Locked instrument is affected by all of the parameters: temperature, pressure and elongation. It behaves as expected on all three bench test models tested for this thesis: the Aluminum model, the PVC model and the Open Channel model. The results of testing show observed frequency changes in accordance with the proposed frequency equation, i.e., the frequency changes as expected due to temperature and pressure effects, due to elongation, and due to a combination of both effects simultaneously, within specified operating limits of temperature and pressure ranges as described within the body of this thesis. A new frequency equation has been established indicating temperature and pressure dependence, as well as elongation dependence, and values for the constants c_1 and c_2 have also been established based on the type of bench test model employed.

B. FUTURE STUDIES

The PVC model resembles the typical human skull, in the relationships discussed above, however further study will be needed to quantify the pressure needed to expand the model. Further study into other materials will enable another type of easily expandable material to be used for a bench test model, as the concept of elongation due to pressure (as in the human skull) is ideal for direct mathematical comparisons to the VFPPLL's relationship of intracranial pressure to intracranial distance.

Cadaver studies will be continuing through the Space Physiology Laboratory at NASA Ames Research Center, which will expand the database relating ICD to ICP. When

the relationship is refined with more data, a reasonable mathematical relationship can be developed. The VFPPLL frequency observations can then be translated into elongations (intracranial distances), and accurately related to increased intracranial pressures.

Further study into the physical parts of the open channel model is needed to accurately compare its elongation to calculations from the frequency observations of the VFPPLL instrument. The instrument's sensitivity for measurement is on the order of approximately 0.1 μm , therefore much more sophisticated equipment will be needed to construct an open channel bench test model with a level of comparable sensitivity.

APPENDIX A. ALUMINUM MODEL

A. NUMERICAL DATA

All data collected on the Aluminum Model during the testing phase of this thesis is included in this appendix. Figures A.1, A.2 and A.3 represent the data for the 9 individual temperature trials, 3 each for the HOT, ROOM TEMP and COLD trials, respectively. Figures A.4, A.5 and A.6 represent the data for the average values (see discussion on the actual averaging analysis in the Aluminum Model section of Chapter IV, for which data points were used in the average values) of the HOT, ROOM TEMP and COLD trials collectively. Figure A.4 is the frequency vs. pressure average analysis, Figure A.5 is the elongation vs. pressure averaging analysis and Figure A.6 is the frequency vs. elongation averaging analysis.

B. GRAPHS

The graphs presented in this appendix represent all graphed data points collected for all temperature trials on the Aluminum Model. All individual temperature trial graphs utilize the same coloring scheme to represent data series; i.e., the dark blue series represents frequency observations from the VFPPLL instrument vs. pressure, the magenta series represents the calculated elongations from the strain gage readings vs. pressure, and the red series represents the VFPPLL frequency vs. strain gage calculated elongations. For each temperature trial, the relationships between frequency and pressure, elongation and pressure, and frequency and elongation are shown. Table A.1 is an easy reference showing which graph is in which figure.

<i>Figure Number</i>	<i>Graph</i>
Figure A.7	HOT (1) Frequency and Axial Elongation vs. Pressure
Figure A.8	HOT (2) Frequency and Axial Elongation vs. Pressure
Figure A.9	HOT (3) Frequency and Axial Elongation vs. Pressure
Figure A.10	HOT (1) Frequency vs. Elongation
Figure A.11	HOT (2) Frequency vs. Elongation
Figure A.12	HOT (3) Frequency vs. Elongation
Figure A.13	ROOM TEMP (1) Frequency and Axial Elongation vs. Pressure
Figure A.14	ROOM TEMP (2) Frequency and Axial Elongation vs. Pressure
Figure A.15	ROOM TEMP (3) Frequency and Axial Elongation vs. Pressure
Figure A.16	ROOM TEMP (1) Frequency vs. Elongation
Figure A.17	ROOM TEMP (2) Frequency vs. Elongation
Figure A.18	ROOM TEMP (3) Frequency vs. Elongation
Figure A.19	COLD (1) Frequency and Axial Elongation vs. Pressure
Figure A.20	COLD (2) Frequency and Axial Elongation vs. Pressure
Figure A.21	COLD (3) Frequency and Axial Elongation vs. Pressure
Figure A.22	COLD (1) Frequency vs. Elongation
Figure A.23	COLD (2) Frequency vs. Elongation
Figure A.24	COLD (3) Frequency vs. Elongation

Table A.1 Figure Number and Representative Graph.

ROOM TEMP (1)	pressure	frequency	strain gage reading			elongation	
	(psi)	(kHz)	axial (norm)	axial	hoop	measured (μm)	theoretical (μm)
temp = 79 F	0	484.490	0	624	-3	0.000	0.000
measured before	10	484.421	5	629	21	0.748	0.610
	20	484.444	9	633	47	1.346	1.221
time = 1548	30	484.426	13	637	74	1.945	1.831
	41	484.432	18	642	102	2.693	2.503
t = 149.2 μs	51	484.436	24	648	131	3.590	3.113
x ₀ = 221.711 mm	60	484.404	29	653	152	4.338	3.663
	70	484.436	34	658	178	5.086	4.273
	80	484.448	40	664	205	5.984	4.884
	90	484.418	46	670	231	6.882	5.494
	101	484.463	52	676	261	7.779	6.166
	110	484.455	56	680	280	8.378	6.715
	120	484.429	61	685	306	9.126	7.326
	130	484.374	66	690	328	9.874	7.936
	141	484.404	72	696	355	10.771	8.608
	CORRELATIONS			SLOPES			
	freq vs. press	elong vs. press	freq vs. elong		freq vs. press	elong vs. press	freq vs. elong
	-0.42991	0.99919	-0.41625		-0.00026	0.07781	-0.00328
ROOM TEMP (2)	pressure	frequency	strain gage reading			elongation	
	(psi)	(kHz)	axial (norm)	axial	hoop	measured (μm)	theoretical (μm)
temp = 79 F ?	0	484.280	0	624	-4	0.000	0.000
not measured...	11	484.291	5	629	22	0.748	0.672
	20	484.295	9	633	45	1.346	1.221
time = 1555	30	484.283	14	638	72	2.094	1.831
	40	484.294	20	644	100	2.992	2.442
t = 149.2 μs	50	484.300	26	650	128	3.890	3.052
x ₀ = 221.711 mm	60	484.315	30	654	154	4.488	3.663
	70	484.320	37	661	180	5.535	4.273
	80	484.326	42	666	205	6.283	4.884
	90	484.342	46	670	229	6.882	5.494
	100	484.370	52	676	257	7.779	6.105
	110	484.390	55	679	274	8.228	6.715
	120	484.385	62	686	303	9.275	7.326
	130	484.408	67	691	330	10.023	7.936
	140	484.414	73	697	357	10.921	8.547
	CORRELATIONS			SLOPES			
	freq vs. press	elong vs. press	freq vs. elong		freq vs. press	elong vs. press	freq vs. elong
	0.96123	0.99943	0.95818		0.00102	0.07817	0.01297
ROOM TEMP (3)	pressure	frequency	strain gage reading			elongation	
	(psi)	(kHz)	axial (norm)	axial	hoop	measured (μm)	theoretical (μm)
temp = 80 F	0	484.672	0	624	-2	0.000	0.000
measured after	10	484.721	4	628	18	0.598	0.610
	21	484.705	9	633	47	1.346	1.282
time = 1610	30	484.586	14	638	73	2.094	1.831
	40	484.599	19	643	98	2.842	2.442
t = 149.2 μs	51	484.600	25	649	129	3.740	3.113
x ₀ = 221.711 mm	60	484.625	30	654	152	4.488	3.663
	70	484.646	36	660	181	5.386	4.273
	80	484.662	41	665	202	6.134	4.884
	90	484.672	46	670	230	6.882	5.494
	100	484.686	51	675	253	7.630	6.105
	110	484.721	56	680	280	8.378	6.715
	120	484.680	62	686	307	9.275	7.326
	130	484.645	67	691	330	10.023	7.936
	140	484.655	74	698	355	11.070	8.547
	CORRELATIONS			SLOPES			
	freq vs. press	elong vs. press	freq vs. elong		freq vs. press	elong vs. press	freq vs. elong
	0.10586	0.99958	0.10902		0.00010	0.07916	0.00131
	30-110 psi range	30-110 psi range	30-110 psi range		30-110 psi range	30-110 psi range	30-110 psi range
	0.98600	0.99965	0.98524		0.00164	0.53007	0.02066

Figure A.2 Numerical Data for ROOM TEMP Trials.

COLD (1)	pressure	frequency	strain gage reading		hoop	elongation	
	(psi)	(kHz)	axial (norm)	axial		measured (μm)	theoretical (μm)
temp = 48 F	0	485.454	0	630	4	0.000	0.000
measured before	10	485.496	0	630	23	0.000	0.610
	20	485.488	8	638	43	1.197	1.221
time = 1635	30	485.560	16	646	76	2.394	1.831
	40	485.594	20	650	101	2.992	2.442
t = 171.2 μs	50	485.661	26	656	127	3.890	3.052
x ₀ = 254.403 mm	60	485.587	31	661	150	4.638	3.663
	70	485.544	40	670	177	5.984	4.273
	80	485.549	45	675	206	6.732	4.884
	90	485.679	49	679	229	7.330	5.494
	100	485.686	55	685	253	8.228	6.105
	111	485.735	62	692	282	9.275	6.776
	122	485.797	66	696	309	9.874	7.448
	130	485.837	70	700	326	10.472	7.936
	140	485.872	77	707	354	11.519	8.547
CORRELATIONS							
freq vs. press	elong vs. press	freq vs. elong	SLOPES				
0.91932	0.99807	0.90512	freq vs. press	elong vs. press	freq vs. elong		
			0.00266	0.08495	0.03081		
COLD (2)	pressure	frequency	strain gage reading		hoop	elongation	
	(psi)	(kHz)	axial (norm)	axial		measured (μm)	theoretical (μm)
temp = 48 F ?	0	485.709	0	625	3	0.000	0.000
not measured...	10	485.758	7	632	29	1.047	0.610
	20	485.812	13	638	48	1.945	1.221
time = 1645	30	485.847	18	643	74	2.693	1.831
	40	485.879	25	650	102	3.740	2.442
t = 171.2 μs	50	485.920	32	657	130	4.787	3.052
x ₀ = 254.403 mm	60	485.952	38	663	156	5.685	3.663
	70	486.002	43	668	180	6.433	4.273
	80	486.062	49	674	205	7.330	4.884
	90	486.123	56	681	235	8.378	5.494
	100	486.207	61	686	256	9.126	6.105
	110	486.271	66	691	279	9.874	6.715
	120	486.319	71	696	301	10.622	7.326
	130	486.396	77	702	331	11.519	7.936
	141	486.314	84	709	359	12.566	8.608
CORRELATIONS							
freq vs. press	elong vs. press	freq vs. elong	SLOPES				
0.98757	0.99940	0.98445	freq vs. press	elong vs. press	freq vs. elong		
			0.00491	0.08831	0.05541		
COLD (3)	pressure	frequency	strain gage reading		hoop	elongation	
	(psi)	(kHz)	axial (norm)	axial		measured (μm)	theoretical (μm)
temp = 60 F	0	486.300	0	626	5	0.000	0.000
measured after	10	486.331	6	632	28	0.898	0.610
	20	486.380	11	637	49	1.646	1.221
time = 1655	30	486.448	17	643	75	2.543	1.831
	40	486.519	23	649	104	3.441	2.442
t = 171.2 μs	50	486.564	31	657	134	4.638	3.052
x ₀ = 254.403 mm	60	486.617	36	662	158	5.386	3.663
	70	486.676	42	668	181	6.283	4.273
	81	486.759	48	674	213	7.181	4.945
	90	486.819	54	680	237	8.078	5.494
	100	486.875	60	686	260	8.976	6.105
	110	486.936	65	691	285	9.724	6.715
	120	486.992	70	696	306	10.472	7.326
	130	487.042	76	702	329	11.370	7.936
	140	487.103	82	708	356	12.267	8.547
CORRELATIONS							
freq vs. press	elong vs. press	freq vs. elong	SLOPES				
0.99918	0.99960	0.99875	freq vs. press	elong vs. press	freq vs. elong		
			0.00593	0.08813	0.06727		

Figure A.3 Numerical Data for COLD Temperature Trials.

[illegible]

Figure A.4 Averaging Analysis for Frequency vs. Pressure Data.

[illegible]

Figure A.6 Averaging Analysis for Frequency vs. Elongation Data.

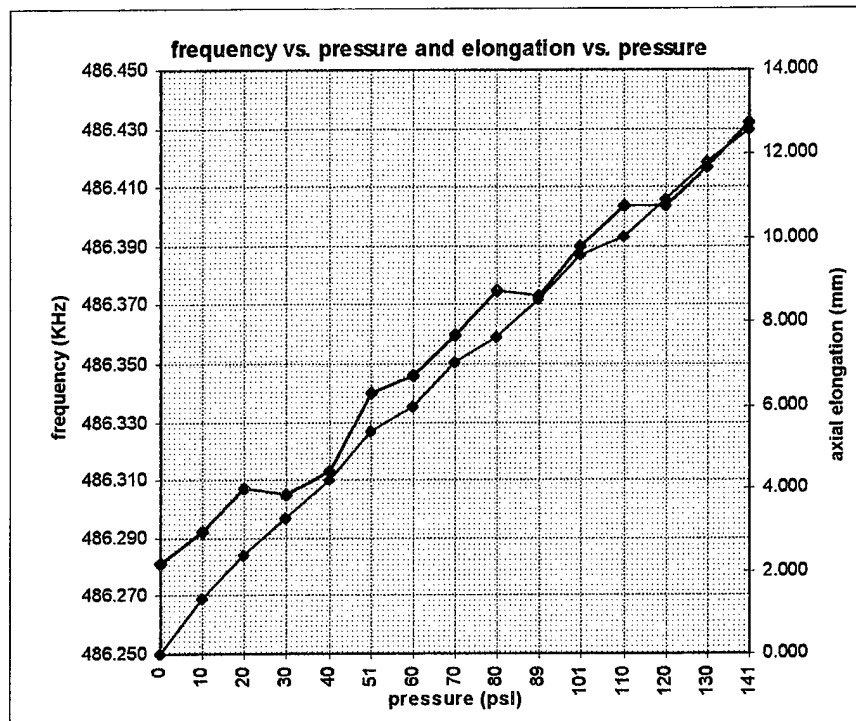


Figure A.7 HOT (1) Frequency and Axial Elongation vs. Pressure.

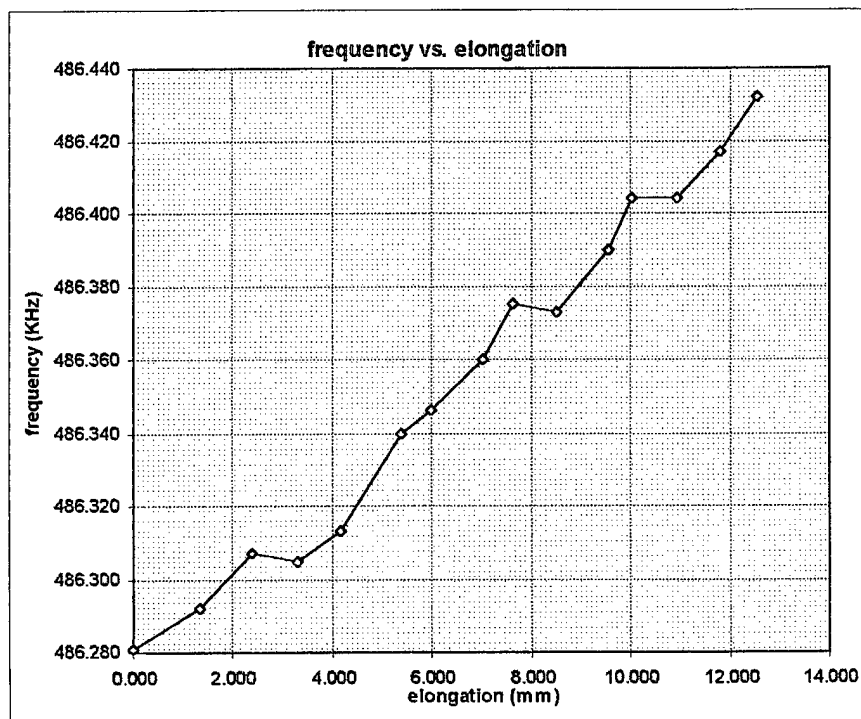


Figure A.8 HOT (1) Frequency vs. Elongation.

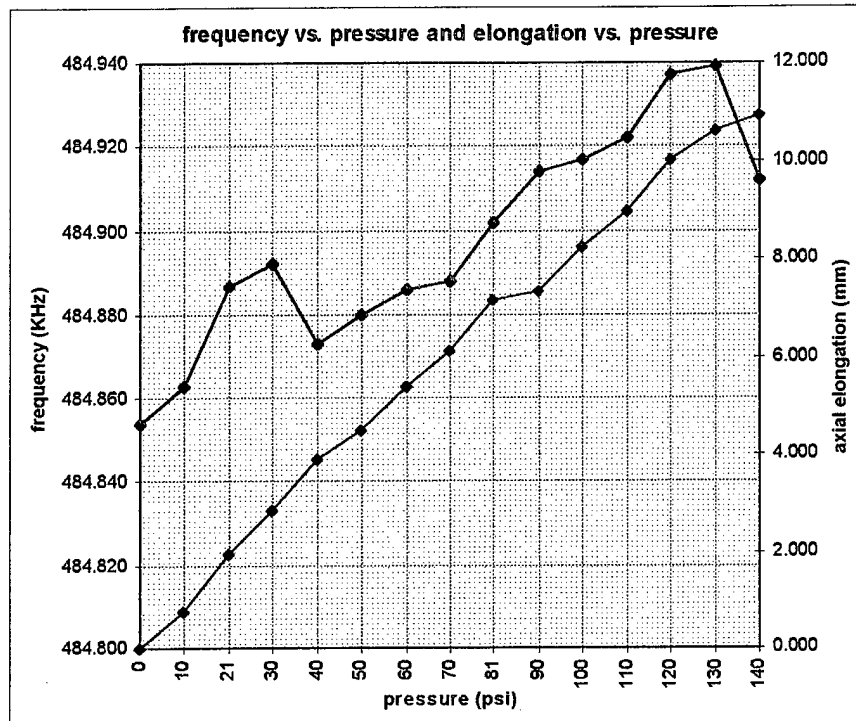


Figure A.9 HOT (2) Frequency and Axial Elongation vs. Pressure.

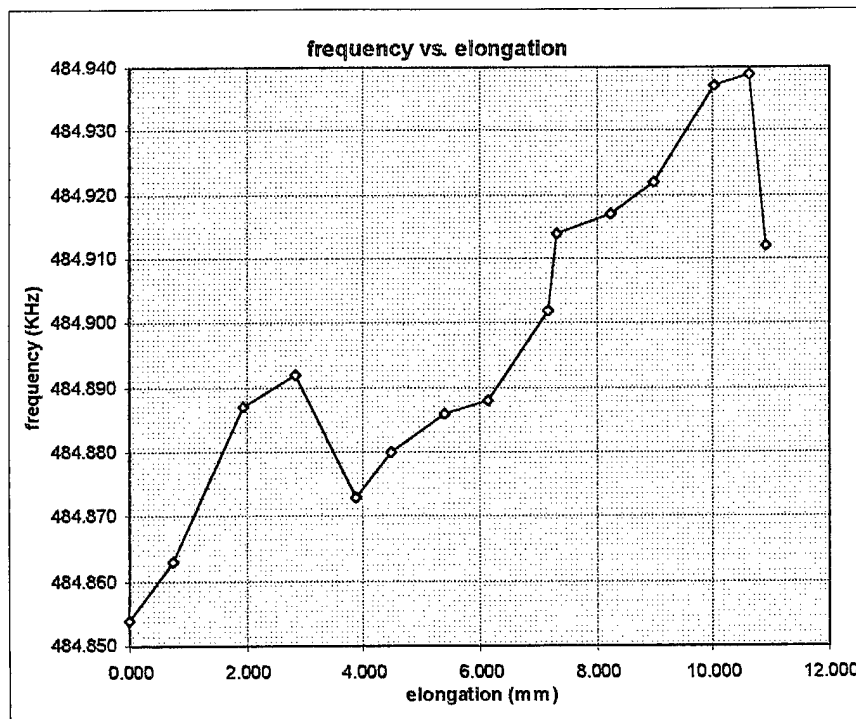


Figure A.10 HOT (2) Frequency vs. Elongation.

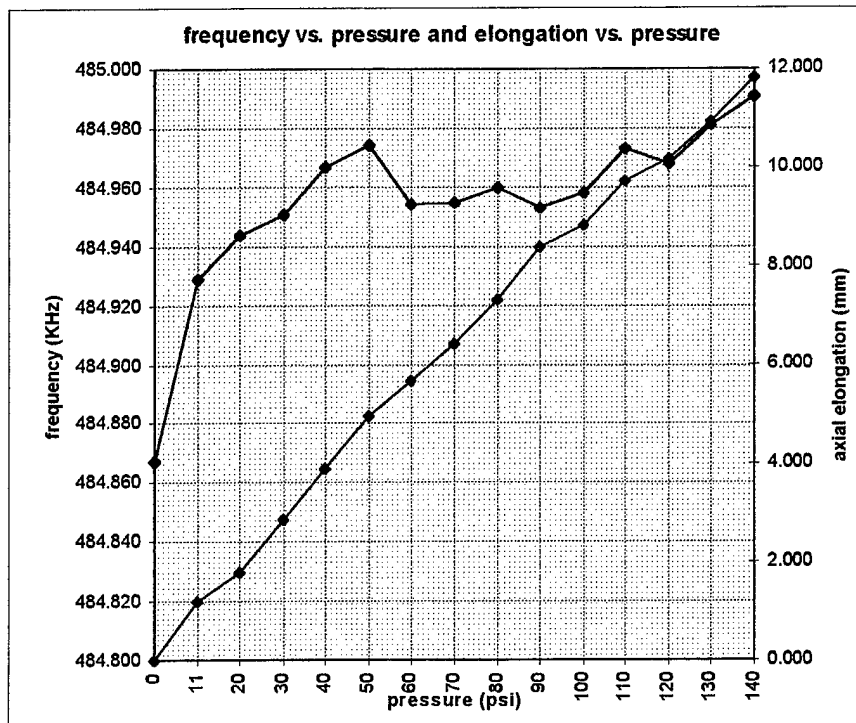


Figure A.11 HOT (3) Frequency and Axial Elongation vs. Pressure.

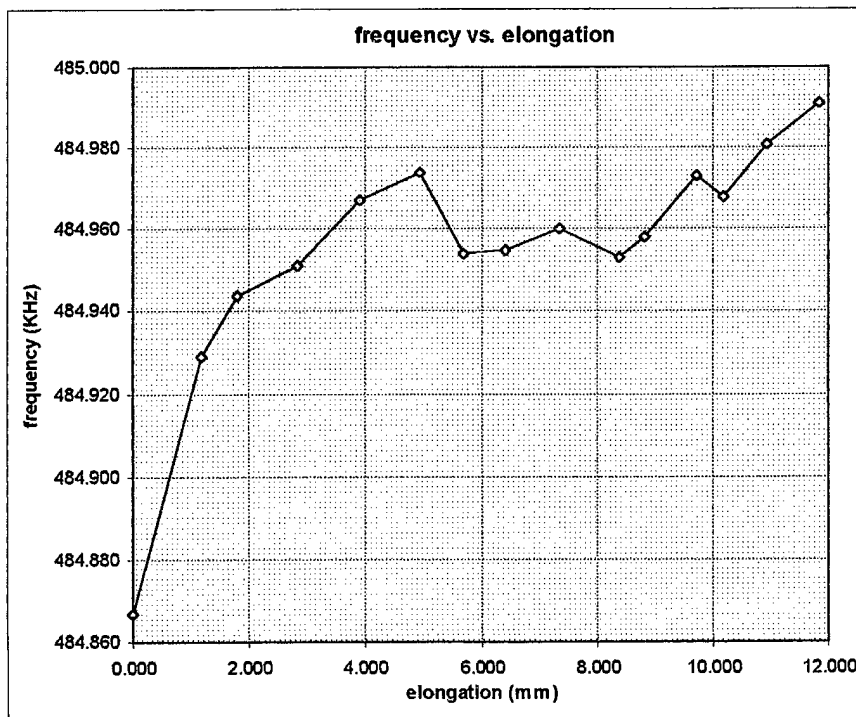


Figure A.12 HOT (3) Frequency vs. Elongation.

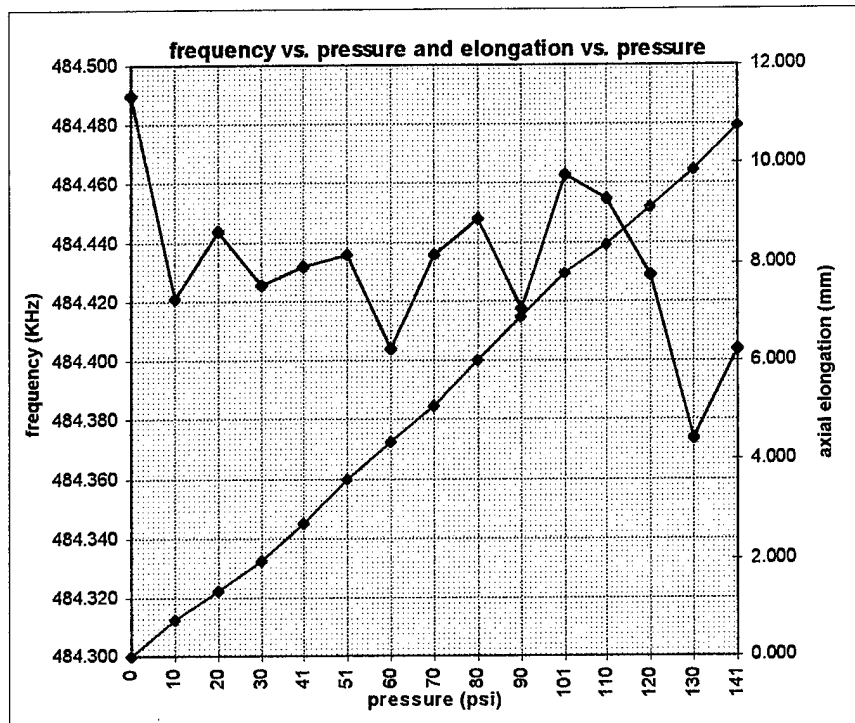


Figure A.13 ROOM TEMP (1) Frequency and Axial Elongation vs. Pressure.

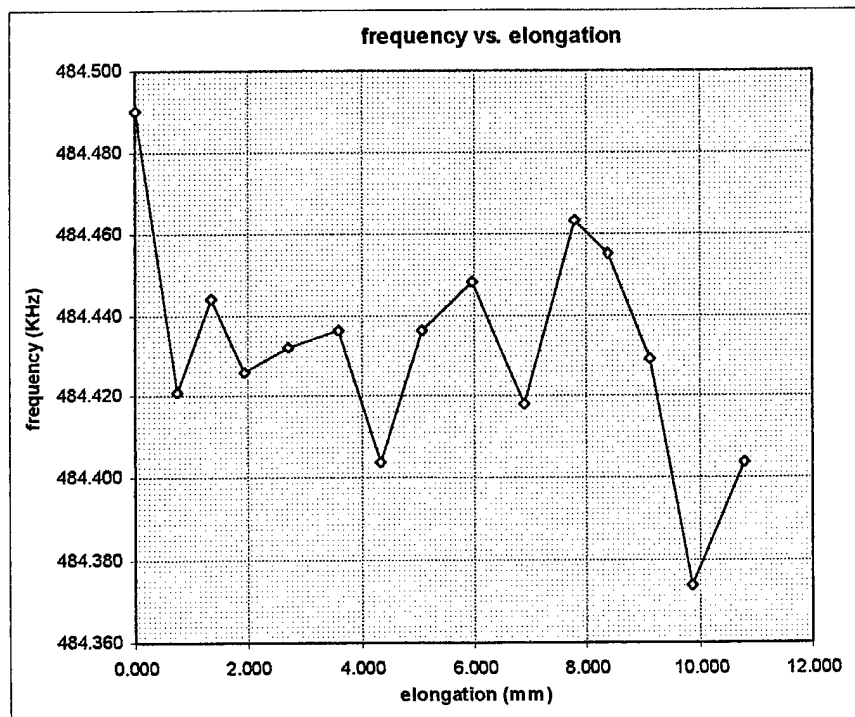


Figure A.14 ROOM TEMP (1) Frequency vs. Elongation.

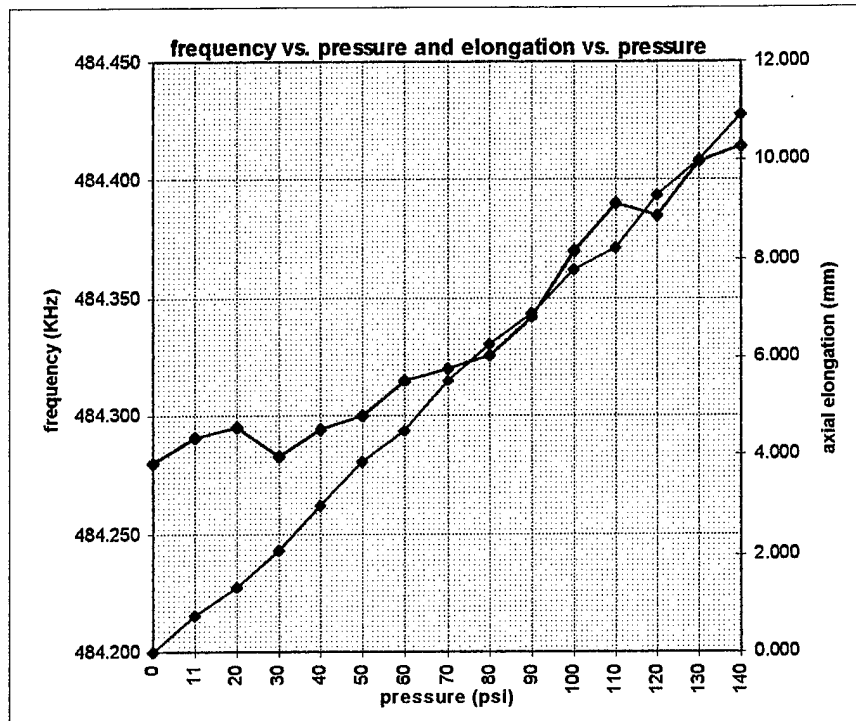


Figure A.15 ROOM TEMP (2) Frequency and Axial Elongation vs. Pressure.

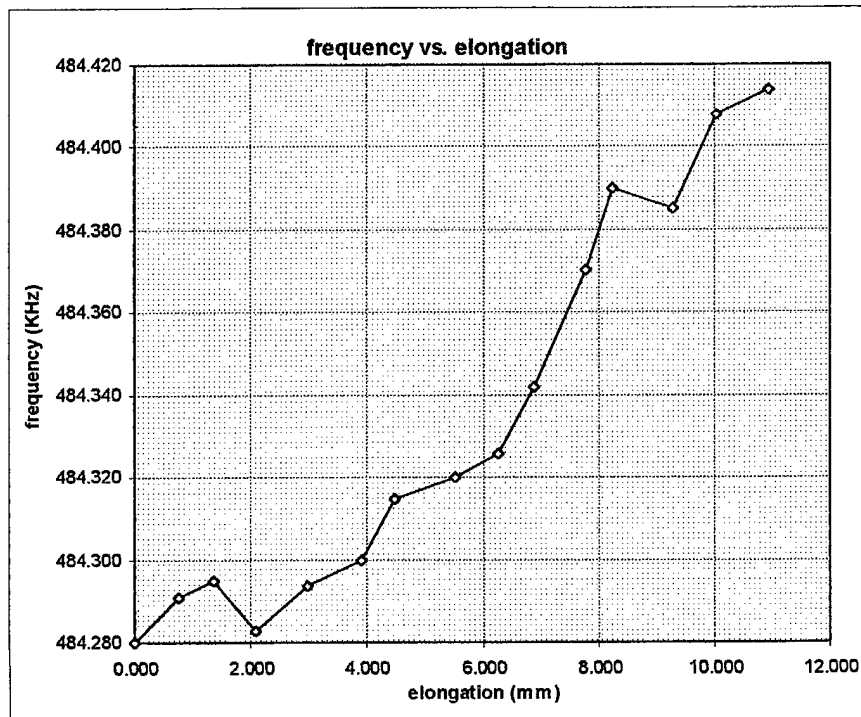


Figure A.16 ROOM TEMP (2) Frequency vs. Elongation.

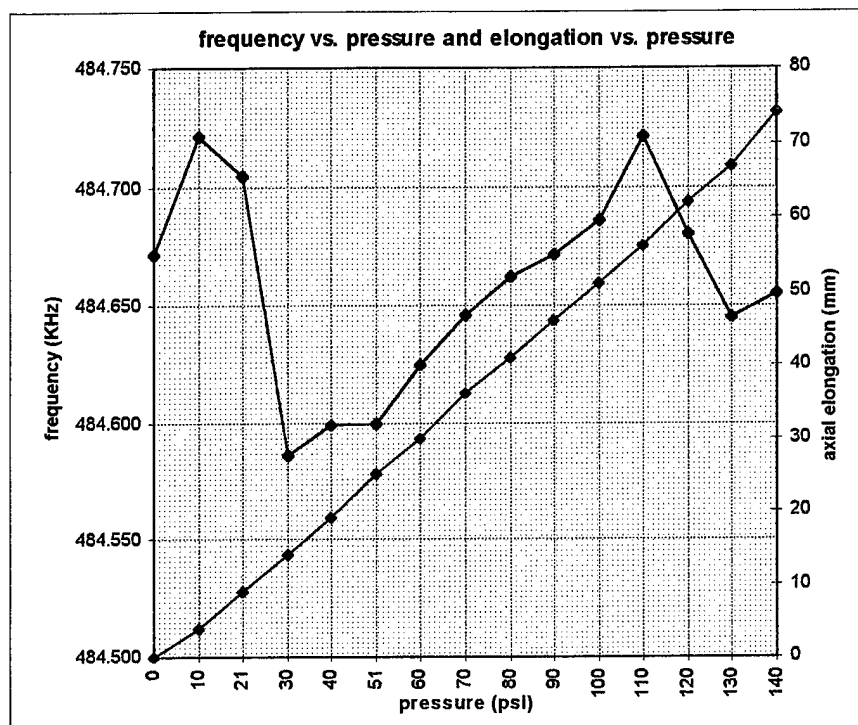


Figure A.17 ROOM TEMP (3) Frequency and Axial Elongation vs. Pressure.

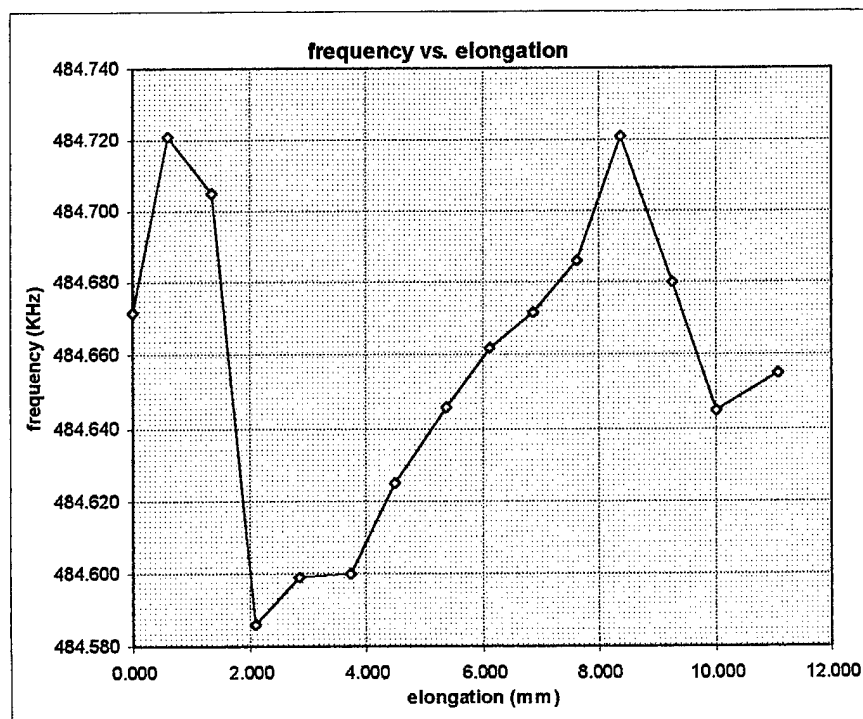


Figure A.18 ROOM TEMP (3) Frequency vs. Elongation.

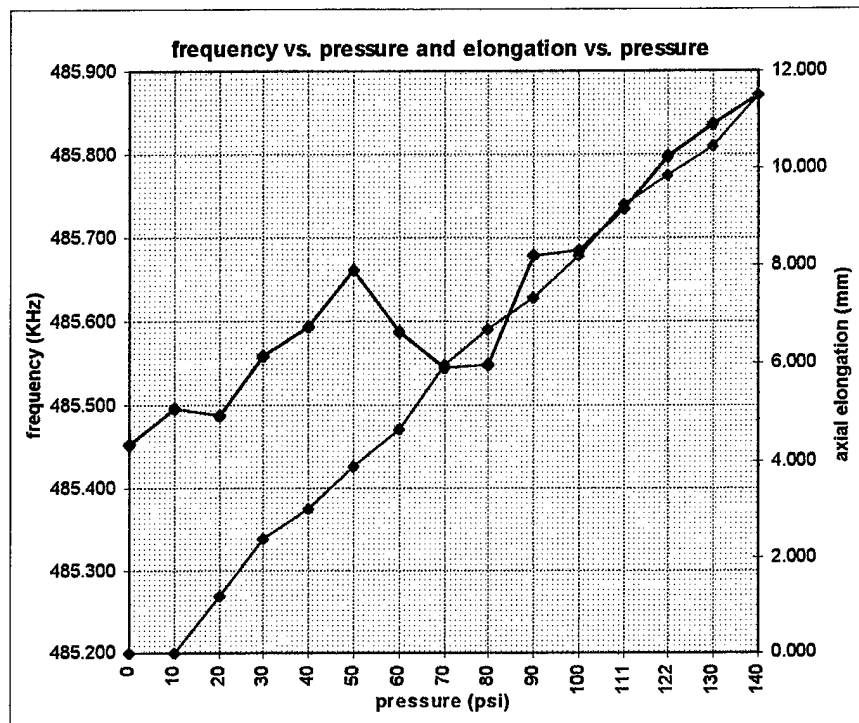


Figure A.19 COLD (1) Frequency and Axial Elongation vs. Pressure.

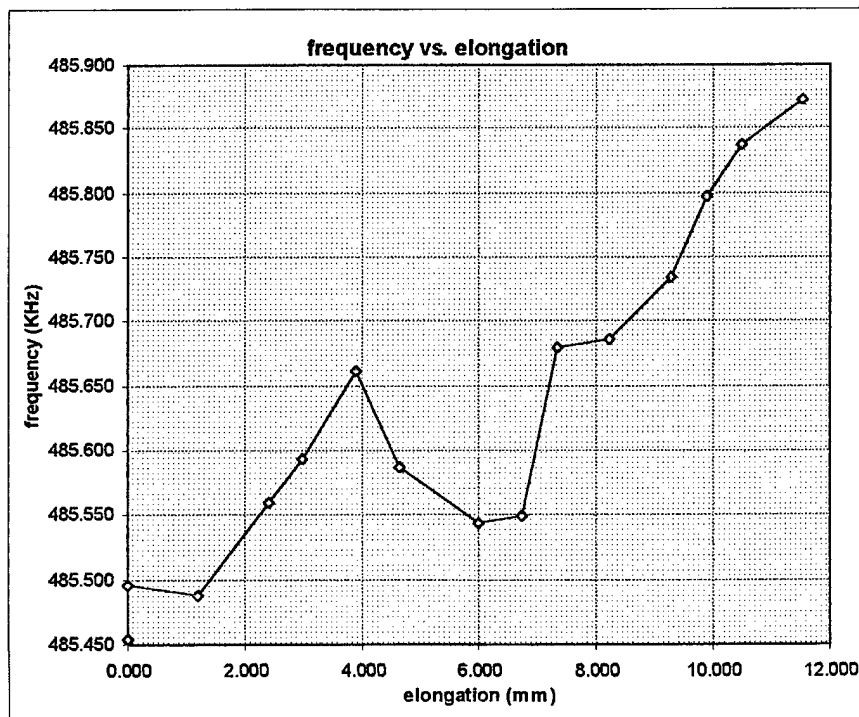


Figure A.20 COLD (1) Frequency vs. Elongation.

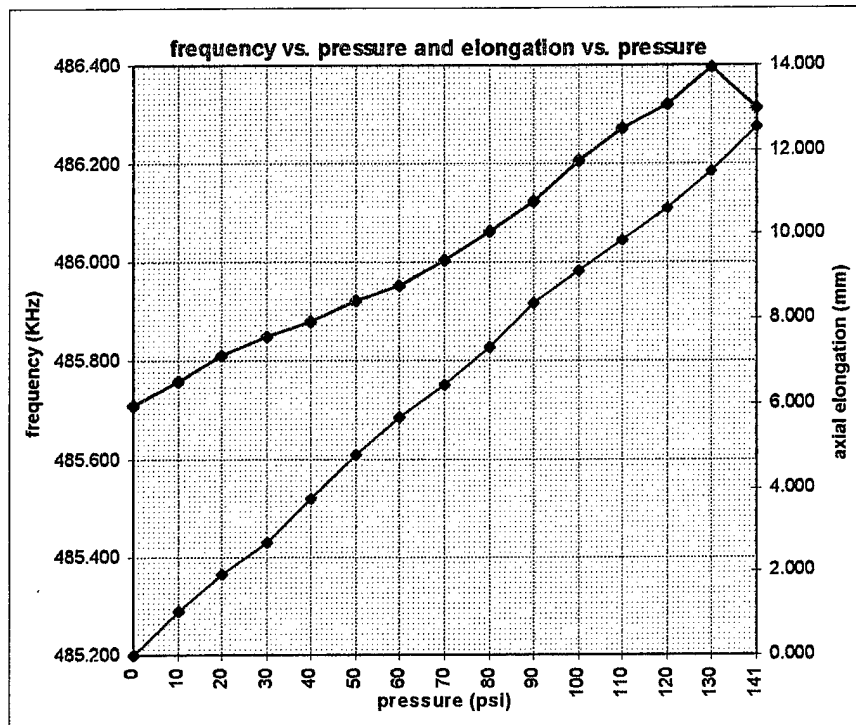


Figure A.21 COLD (2) Frequency and Axial Elongation vs. Pressure.

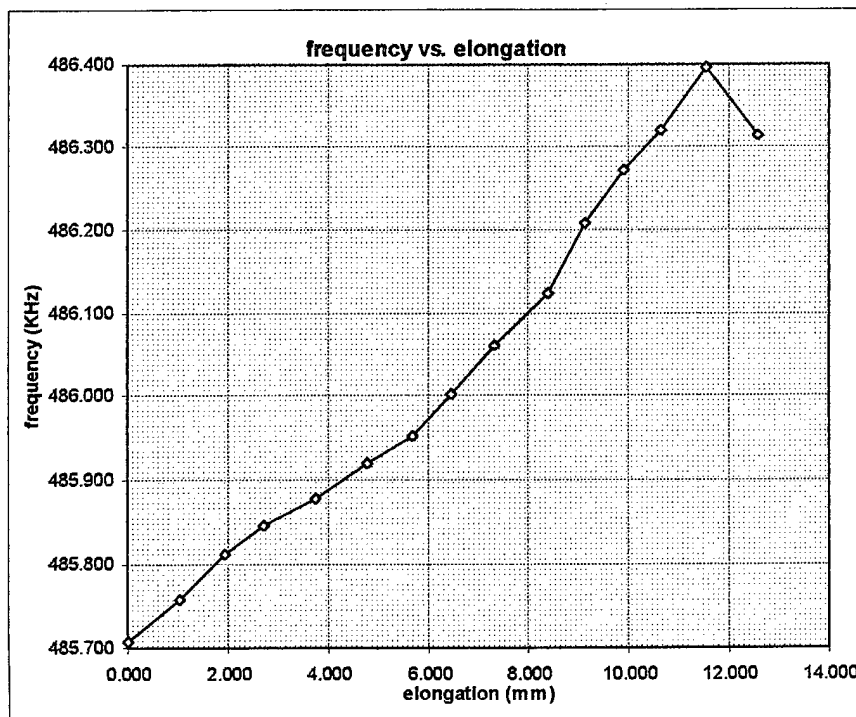


Figure A.22 COLD (2) Frequency vs. Elongation.

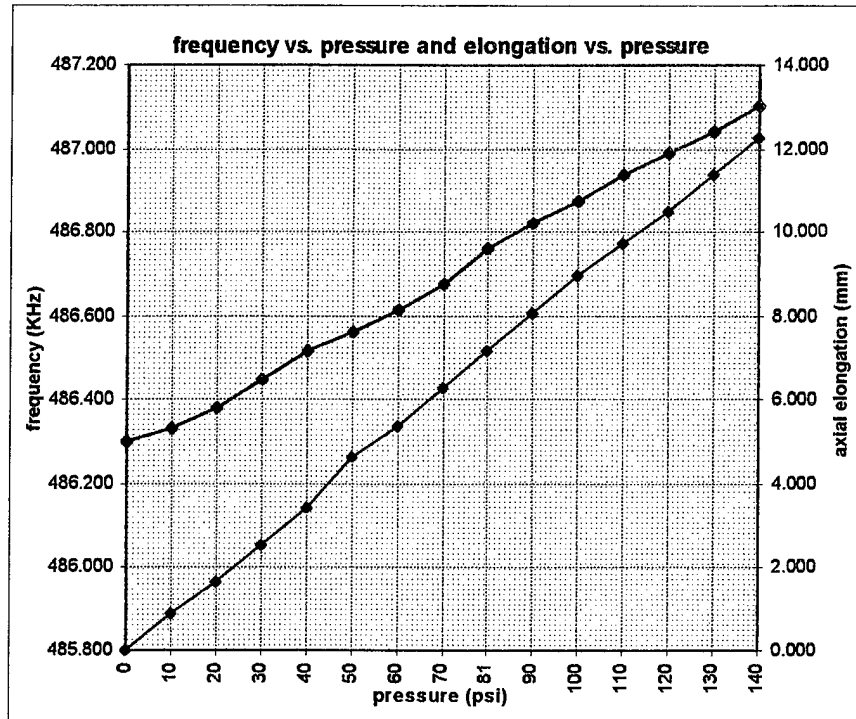


Figure A.23 COLD (3) Frequency and Axial Elongation vs. Pressure.

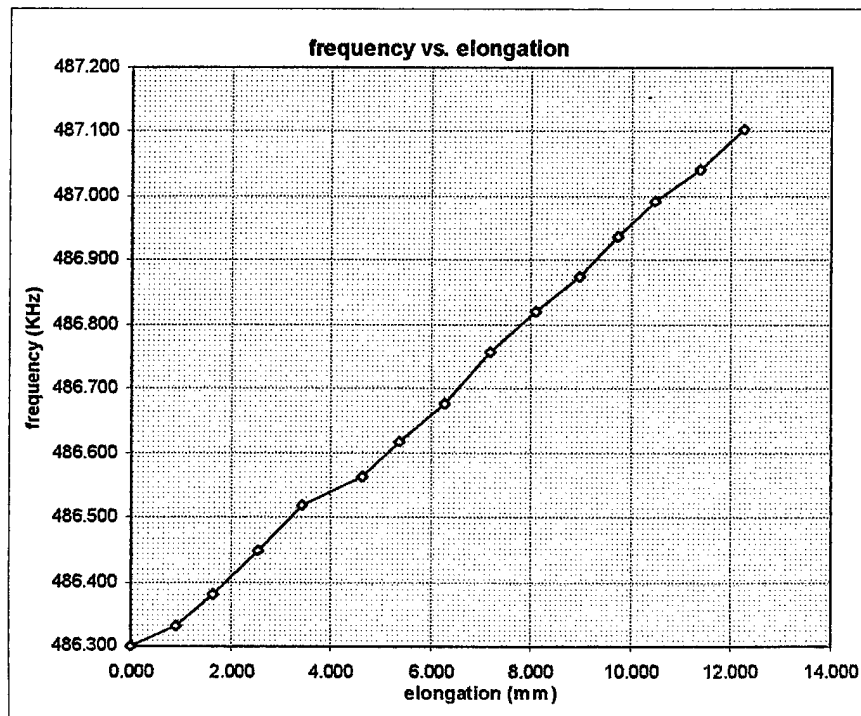


Figure A.24 COLD (3) Frequency vs. Elongation.

APPENDIX B. PVC MODEL

A. NUMERICAL DATA

All data collected on the PVC Model during the testing phase of this thesis is included in this appendix. Figures B.1, B.2 and B.3 represent data for the 9 individual trials; Figure B.1 contains Runs 1, 2 and 3, Figure B.2 contains Runs 3, 4 and 5, and Figure B.3 contains Runs 7, 8 and 9.

B. GRAPHS

The graphs presented in this appendix represent all graphed data collected on the PVC Model. All graphs demonstrate the relationship between frequency and elongation, with the purple series representing the frequency derived (from the VFPPLL instrument) elongations and the green series representing the calculated elongations from the actual observed strain gage readings. Figures B.4 and B.5 contain Runs 1 and 2, Figures B.6 and B.7 contain Runs 3 and 4, Figures B.8 and B.9 contain Runs 5 and 6, Figures B.10 and B.11 contain Runs 7 and 8, and Figure B.12 contains Run 9. Of note, Figures B.2 and B.3 are a repeat of Figures 4.7 and 4.8; they are repeated here for convenience of the reader.

RUN 1						
ssw=1.486E3 m/s	microstrain		(microns)	(kHz)	(microns)	c ₂
x ₀ = ssw*t	hoop	(normal)	measured	RUN 1	calculated	Δf / Δx
x ₀ is round-trip	strain 1	strain 1	elongation	frequency	elongation	measured
	-10	0	0.0	491.704	0.0	0.00000
time (μs)	31	41	10.3	491.654	13.8	-0.00244
364.8	79	89	22.3	491.628	20.9	-0.00171
x ₀ (mm)	123	133	33.3	491.599	28.9	-0.00158
542.0928	194	204	51.0	491.535	46.6	-0.00166
CORREL	238	248	62.0	491.526	49.1	-0.00144
-0.98874	409	419	104.8	491.473	63.7	-0.00110
SLOPE	520	530	132.5	491.343	99.5	-0.00136
-0.00262	698	708	177.0	491.204	137.8	-0.00141
(measured)					overall	-0.00141
SLOPE						
-0.00363			c ₂ = -f ₀ / x ₀ =	-0.00181	kHz/micron	
(calculated)			Δf / Δx	-0.00141	kHz/micron	
RUN 2						
ssw=1.486E3 m/s	microstrain		(microns)	(kHz)	(microns)	c ₂
x ₀ = ssw*t	hoop	(normal)	measured	RUN 1	calculated	Δf / Δx
x ₀ is round-trip	strain 1	strain 1	elongation	frequency	elongation	measured
	-26	0	0.0	483.325	0.0	0.00000
time (μs)	42	68	17.0	483.259	18.6	-0.00194
366.4	143	169	42.3	483.177	41.7	-0.00175
x ₀ (mm)	275	301	75.3	483.096	64.5	-0.00152
544.4704	398	424	106.0	482.997	92.4	-0.00155
CORREL	483	509	127.3	482.956	103.9	-0.00145
-0.99769	615	641	160.3	482.825	140.8	-0.00156
SLOPE					overall	-0.00156
-0.00299						
(measured)						
SLOPE			c ₂ = -f ₀ / x ₀ =	-0.00178	kHz/micron	
-0.00355			Δf / Δx	-0.00156	kHz/micron	
(calculated)						
RUN 3						
	end; t = 362.8 - may have jumped peaks					
ssw=1.486E3 m/s	microstrain		(microns)	(kHz)	(microns)	c ₂
x ₀ = ssw*t	hoop	(normal)	measured	RUN 1	calculated	Δf / Δx
x ₀ is round-trip	strain 1	strain 1	elongation	frequency	elongation	measured
	-30	0	0.0	483.204	0.0	0.00000
time (μs)	172	202	50.5	483.787	-162.8	0.00577
363.2	285	315	78.8	483.428	-62.5	0.00142
x ₀ (mm)	406	436	109.0	483.219	-4.2	0.00007
539.7152	475	505	126.3	482.886	88.8	-0.00126
CORREL	592	622	155.5	482.748	127.3	-0.00147
-0.72004	610	640	160.0	482.706	139.1	-0.00156
SLOPE					overall	-0.00156
-0.00484						
(measured)			c ₂ = -f ₀ / x ₀ =	-0.00179	kHz/micron	
SLOPE			Δf / Δx	-0.00156	kHz/micron	
-0.00358						
(calculated)						

Figure B.1 PVC Model Numerical Data Runs 1, 2 and 3.

RUN 4						
Note: LOST SIGNAL!						
ssw=1.486E3 m/s	microstrain		(microns)	(kHz)	(microns)	c ₂
x ₀ = ssw*t	hoop	(normal)	measured	RUN 1	calculated	Δf / Δx
x ₀ is round-trip	strain 1	strain 1	elongation	frequency	elongation	measured
	3	0	0.0	483.223	0.0	0.00000
time (μs)	125	122	30.5	483.516	-81.7	0.00480
362.8	275	272	68.0	483.758	-149.2	0.00393
x ₀ =	303	300	75.0	483.835	-170.7	0.00408
539.1208	383	380	95.0	483.267	-12.3	0.00023
CORREL (last 2 pts)	CORREL	(first 3 pts)			overall	0.00023
-1.00000	0.99347					
SLOPE (last 2 pts)	SLOPE	(first 3 pts)				
-0.02840	0.00781					
(measured)			c ₂ = -f ₀ / x ₀ =	-0.00179	kHz/micron	
SLOPE			Δf / Δx	0.00023	kHz/micron	
-0.00359						
(calculated)						
RUN 5						
ssw=1.486E3 m/s	microstrain		(microns)	(kHz)	(microns)	c ₂
x ₀ = ssw*t	hoop	(normal)	measured	RUN 1	calculated	Δf / Δx
x ₀ is round-trip	strain 1	strain 1	elongation	frequency	elongation	measured
	-4	0	0.0		0.0	0.00000
time (μs)	126	130	32.5	480.356		
359.2	274	278	69.5	480.438	-22.8	0.00111
x ₀ (mm)	398	402	100.5	480.164	53.3	-0.00141
533.7712	570	574	143.5	479.135	339.2	-0.00550
CORREL					overall	-0.00550
-0.86480						
SLOPE			c ₂ = -f ₀ / x ₀ =	-0.00180	kHz/micron	
-0.01108			Δf / Δx	-0.00550	kHz/micron	
(measured)						
SLOPE						
-0.00360						
(calculated)						
RUN 6						
ssw=1.486E3 m/s	microstrain		(microns)	(kHz)	(microns)	c ₂
x ₀ = ssw*t	hoop	(normal)	measured	RUN 1	calculated	Δf/Δx
x ₀ is round-trip	strain 1	strain 1	elongation	frequency	elongation	measured
	22	0	0.0	480.462	0.0	0.00000
time (μs)	155	133	33.3	480.688	-62.8	0.00340
359.2	259	237	59.3	480.213	69.2	-0.00210
x ₀ (mm)	307	285	71.3	480.096	101.7	-0.00257
533.7712	344	322	80.5	480.235	63.0	-0.00141
CORREL	(middle 3)				overall	-0.00141
-0.69955	-0.99203					
SLOPE	(middle 3)		c ₂ = -f ₀ / x ₀ =	-0.00180	kHz/micron	
-0.00507	-0.01601		Δf / Δx	-0.00141	kHz/micron	
(measured)						
SLOPE						
-0.00360						
(calculated)						

Figure B.2 PVC Model Numerical Data Runs 4, 5 and 6.

RUN 7						
ssw=1.486E3 m/s	microstrain		(microns)	(kHz)	(microns)	c ₂
x ₀ = ssw*t	hoop	(normal)	measured	RUN 1	calculated	Δf / Δx
x ₀ is round-trip	strain 1	strain 1	elongation	frequency	elongation	measured
	37	0	0.0	477.498	0.0	0.0000
time (ms)	154	117	29.3	477.977	-133.3	0.00819
357.6	224	187	46.8	478.339	-234.0	0.00899
x ₀ =	245	208	52.0	477.574	-21.1	0.00073
531.3936	277	240	60.0	477.342	43.4	-0.00130
CORREL	317	280	70.0	477.250	69.0	-0.00177
-0.59225	347	310	77.5	477.220	77.3	-0.00179
SLOPE	366	329	82.3	477.200	82.9	-0.00181
-0.00800	401	364	91.0	477.166	92.4	-0.00182
(measured)	410	373	93.3	477.158	94.6	-0.00182
SLOPE					overall	-0.00182
-0.00359						
(calculated)			c ₂ = -f ₀ / x ₀ =	-0.00180	kHz/micron	
			Δf / Δx	-0.00182	kHz/micron	
RUN 8						
ssw=1.486E3 m/s	microstrain		(microns)	(kHz)	(microns)	c ₂
x ₀ = ssw*t	hoop	(normal)	measured	RUN 1	calculated	Δf / Δx
x ₀ is round-trip	strain 1	strain 1	elongation	frequency	elongation	measured
	-7	0	0.0	480.199	0.0	0.00000
time (ms)	109	116	29.0	480.148	14.6	-0.00088
369.6	170	177	44.3	480.122	22.0	-0.00087
x ₀ =	222	229	57.3	480.099	28.6	-0.00087
549.2256	252	259	64.8	480.039	45.7	-0.00124
CORREL	290	297	74.3	479.977	63.5	-0.00149
-0.96650	296	303	75.8	479.984	61.5	-0.00142
SLOPE	321	328	82.0	479.963	67.5	-0.00144
-0.00323	356	363	90.8	479.924	78.6	-0.00152
(measured)	358	365	91.3	479.930	76.9	-0.00147
SLOPE					overall	-0.00147
-0.00350						
(calculated)			c ₂ = -f ₀ / x ₀ =	-0.00175	kHz/micron	
			Δf / Δx	-0.00147	kHz/micron	
RUN 9						
ssw=1.486E3 m/s	microstrain		(microns)	(kHz)	(microns)	c ₂
x ₀ = ssw*t	hoop	(normal)	measured	RUN 1	calculated	Δf / Δx
x ₀ is round-trip	strain 1	strain 1	elongation	frequency	elongation	measured
	11	0	0.0	480.177	0.0	0.00000
time (μs)	124	113	28.3	480.124	15.1	-0.00094
368.0	202	191	47.8	480.089	25.1	-0.00092
x ₀ (mm)	256	245	61.3	480.008	48.1	-0.00138
546.848	301	290	72.5	479.991	53.0	-0.00128
CORREL	317	306	76.5	479.927	71.2	-0.00163
-0.96767	341	330	82.5	479.908	76.6	-0.00163
SLOPE	353	342	85.5	479.911	75.7	-0.00156
-0.00333					overall	-0.00156
(measured)						
SLOPE			c ₂ = -f ₀ / x ₀ =	-0.00176	kHz/micron	
-0.00351			Δf / Δx	-0.00156	kHz/micron	
(calculated)						

Figure B.3 PVC Model Numerical Data Runs 7, 8 and 9.

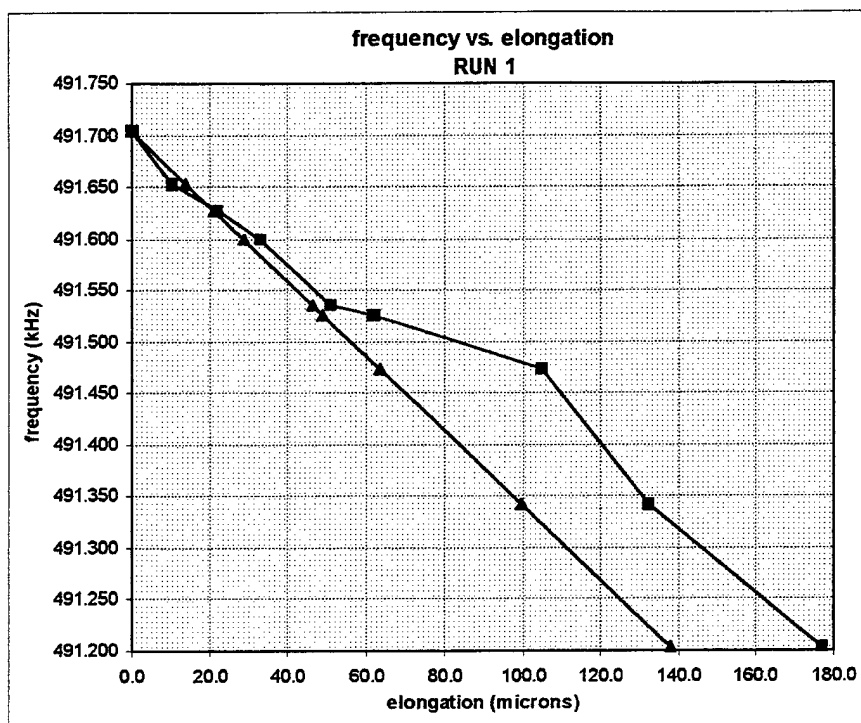


Figure B.4 PVC Model Run 1; Frequency vs. Elongation.

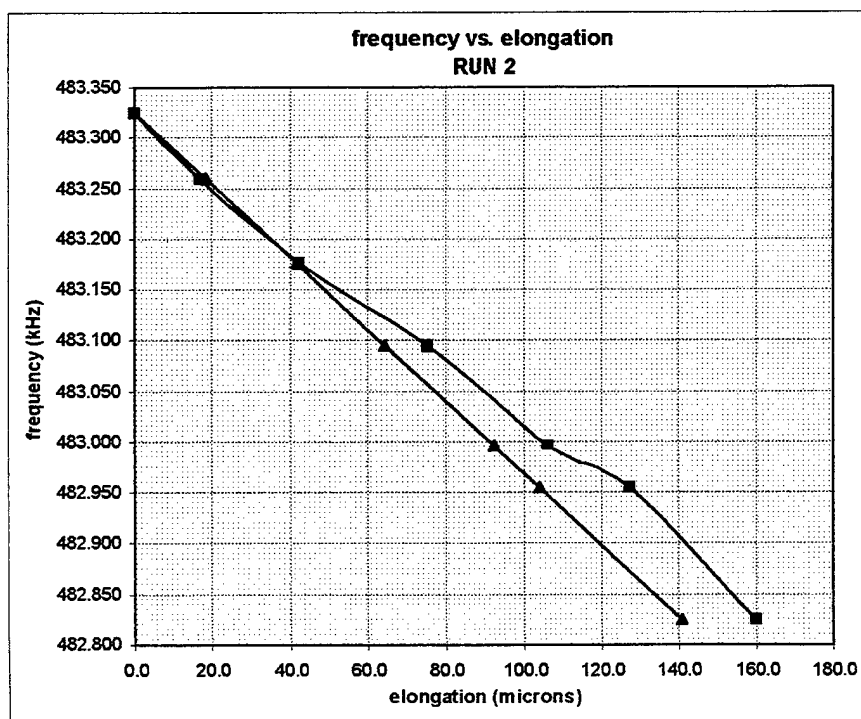


Figure B.5 PVC Model Run 2; Frequency vs. Elongation.

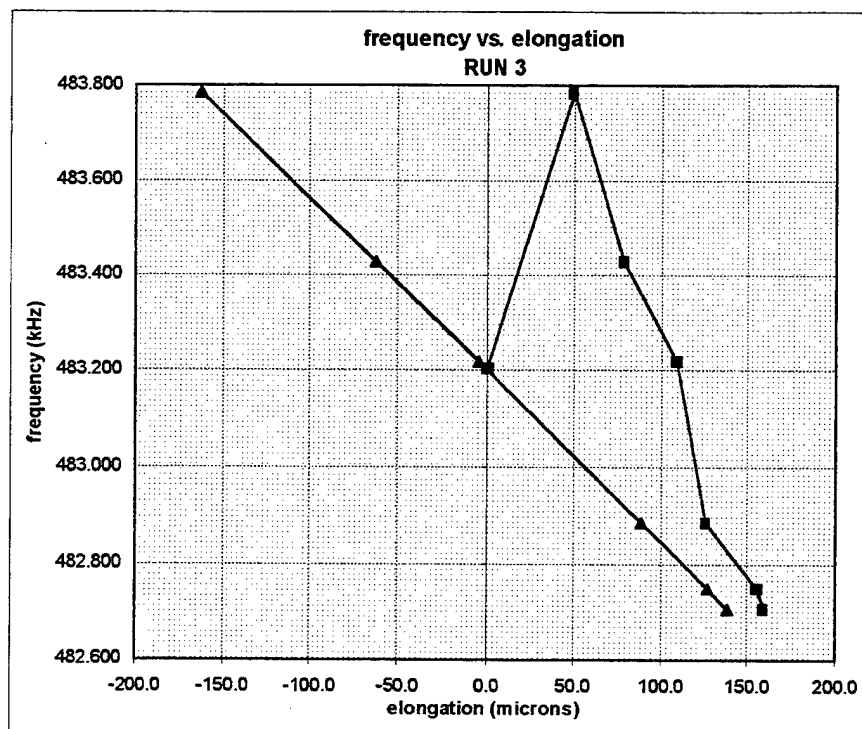


Figure B.6 PVC Model Run 3; Frequency vs. Elongation.

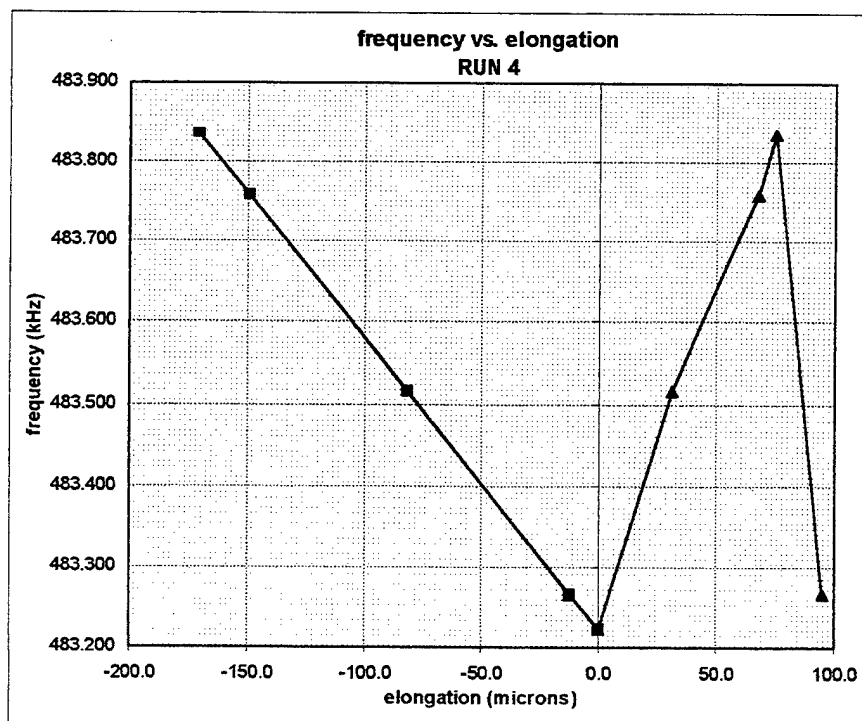


Figure B.7 PVC Model Run 4; Frequency vs. Elongation.

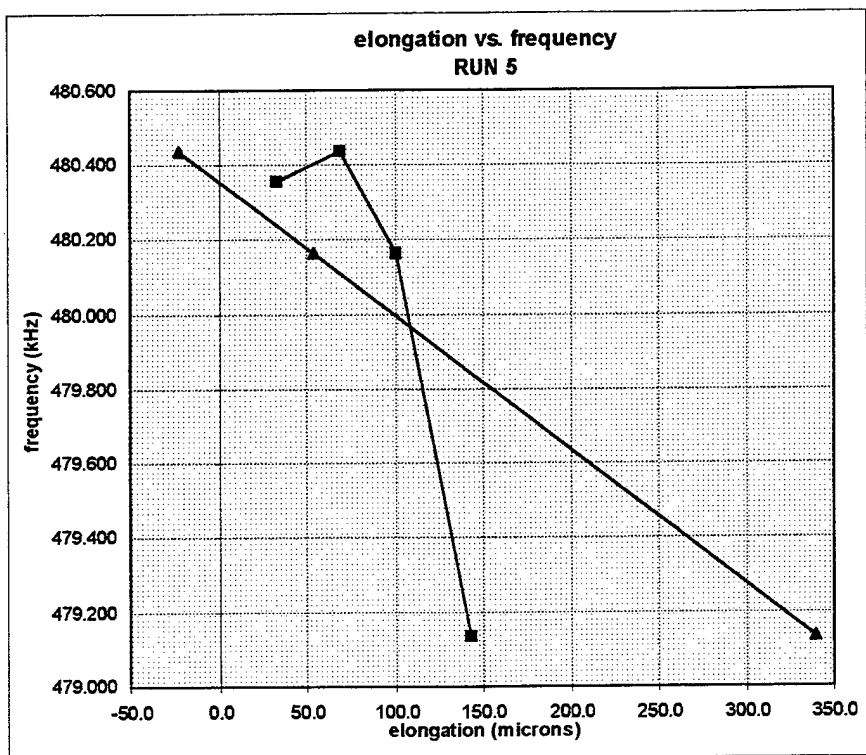


Figure B.8 PVC Model Run 5; Frequency vs. Elongation.

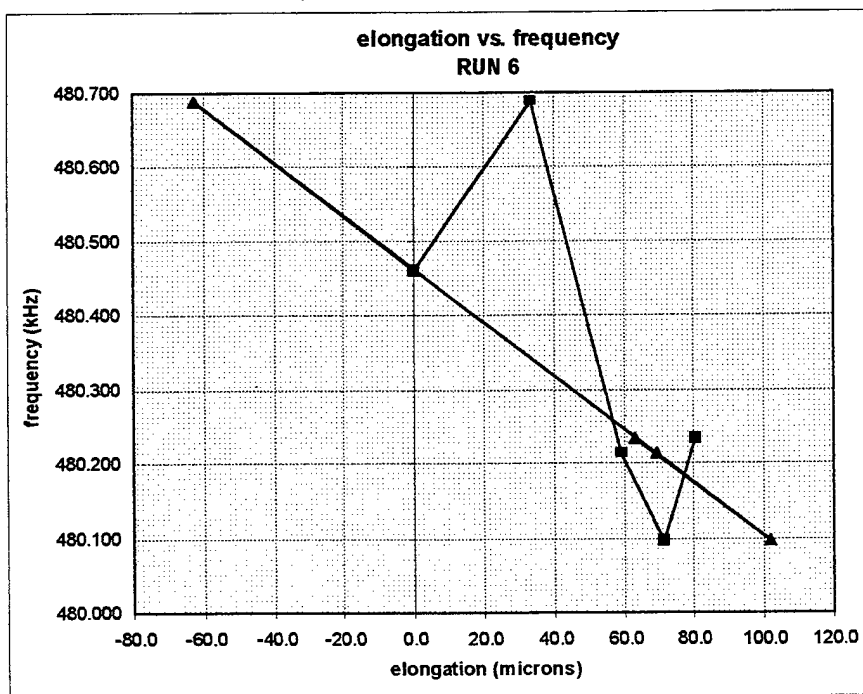


Figure B.9 PVC Model Run 6; Frequency vs. Elongation.

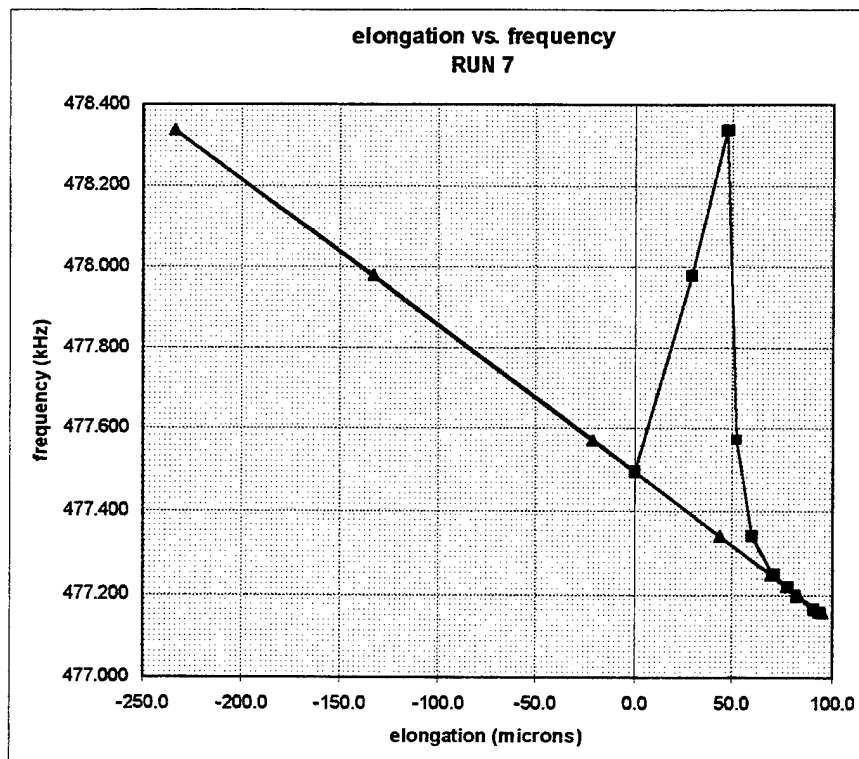


Figure B.10 PVC Model Run 7; Frequency vs. Elongation.

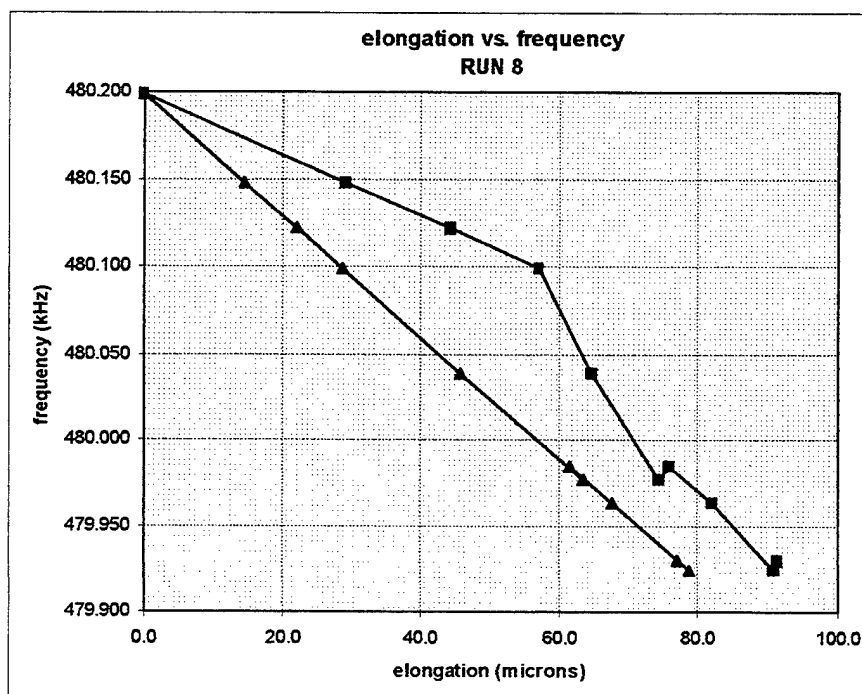


Figure B.11 PVC Model Run 8; Frequency vs. Elongation.

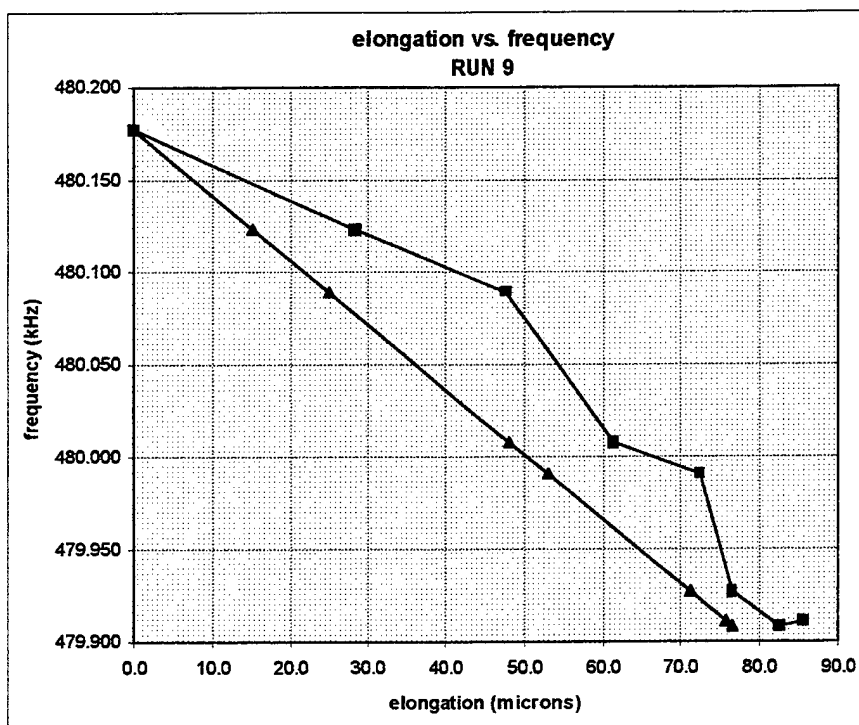


Figure B.12 PVC Model Run 9; Frequency vs. Elongation.

APPENDIX C. OPEN CHANNEL MODEL

A. NUMERICAL DATA

All data collected on the Open Channel Model during the testing phase of this thesis is included in this appendix. Figures C.1, C.2, C.3, C.4, C.5, C.6, C.7 and C.8 represent the data for the 16 individual trials; Figure C.1 contains Runs 1 and 2, Figure C.2 contains Runs 3 and 4, Figure C.3 contains Runs 5 and 6, Figure C.4 contains Runs 7 and 8, Figure C.5 contains Runs 9 and 10, Figure C.6 contains Runs 11 and 12, Figure C.7 contains Runs 13 and 14, and Figure C.8 contains Runs 15 and 16.

B. GRAPHS

The graphs presented in this appendix represent all graphed data collected on the Open Channel Model. All graphs demonstrate the relationship between frequency and elongation, with the purple series representing the frequency derived (from the VFPPLL instrument) elongations and the green series representing the physically effected elongations. Figures C.9 and C.10 contain Runs 1 and 2, Figures C.11 and C.12 contain Runs 3 and 4, Figures C.13 and C.14 contain Runs 5 and 6, Figures C.15 and C.16 contain Runs 7 and 8, Figures C.17 and C.18 contain Runs 9 and 10, Figures C.19 and C.20 contain Runs 11 and 12, Figures C.21 and C.22 contain Runs 13 and 14, and Figures C.23 and C.24 contain Runs 15 and 16, respectively.

[illegible]

Figure C.1 Open Channel Model Numerical Data Runs 1 and 2.

RUN 3	t = 148.0 μ s					
x_0 (mm)	(mm)	(mm)	total (mm)	total (mm)	(kHz)	(mm)
219.928	1/6 turn	calc Δx	calc Δx	Δx	frequency	x
(round-trip)			0.000	0.000	494.202	219.928
	-0.132	-0.199	-0.199	-0.132	495.096	219.729
	-0.132	-0.151	-0.350	-0.265	495.777	219.578
	-0.132	-0.115	-0.465	-0.397	496.296	219.463
	-0.132	0.036	-0.429	-0.529	496.134	219.499
	-0.132	-0.033	-0.463	-0.661	496.284	219.465
	-0.132	-0.052	-0.515	-0.794	496.520	219.413
	-0.132	-0.068	-0.583	-0.926	496.828	219.345
	-0.132	-0.125	-0.708	-1.058	497.393	219.220
	-0.132	-0.098	-0.806	-1.191	497.835	219.122
	-0.132	-0.160	-0.966	-1.323	498.561	218.962
	-0.132	-0.139	-1.105	-1.455	499.192	218.823
CORREL	0.96962		$c_2 = -f_0 / x_0 =$	-4.49422	kHz/mm	
SLOPE	-4.51493					
RUN 4	t = 154.8 μ s					
x_0 (mm)	(mm)	(mm)	total (mm)	total (mm)	(kHz)	(mm)
230.033	1/6 turn	calc Δx	calc Δx	Δx	frequency	x
(round-trip)			0.000	0.000	485.445	230.033
	-0.132	-0.207	-0.207	-0.132	486.320	229.825
	-0.132	-0.193	-0.400	-0.265	487.136	229.632
	-0.132	-0.151	-0.551	-0.397	487.775	229.482
	-0.132	-0.072	-0.623	-0.529	488.081	229.409
	-0.132	-0.123	-0.747	-0.661	488.604	229.286
	-0.132	-0.106	-0.853	-0.794	489.055	229.180
	-0.132	-0.106	-0.958	-0.926	489.504	229.074
	-0.132	-0.113	-1.071	-1.058	489.985	228.961
	-0.132	-0.149	-1.220	-1.191	490.618	228.813
CORREL	0.99226		$c_2 = -f_0 / x_0 =$	-4.22066	kHz/mm	
SLOPE	-4.24065					

Figure C.2 Open Channel Model Numerical Data Runs 3 and 4.

[illegible]

[illegible]

Figure C.4 Open Channel Model Numerical Data Runs 7 and 8.

[illegible]

Figure C.6 Open Channel Model Numerical Data Runs 11 and 12.

[illegible]

Figure C.8 Open Channel Model Numerical Data Runs 15 and 16.

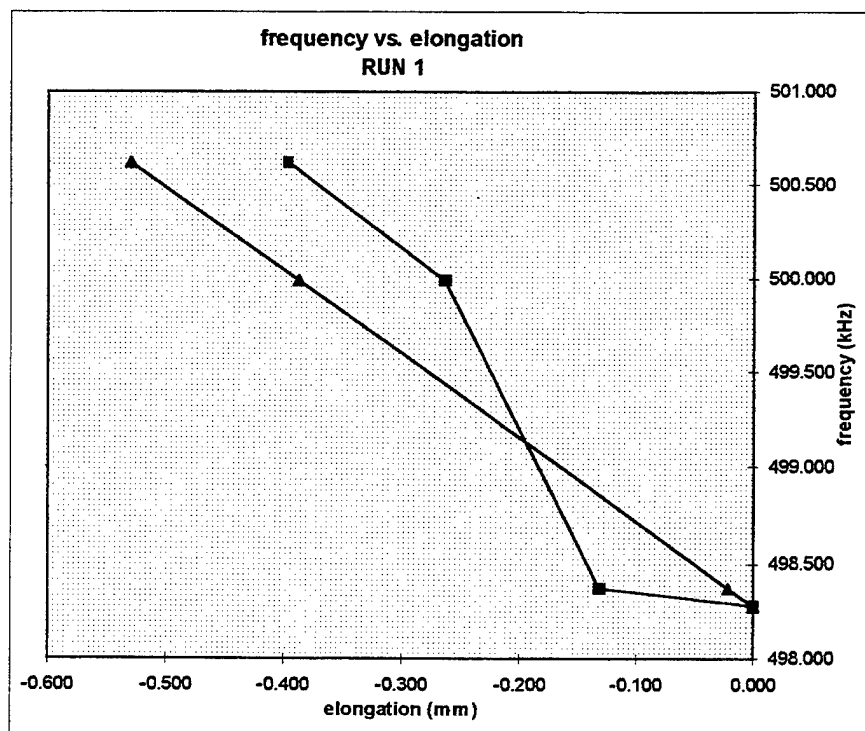


Figure C.9 Open Channel Model Run 1; Frequency vs. Elongation.

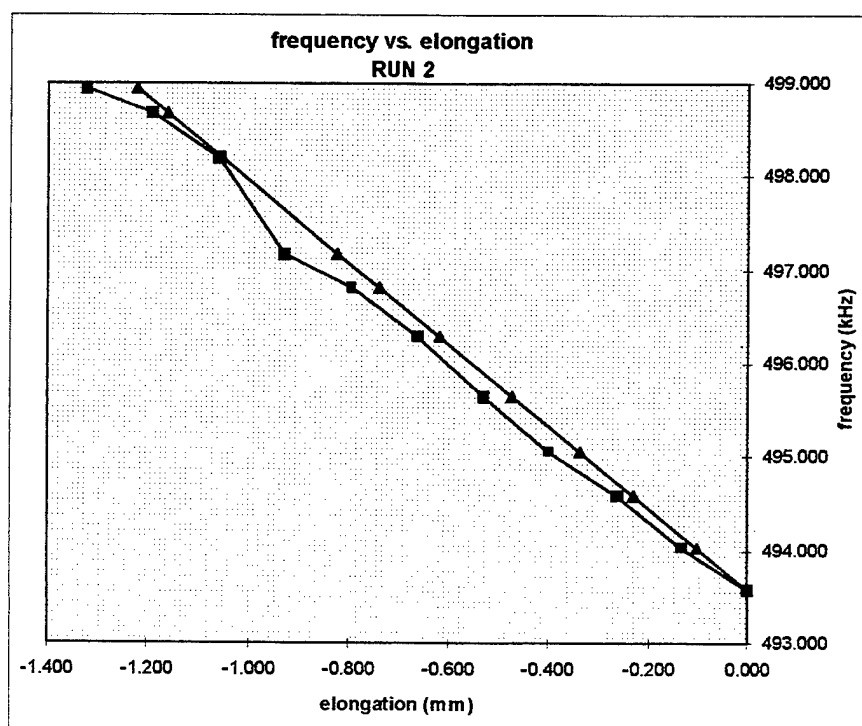


Figure C.10 Open Channel Model Run 2; Frequency vs. Elongation.

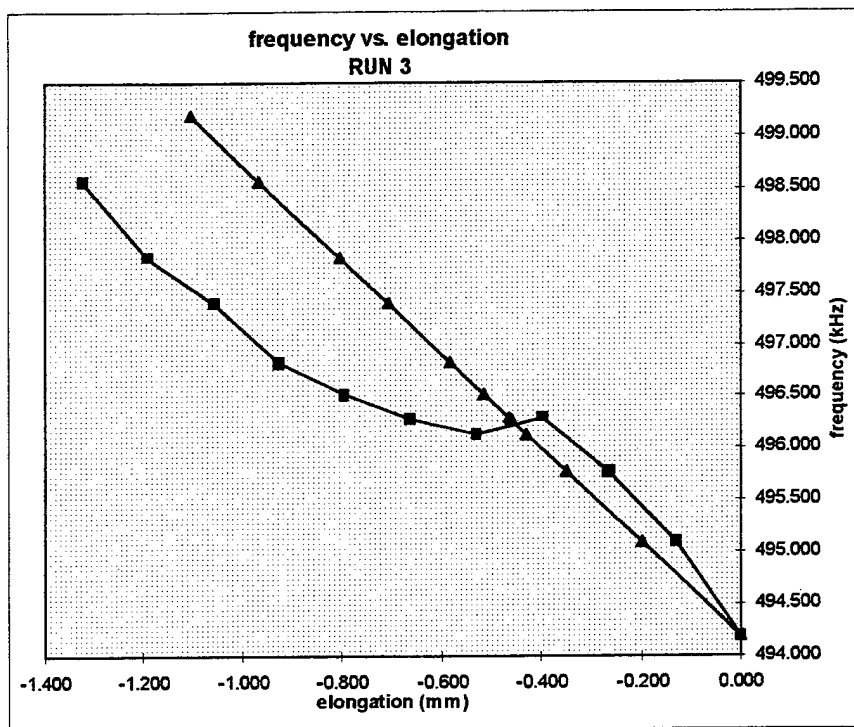


Figure C.11 Open Channel Model Run 3; Frequency vs. Elongation.

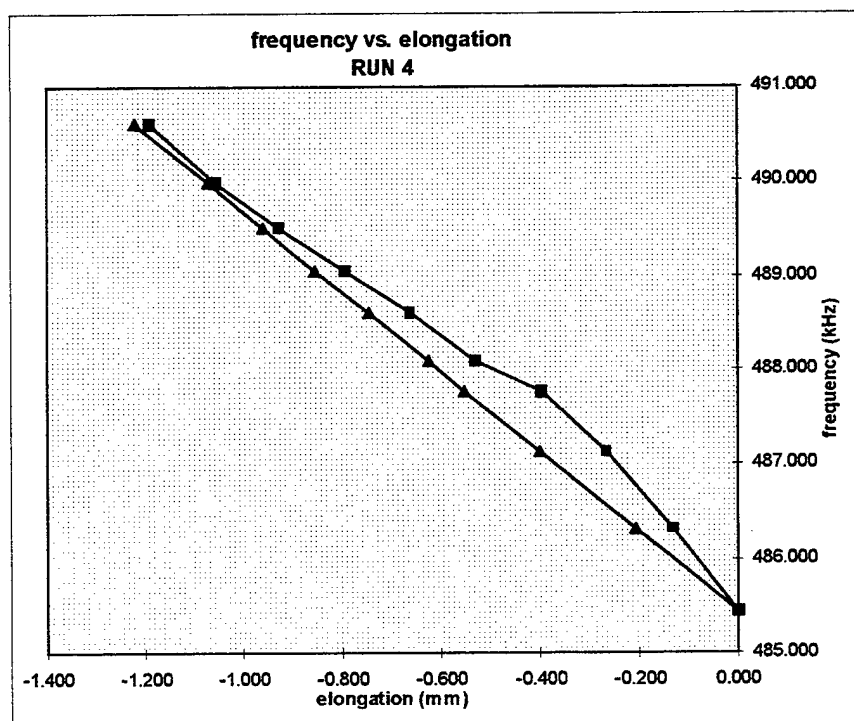


Figure C.12 Open Channel Model Run 4; Frequency vs. Elongation.

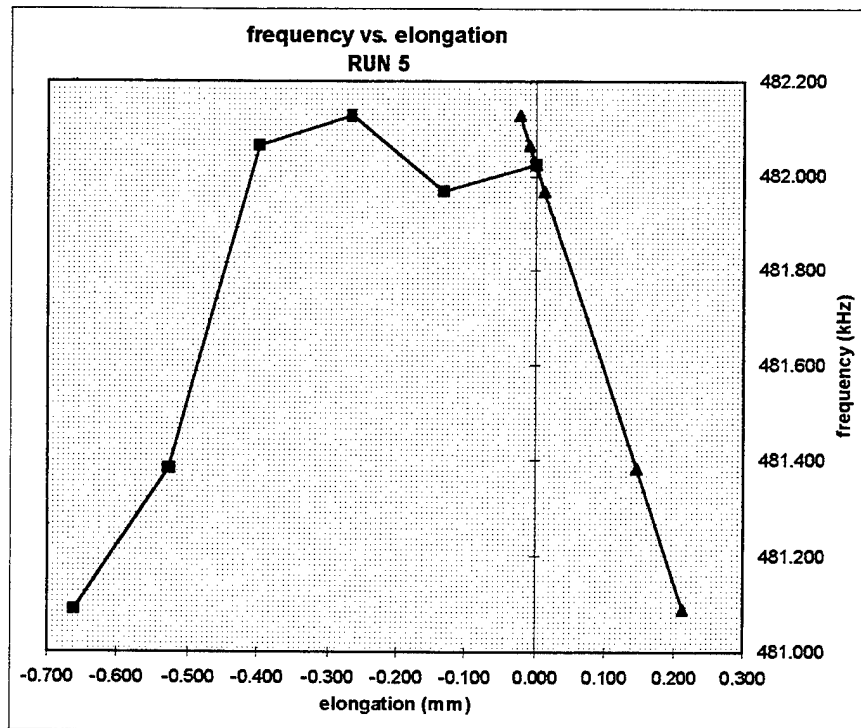


Figure C.13 Open Channel Model Run 5; Frequency vs. Elongation.

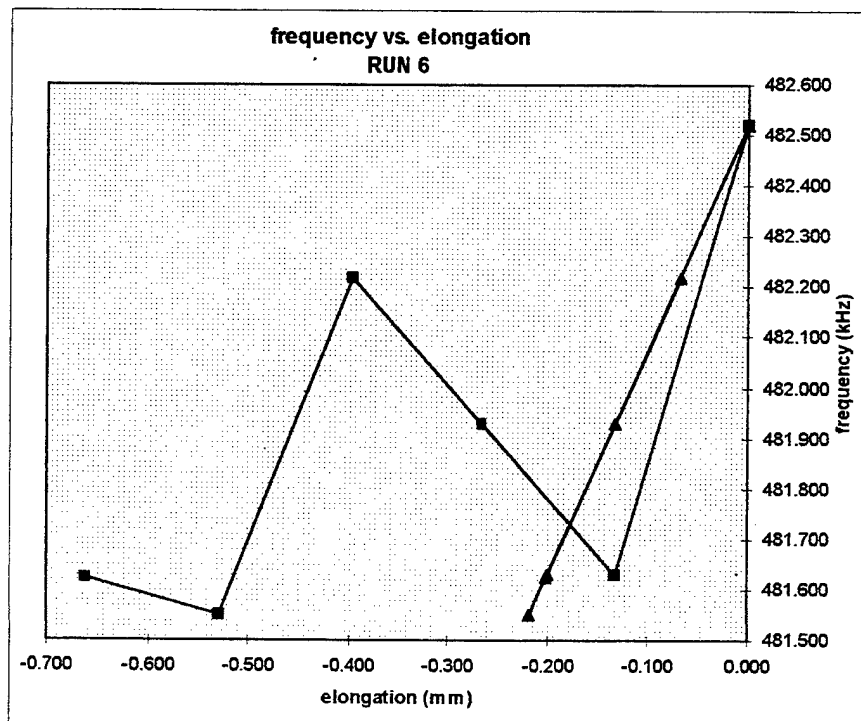


Figure C.14 Open Channel Model Run 6; Frequency vs. Elongation.

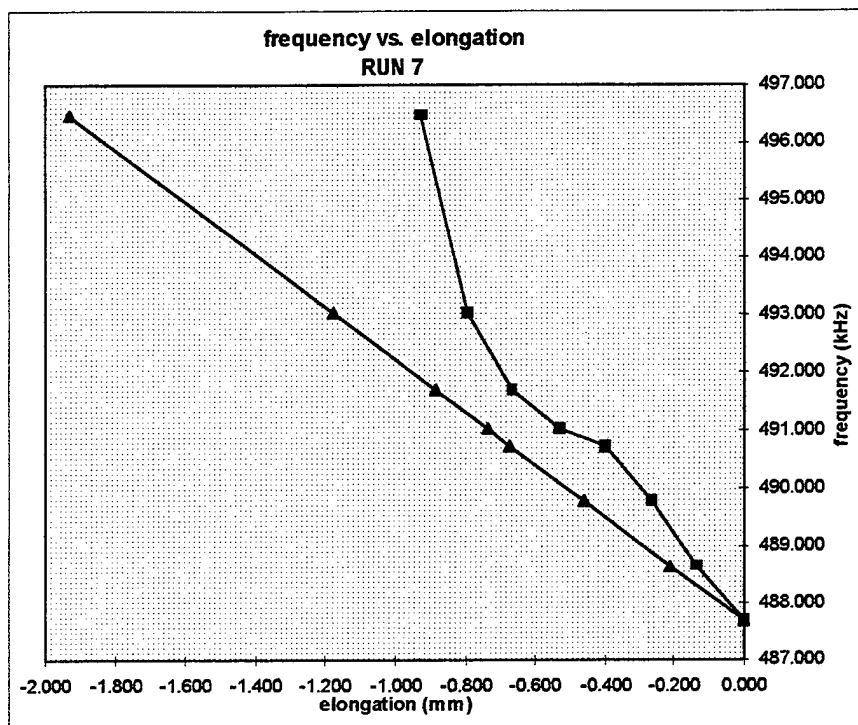


Figure C.15 Open Channel Model Run 7; Frequency vs. Elongation.

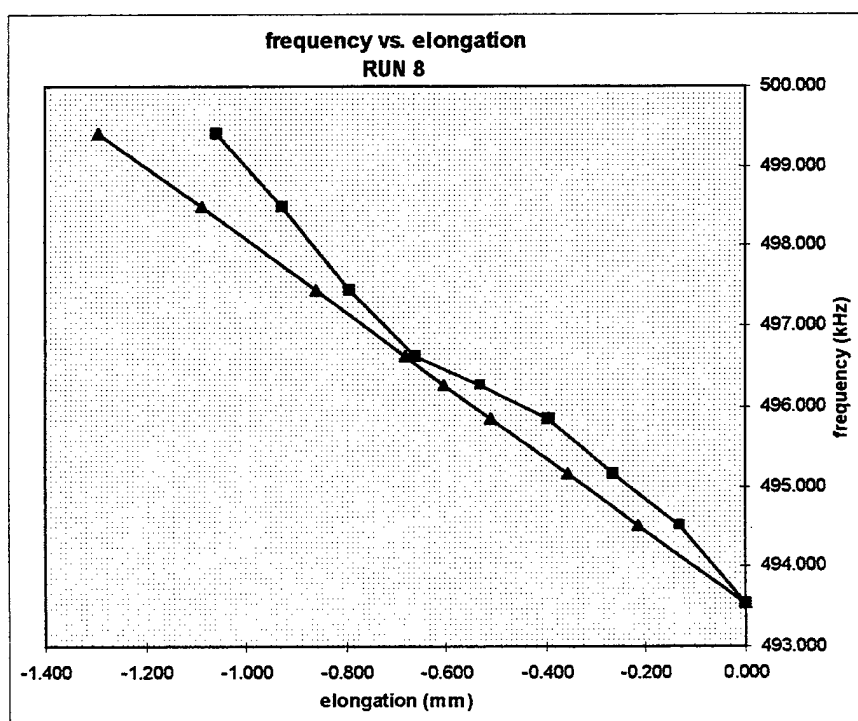


Figure C.16 Open Channel Model Run 8; Frequency vs. Elongation.

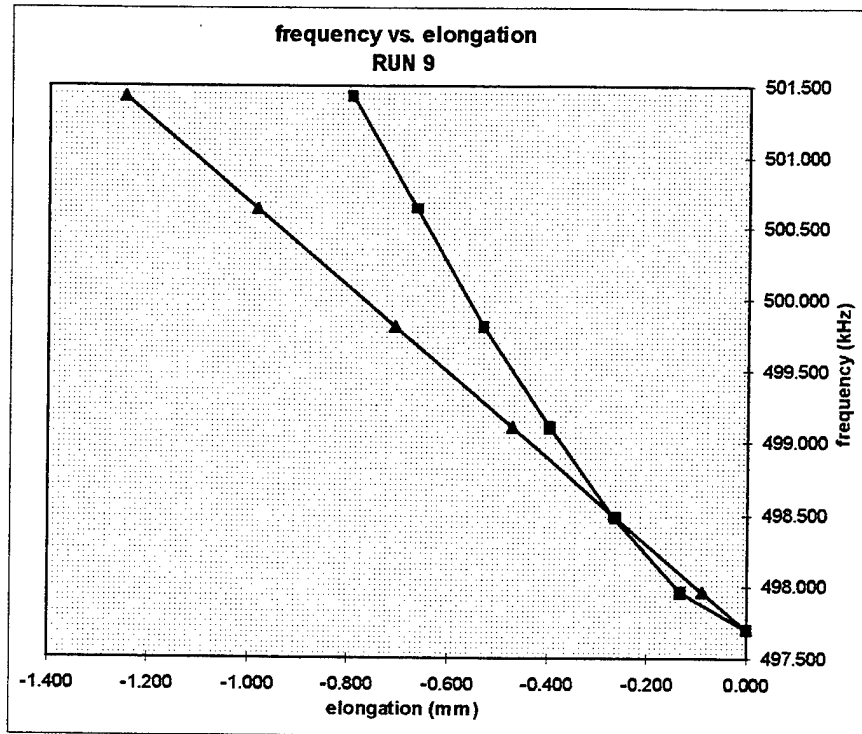


Figure C.17 Open Channel Model Run 9; Frequency vs. Elongation.

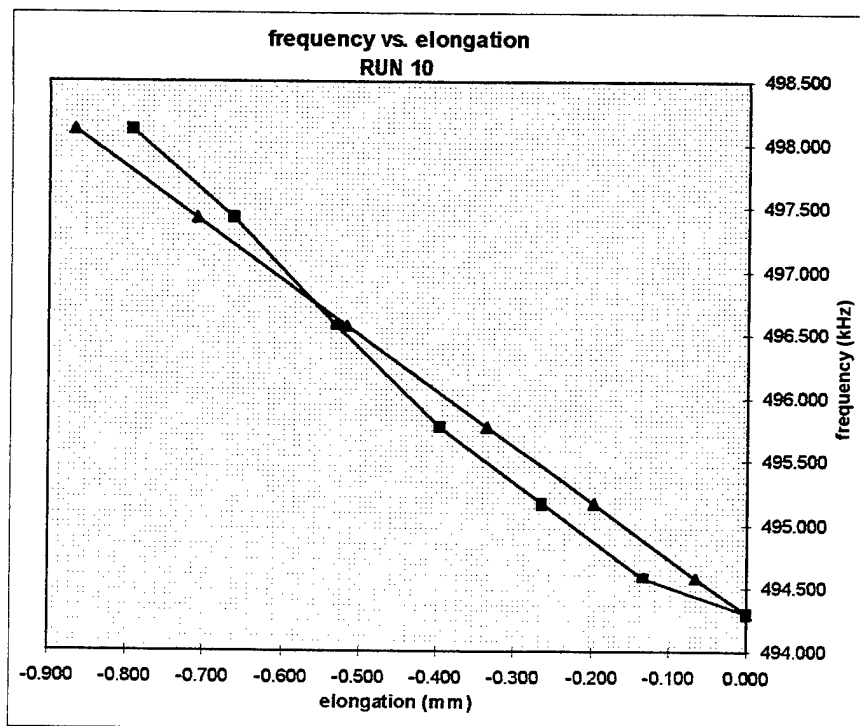


Figure C.18 Open Channel Model Run 10; Frequency vs. Elongation.

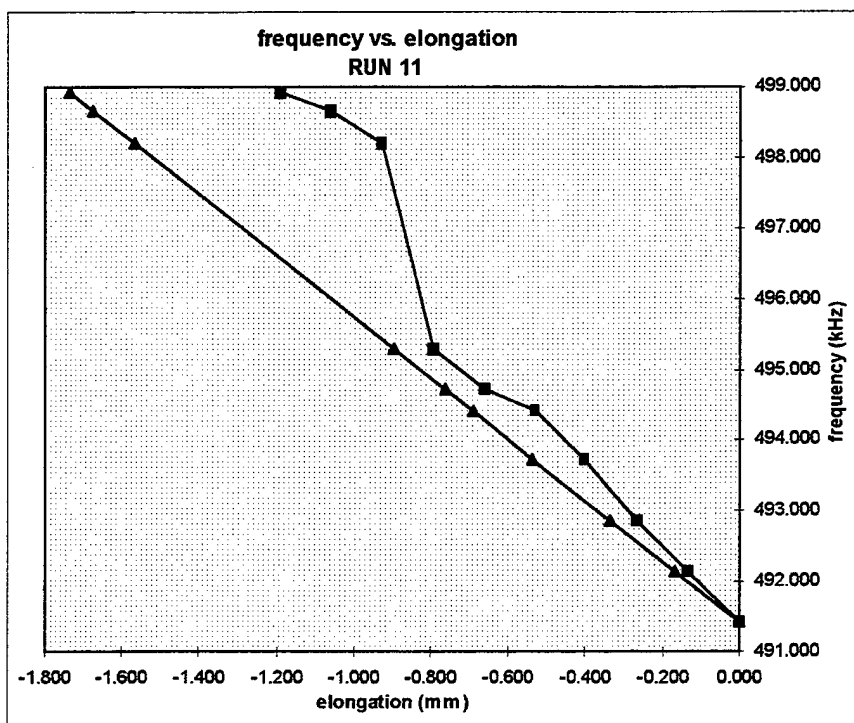


Figure C.19 Open Channel Model Run 11; Frequency vs. Elongation.

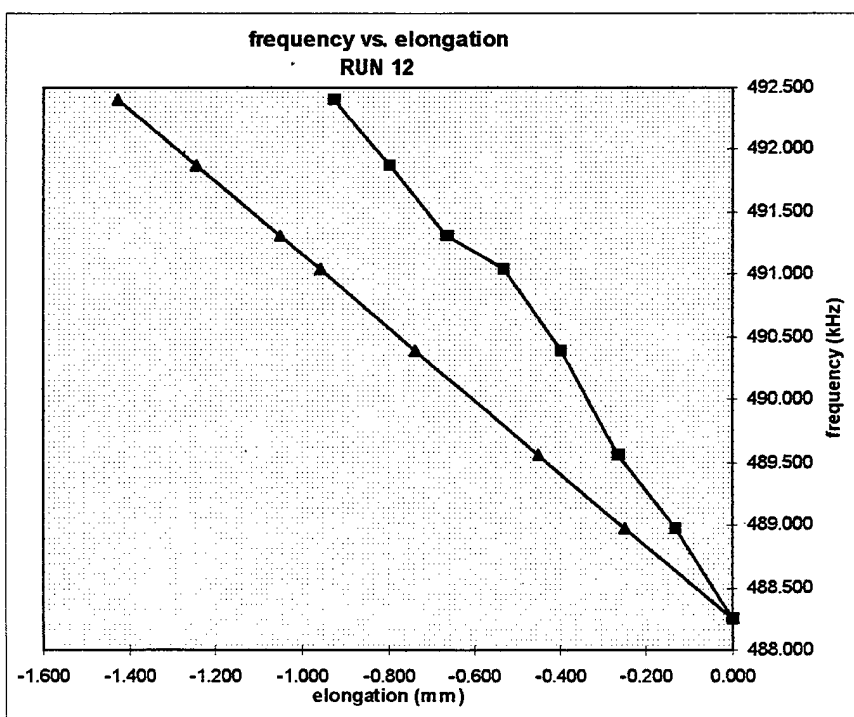


Figure C.20 Open Channel Model Run 12; Frequency vs. Elongation.

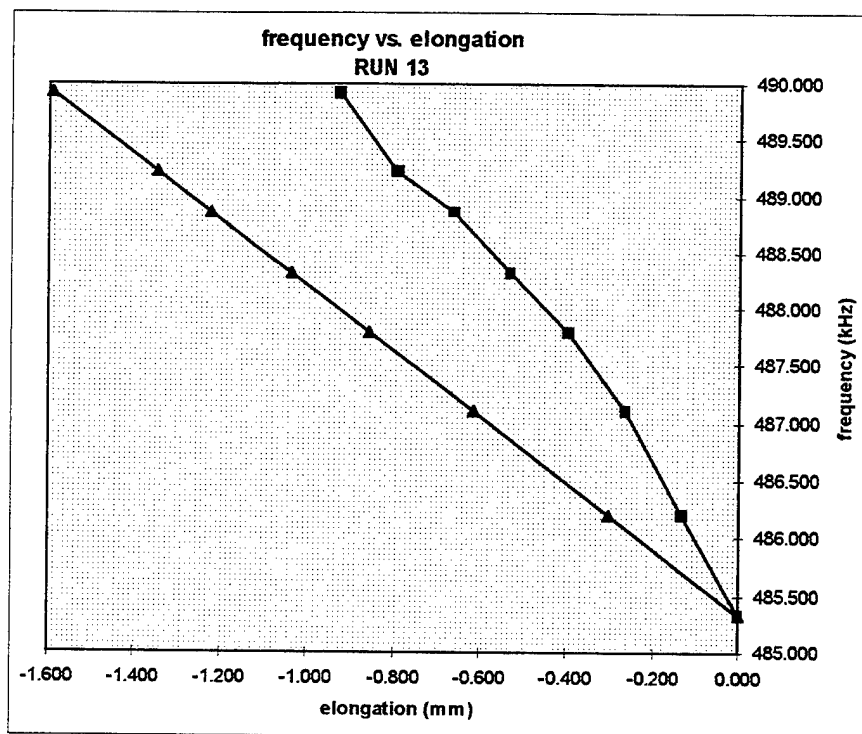


Figure C.21 Open Channel Model Run 13; Frequency vs. Elongation.

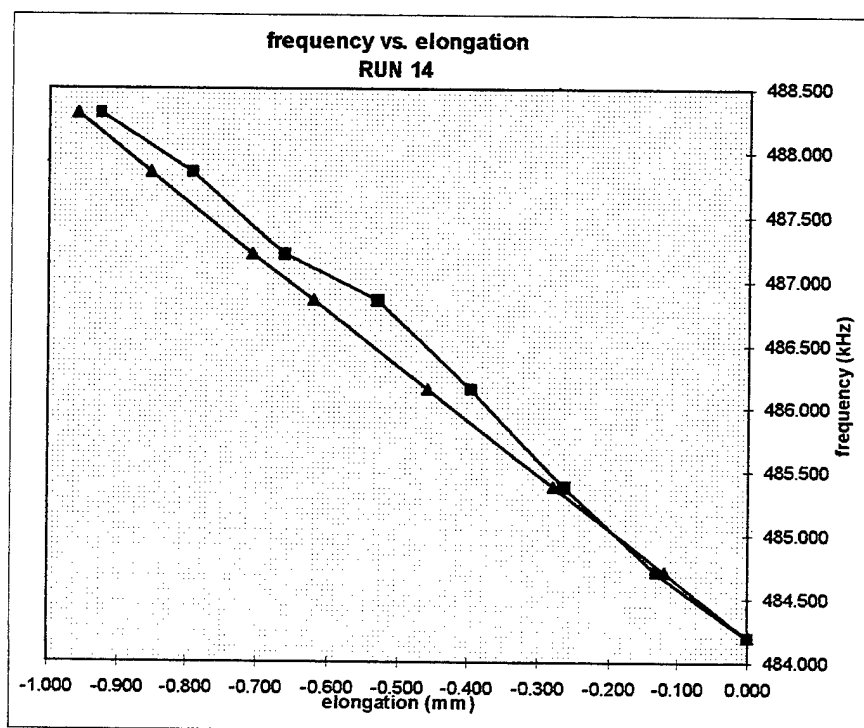


Figure C.22 Open Channel Model Run 14; Frequency vs. Elongation.

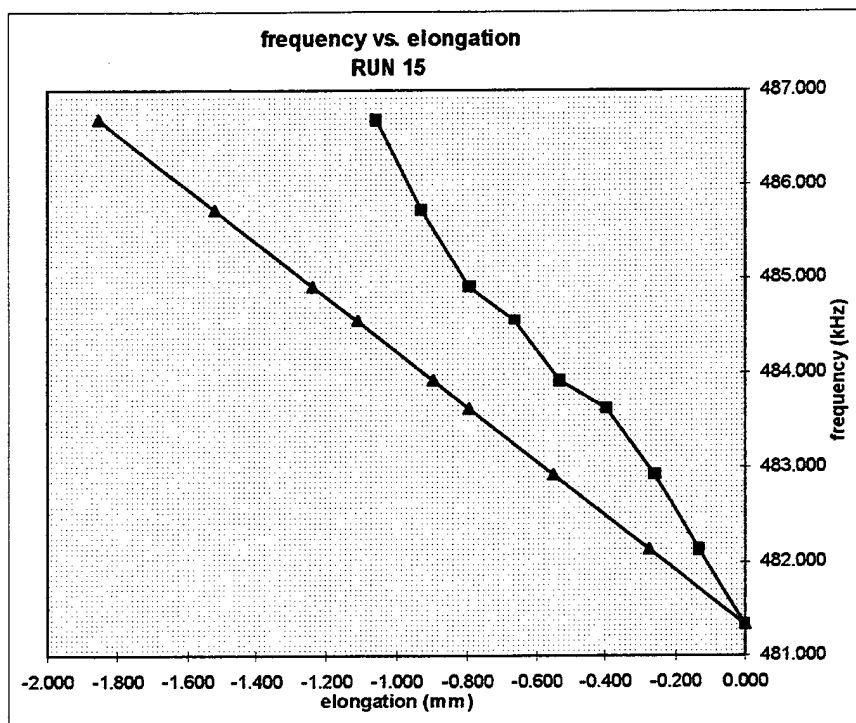


Figure C.23 Open Channel Model Run 15; Frequency vs. Elongation.

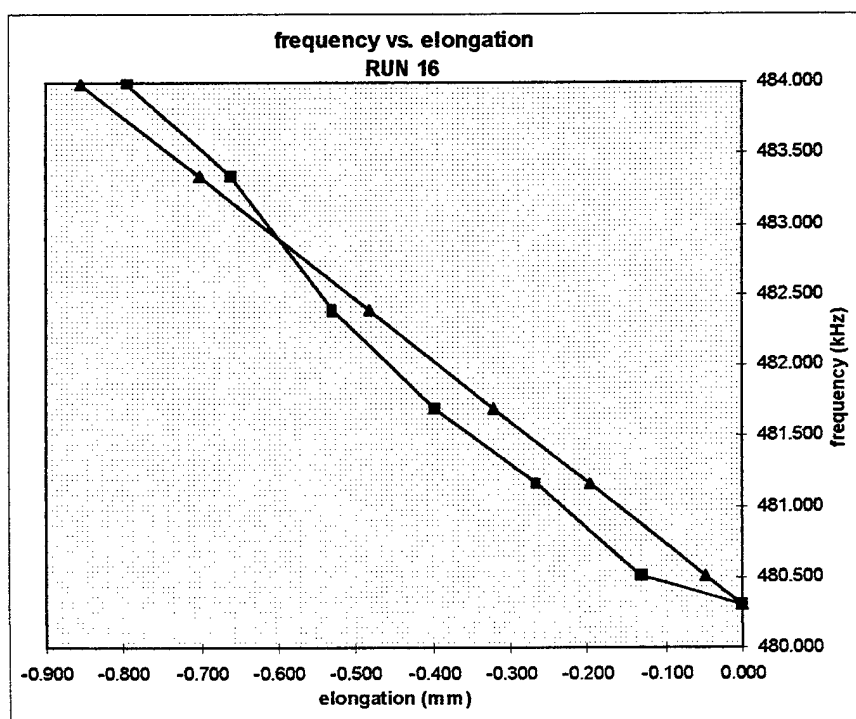


Figure C.24 Open Channel Model Run 16; Frequency vs. Elongation.

APPENDIX D. CADAVERS

A. NUMERICAL DATA

Representative numerical data collected on Cadavers A, B and C during the testing phase of this thesis is included in Chapter V. Figure D.1 contains the remaining reduced and processed data on Cadaver C.

B. GRAPHS

Figure D.2 represents all cadaver data points on one graph for comparative value only.

Figure D.3 represents all data points on Cadaver C, presented on one graph for clarity.

				Cadaver C					
	run 1			run 2			run 3		
	ICD (mm)	ICP (mmHg)		ICD (mm)	ICP (mmHg)		ICD (mm)	ICP (mmHg)	
	4.9	0		5.15	0		5.58	0	
	15.01	0.058		17.25	0.038		17.82	0.162	
	25.27	0.213		26.21	0.174		26.98	0.494	
	34.65	0.324		36.59	0.369		37.82	0.844	
	44.26	0.405		45.76	0.424		43.54	1.325	
	35.04	0.396		34.34	0.38				
	23.66	0.296		23.46	0.274				
	12.95	0.162		12.63	0.088				
	4.95	0.029		3.04	-0.167				
	run 4			run 5					
	ICD (mm)	ICP (mmHg)		ICD (mm)	ICP (mmHg)				
	6.64	0		6.17	0				
	16.77	0.062		14.87	0.182				
	28.49	0.237		28.48	0.508				
				40.38	0.988				
				44.51	1.338				

Figure D.1 All Cadaver C Numerically Reduced Data.

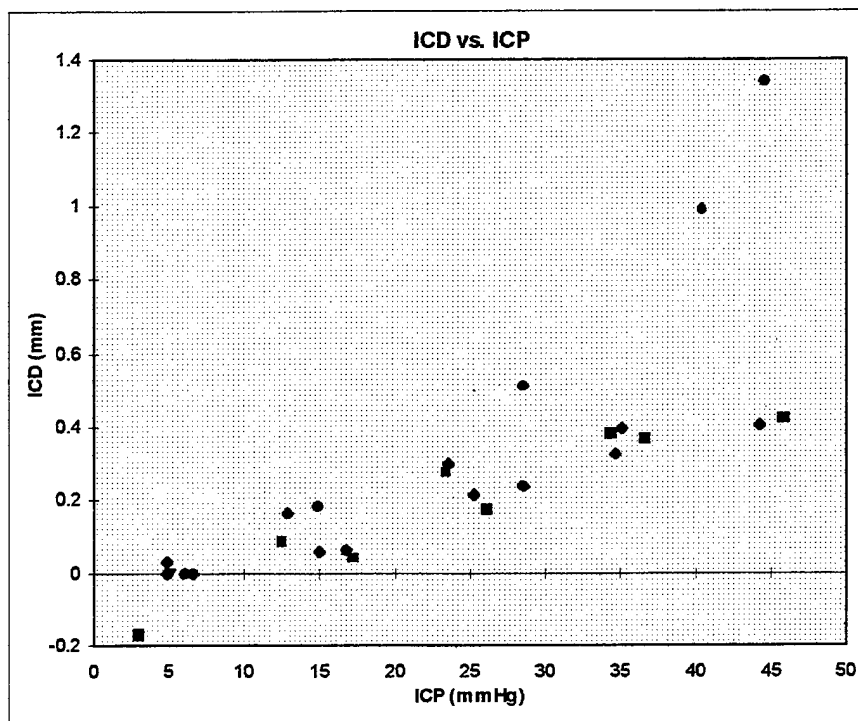


Figure D.2 All Cadaver C Data Points; ICD vs. ICP.

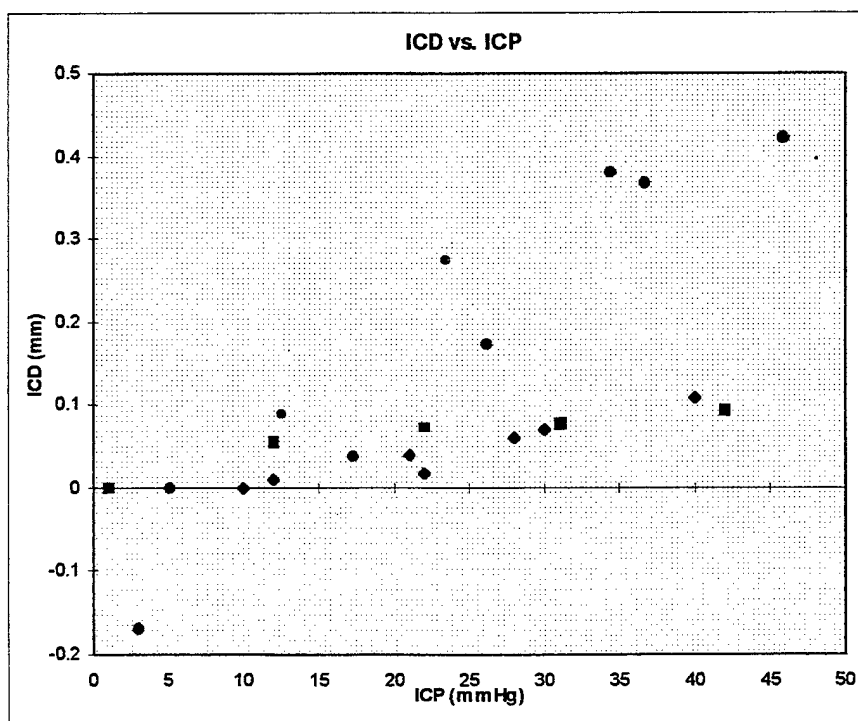


Figure D.3 Data Points from Cadavers A, B and C; ICD vs. ICP.

LIST OF REFERENCES

1. Jennings et al., *Aviation and Space Environmental Medicine*, 64:423(27), 1993.
2. Ballard, R. E., Wilson, M., Watenpaugh, D. E., Hargens, A. R., Shuer, L. M., Cantrell, J., and Yost, W. T., NASA Ames Research Center Proposal, Title Noninvasive Intracranial Volume and Pressure Measurements Using Ultrasound, 1996.
3. Miller et al., *Journal of Neurotrauma*, 9:S317-326, 1992.
4. Bellamy, R. F., The causes of death in conventional land warfare: implications for combat casualty care research, *Military Medicine*, 149:55-62, 1984.
5. Bowden, T. E., and Bellamy, R. F., eds., *Emergency War Surgery*, Washington, DC: U.S. Government Printing Office, Chapter XXII: Craniocerebral injury, p.283-295, 1988.
6. Hargens, A. R., NASA, Ames Research Center Proposal Title: Intracranial volume and pressure measurements using ultrasound, 23 Mar 1995.
7. Nakatani, S., Ozaki, K., Wakayama, A., and Mogami, N., "Intracranial pressure and pressure waves evaluated by transcranial Doppler sonography: clinical and experimental studies." In: Abstract Book, First International Conference on Transcranial Doppler Sonography, Rome, 1986.
8. North, J. B., Reilly, P. L., "A comparison between three models of ICP recording." In: Intracranial Pressure VI, Heidelberg, Springer, pp. 177-180, 1986.
9. Powell, M., and Crockard, A., "Difficulties in interpretation of extradural pressure (EDP) measurement in acutely raised intracranial pressure (ICP)." In: Intracranial Pressure VI, Heidelberg, Springer, pp. 203-206, 1986.
10. Barlow, P., Mendelow, A. D., Rowan, A., Lawrence, A., and Barlow, M., "Clinical evaluation of the Gaeltec ICT/b pressure transducer." In: Intracranial Pressure VI, Heidelberg, Springer, pp. 181-183, 1986.
11. Sundbarg, G., Messeter, K., Nordstrom, C. H., Soderstrom, S., "Intracerebral versus intraventricular pressure recording." In: Intracranial Pressure VI, Heidelberg, Springer, pp. 187-192, 1986.

12. Maas, A. I. R., and DeJong, D. A., "The Rotterdam teletransducer: telemetric epidural pressure monitoring - results of comparative EDP - VFP measurements." In: *Intracranial Pressure VI*, Heidelberg, Springer, pp. 207-212, 1986.
13. Hargens, A., Meyer, J., Aratow, M., Keil, L., Shuer, L., Semmlow, J., Watenpaugh, D., "Development and Experimental Verification of a Noninvasive Intracranial Pressure Recording System", 13 Dec 1989.
14. Heisey and Adams, *Neurosurgery*, 33:869-877, 1993.
15. Hiefetz and Weiss, *Journal of Neurosurgery*, 55:811-812, 1981.
16. Yost, W. T., and Cantrell, J.H., Fundamental aspects of pulse phase-locked loop technology-based methods for measurement of ultrasonic velocity, *The Journal of the Acoustical Society of America*, Vol. 91, No. 3, March 1992.
17. Logan, D. L., *Properties of Selected Engineering Materials*, p. 719-710, HarperCollins Publishers Inc., New York, NY, 1991.
18. Beer, F. P., and Johnston, E. R., Jr., *Mechanics of Materials*, p. 64, McGraw-Hill, Inc., New York, NY, 1981.
19. Halliday, D., and Resnick, R., *Fundamentals of Physics*, p. 316-321, John Wiley & Sons, Inc., New York, NY, 1981.
20. Shames, I. H., *Mechanics of Fluids*, Second Edition, p. 434-438, McGraw-Hill, Inc., New York, NY, 1982.

INITIAL DISTRIBUTION LIST

1. Defense Technical Information Center. 2
 8725 John J. Kingman Rd., STE 0944
 Ft. Belvoir, Virginia 22060-6218

2. Dudley Knox Library. 2
 Naval Postgraduate School
 411 Dyer Rd.
 Monterey, California 93943-5101

3. Dr. Rudolf Panholzer. 1
 Chairman, Space Systems Academic Group
 Code SP
 Naval Postgraduate School
 Monterey, California 93943-5101

4. Dr. Daniel J. Collins
 Chairman, Aeronautics and Astronautics Department. 1
 Code AA
 Naval Postgraduate School
 Monterey, California 93943-5101

5. Dr. Sandra L. Scrivener. 4
 Code AA/SS
 Naval Postgraduate School
 Monterey, California 93943-5101

6. Jeff Jenner. 1
 Michael J. Smith Professor of Space Systems
 Code SS/Jj
 Naval Postgraduate School
 Monterey, California 93943

7. Naval Research Laboratory. 1
 Code 9100, Bldg. 259
 4555 Overlook Avenue, SW
 Washington, DC 20363

8. Richard E. Ballard1
Life Science Division (239-11)
Gravitational Research Branch
NASA Ames Research Center
Moffett Field, California 94035-1000
9. Toshiaki Ueno, M.D., D.M.Sc.1
Life Science Division (239-11)
Gravitational Research Branch
NASA Ames Research Center
Moffett Field, California 94035-1000
10. W. Tom Yost, Ph.D.1
Langley Research Center
Mail Stop 231
Hampton, Virginia 23681-0001
11. Wen-Jei Yang, Ph.D., P.E.1
The University of Michigan
Mechanical Engineering and Applied Mechanics
Ann Arbor, Michigan 48109-2125
12. LT A. D. Burin.2
7050 Tuttle Court
Waterford, Michigan 48329-4832